DIN 67SD4379
16 OCTOBER 1967

FINAL REPORT

VOYAGER SPACECRAFT

PHASE B, TASK D

VOLUME IV (BOOK 1 OF 5)

EFFECT OF CAPSULE RTG'S ON SPACECRAFT

PREPARED FOR

GEORGE C. MARSHALL SPACE FLIGHT CENTER

UNDER MSFC CONTRACT No. NAS8-22603

GENERAL ELECTRIC

MISSILE AND SPACE DIVISION
Valley Forge Space Technology Center
P.O. Box 8555 • Philadelphia 1, Penna.

VOLUME SUMMARY

The Voyager Phase B, Task D Final Report is contained in four volumes. The volume numbers and titles are as follows:

Volume I	Summary
Volume II	System Description
Book 1	Guidelines and Study Approach, System Functional Description
Book 2	Telecommunication
Book 3	Guidance and Control Computer and Sequencer Power Subsystem Electrical System
Book 4	Engineering Mechanics Propulsion Planet Scan Platform
Book 5	Design Standards Operational Support Equipment Mission Dependent Equipment
Volume III	Implementation Plan
Volume IV	Engineering Tasks
Book 1	Effect of Capsule RTG's on Spacecraft
Book 2	Applicability of Apollo Checkout Equipment
Book 3	Central Computer
Book 4	Mars Atmosphere Definition
Book 5	Photo-Imaging

TABLE OF CONTENTS

Section		Page
1	SUMMARY	1-0
2	STUDY APPROACH	2-0
3	GUIDELINES	3-0
4	THERMAL ANALYSIS	4-0
5	NUCLEAR RADIATION ANALYSIS	5-0
6	MISSION EFFECTS	6-0
7	ASSEMBLY, TEST, AND PRELAUNCH EFFECTS	7-0
Appendix A		A-1
Appendix B		B-1
Appendix C		C-1

List of Illustrations

Figure		Page
2-1	Work Flow Summary	2-1
3-1	Spacecraft Design for Capsule RTG Interaction Study	3-1
3-2	Planetary Vehicle Configuration (Solar Powered Spacecraft)	3-3
3-3	Planetary Vehicle Configuration (RTG Powered Spacecraft)	3-4
4-1	Inside Shroud Temperature Distribution Opposite Lander RTG Radiation Plate	4-1
4-2	Effect of Spacecraft RTG's on Local Shroud Temperatures	4-1
4-3	Temperature of Lander Radiating Plate Versus Radiating Plate Emissivity	4-2
4-4	Effect of Shroud Temperature on Average Electronics Temperature	4-4
4-5	Shroud Cooling to Reduce Shroud Temperature	4-4
4-6	Shroud Cooling Versus Average Electronic Temperatures	4-5
4-7	Temperature History of Outside of Shroud Opposite Capsule RTG Radiating Plate	4-7
5-1	Planetary Vehicle Model With Neutron Flux and Gamma Dose Rate Isopleths	5-1
5-2	Neutron Spectra from Capsule RTG's	5-3
5-3	Gamma Effects Summary	5-5
5-4	Neutron Effects Summary	5-6
5-5	Radiation Effects on Eastman Kodak SO-243 Film	5-9
5-6	Radiation Absorption Versus Shield Weight Eastman Kodak High Definition Aerial Film SO-243	5-9
5-7	Shield Weight Versus Granularity and S/N Eastman Kodak Film SO-243	5-9
6-1	Array Area Requirements	6-1
7-1	Planetary Vehicle Model with Neutron and Gamma Dose Rate Isopleths	7-1
A-1	Planetary Vehicle Model with Neutron Flux and Gamma Dose Rate Isopleths	A-9
A-2	Planetary Vehicle Model for One-Dimensional Neutron Transport Analysis	A-12
A-3	Neutron Flux Energy Distribution	A-14
B-1	Activity Required to Produce a Dose Rate of 1.0×10^{-3} r/hr @ 1 Meter from a Point Source	B-7
C-1	Neutron Sensitivity Summary	C-6
C-2	Gamma Effects Summary	C-7
C-3	Solar Cell Power Degradation	C-12

SECTION 1: SUMMARY

- EFFECT OF CAPSULE RTG'S ON SPACECRAFT

The use of radioisotope thermoelectric generators (RTG's) is being considered for the prime power source for the Voyager surface laboratory system. The objective of this study was to examine the impact of the RTG's in the flight capsule upon the spacecraft, and to determine the necessary spacecraft design provisions for compatibility.

RTG's are characterized by elevated temperature operation and the emission of nuclear radiation. It was the interaction of these characteristics with the spacecraft that was the main concern of this study. Other aspects of the study dealt with the potential reduction of spacecraft power requirements, since the RTG-powered capsule is self-sufficient from a power standpoint.

Representative spacecraft and capsule configurations were first selected, and served as the basis for subsequent thermal and nuclear radiation analyses. A conscious attempt was made in these selections to introduce potential interaction problems. For example, the spacecraft electronic equipment was located close to the spacecraft/capsule interface to aggravate thermal and nuclear interactions. The capsule configuration selected also reflected this approach by confining the heat rejected from the RTG's to a narrow zone, creating possible conditions of excessive temperature. The underlying thought was that if analysis showed the practicality of these worst-case approaches, greater margin would be available with more judicious designs.

The Planetary Vehicle thus defined consisted of a solar-array-powered spacecraft and an RTG-powered capsule. In addition, the thermal and nuclear effects were also studied for the configuration resulting when the spacecraft and capsule are both powered by RTG's.

The study results are summarized below.

- THERMAL INTERACTION

During steady-state prelaunch conditions with the Planetary Vehicle enshrouded, the inside shroud wall temperature in the vicinity of the capsule RTG heat-rejection radiators will be about 260°F. Because the spacecraft is remote from this elevated temperature zone, effects on the spacecraft are only slight and will not result in a substantial increase in shroud cooling requirements. (Shroud cooling is required primarily to remove the inflow of ambient and solar heat.) The use of RTG's in the spacecraft will likewise result in only nominal cooling increases.

During the launch phase the shroud zone in the vicinity of the capsule RTG radiators would rise to 420°F, about 100 degrees higher than if RTG's were not used. With an upper limit on permissible shroud temperature estimated to be around 300°F, some method of removing heat from the shroud wall appears necessary. The heat of vaporization of several pounds of water contained in appropriate cooling coils would suffice for this purpose.

After shroud separation, there are no appreciable RTG thermal effects on the spacecraft.

- NUCLEAR RADIATION INTERACTION

For the spacecraft piece parts, materials, and science instruments, radiation sensitivity levels were determined for threshold effects, moderate effect, and severe damage. Spacecraft radiation environment was determined by mapping the gamma and neutron radiation levels throughout the spacecraft. Total integrated dose rates for the mission were then established, and the radiation effects determined.

Considering first the spacecraft parts and materials (exclusive of science instruments), the effect of gamma radiation is negligible. Neutron radiation produces some threshold and moderate effects which can be overcome by proper part selection and derating, circuit design, and, perhaps in a few cases, by local shielding.

Nuclear radiation interaction with the science payload will be in the form of dynamic interference, i.e., inability of certain instruments to distinguish between the natural particles of interest and those resulting from RTG emission. Of the nine instruments defined as the baseline science, only the ultraviolet spectrometer will be seriously affected by the RTG environment. The difficulty is associated with the reduction of signal-to-noise ratios and the ability to extract useful information from target areas of weak ultraviolet emission. The two infrared spectrometers of the baseline instruments will also be affected, but to a much lesser degree. Other potential alternates or additions to the baseline science were examined. Some of these would also experience dynamic interference, depending on their sensitivity requirements and the presence of certain materials in the spacecraft. This latter point relates to radioactivity induced by the RTG's in various materials. In general, it was found that such activity would decay to insignificance in several hours after capsule separation; however, this assessment is relative to the baseline instruments and could be serious for other very sensitive instruments.

Estimates indicate that 40 or more pounds of shielding would be required for photographic film of a typical photo-imaging system to limit fogging to acceptable levels. An uncertainty exists as a result of limited data on the effect of neutrons on film.

- MISSION EFFECTS

The use of RTG's in the capsule eliminates the capsule requirement for 200 watts of electrical power from the spacecraft. The solar array cannot be made smaller, however, since it is sized to meet late mission requirements. The excess availability of 200 watts in the early portion of the orbiting phase makes it possible to consider:

a. Increasing the science data return.

b. Selection of orbits with early occulations.

The presence of the RTG power source in the capsule allows the consideration of using capsule power as an emergency backup to the spacecraft battery power during maneuvers.

THIS PAGE INTENTIONALLY LEFT BLANK

SECTION 2: STUDY APPROACH

THE APPROACH USED IN THIS STUDY WAS ORGANIZED TO TAKE ADVANTAGE OF RESULTS AND TECHNIQUES DEVELOPED ON THE EARLIER VOYAGER TASK C RTG STUDY.

The Work Flow diagram shown in Figure 2-1 delineates the principal areas of investigation undertaken in this study.

Radiation mapping and sensitivity studies consisted largely of an updating of the results of the earlier Task C RTG study, taking spacecraft and capsule configuration changes into account and incorporating the radiation sensitivities of any newly selected spacecraft components. In addition, a study of the induced radioactivity in spacecraft materials was performed to determine the spacecraft radiation environment after the time of capsule separation.

Thermal analysis was initially limited to effects on the spacecraft. It soon became apparent that these effects were small and that the principal interaction occurred between the capsule and the shroud. Accordingly, more emphasis was placed on this problem.

Activity on the other elements shown on the Work Flow diagram followed from the principal thermal and radiation analyses.

Results in the following sections generally follow the pattern of the Work Flow diagram.

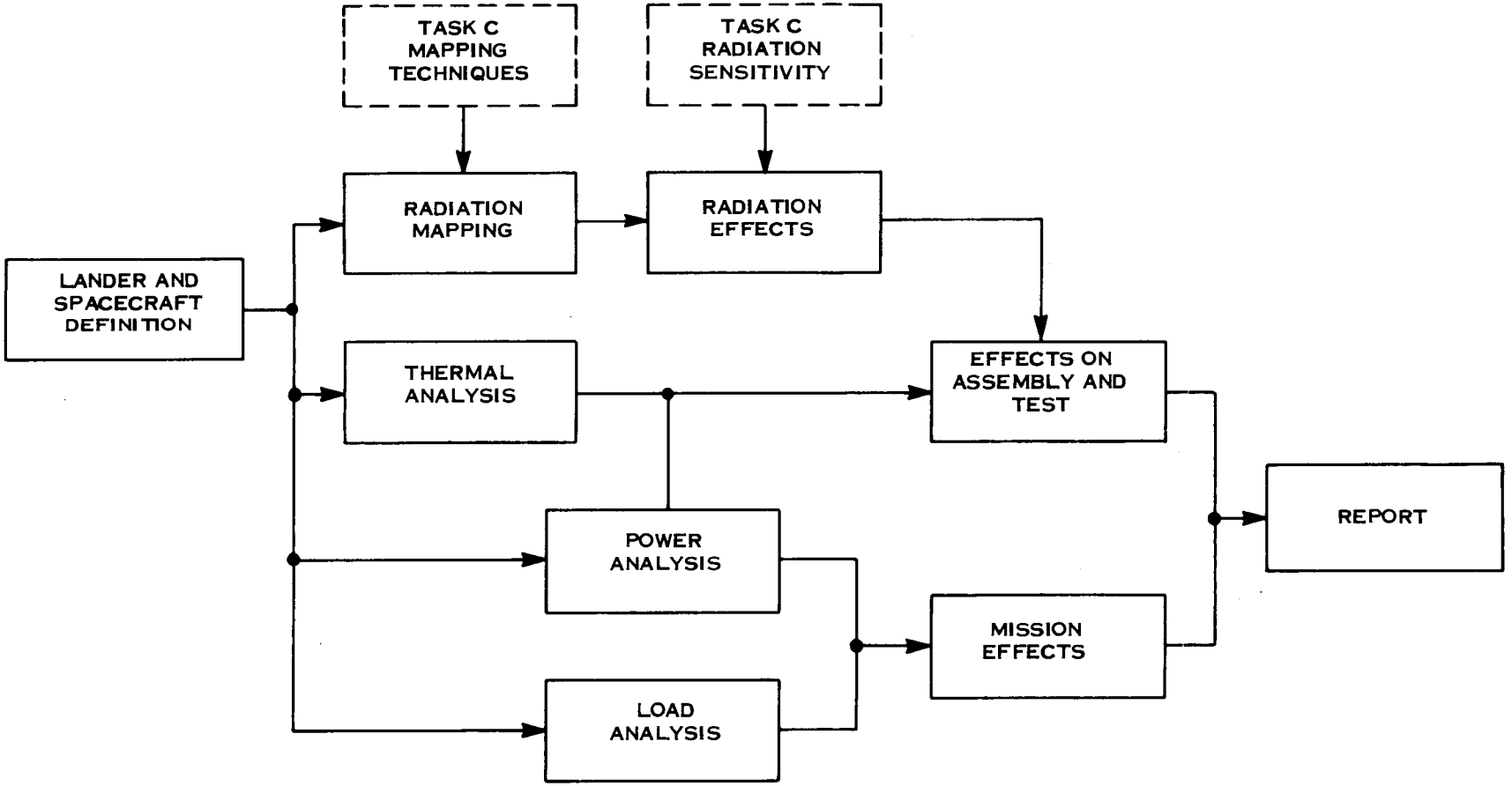

Figure 2-1. Work Flow Summary

SECTION 3: GUIDELINES

CAPSULE DEFINITION

THE CAPSULE CONFIGURATION ADAPTED FOR THIS STUDY CONTAINS THREE CENTRALLY LOCATED RTG'S RATED AT 2400 THERMAL WATTS EACH, FROM WHICH WASTE HEAT IS TRANSFERRED TO AND REJECTED THROUGH RADIATOR PLATES LOCATED ON THE CIRCUMFERENTIAL PERIPHERY OF THE CAPSULE.

Figure 3-1 shows the capsule configuration used in this study. This configuration is based on information supplied by the Jet Propulsion Laboratory through the Marshall Space Flight Center.

Three centrally located RTG's provide electrical power to the capsule. Each is thermally rated at 2400 watts. Assuming a typical conversion efficiency of 5 percent, each would provide an electrical power of 120 watts (360 watts total).

The principal interactions with the spacecraft result from thermal and nuclear radiation:

a. Thermal characteristics are taken to be those defined on the sketch which indicates that all RTG waste heat is transferred by suitable means to three radiator plates located on the circumferential periphery of the capsule. The exact means of heat transfer to the radiator plates is not defined but could presumably be accomplished by pumped fluid loop systems, heat pipes or other methods. For the purpose of this study, it is assumed that the radiator plates provide the only means of RTG waste heat rejection. Although heat leaks in the RTG to radiator plate heat transfer system would likely occur, their consideration would require a detailed analysis of the internal arrangement of the capsule. Such information was not available for this study, and it was therefore considered more appropriate to consider only the idealized conditions suggested by the sketch. These are that RTG waste heat is only rejected at the radiator plates and that all other capsule surfaces are perfect thermal insulators. This latter assumption regarding the entry shape end of the capsule is conservative since heat transfer in that region would decrease thermal interaction with the spacecraft. At the spacecraft interface, the existence of adequate insulation is assumed. As shown in the Thermal Analysis section a nominal amount of insulation can effectively reduce transferred heat to negligible values.

b. Nuclear radiation characteristics are assumed to be based on RTG's fueled with plutonium - 238. In the absence of specific RTG configuration data, the RTG's at each of the three locations are assumed to be of the SNAP-27 design

for which extensive radiation analysis data exist. Any masses in the capsule located between the RTG's and the spacecraft interface are assumed negligible to permit worst case-analysis of radiation effects upon the spacecraft equipment.

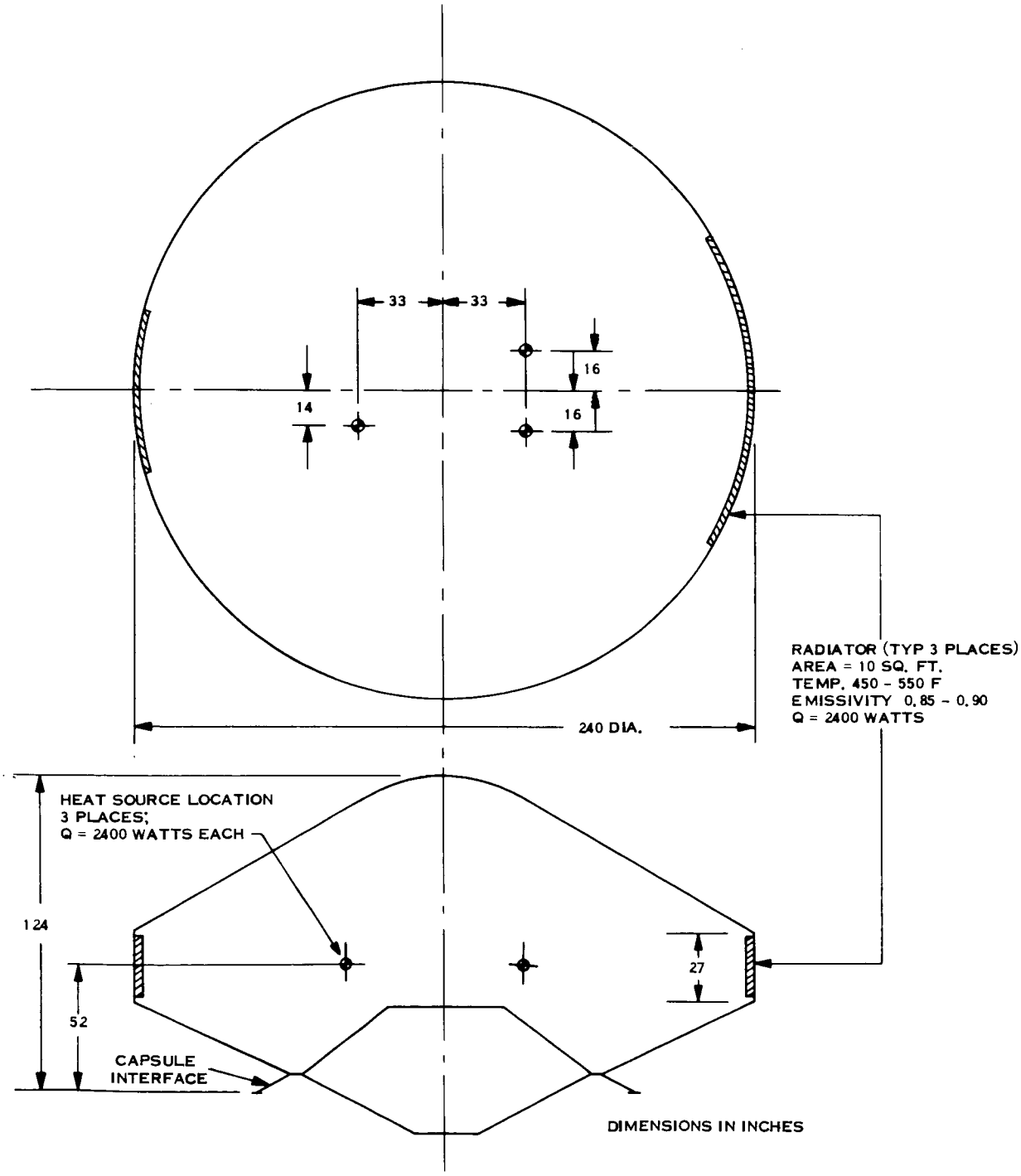

Figure 3-1. Spacecraft Design for Capsule RTG Interaction Study

SECTION 3: GUIDELINES

PLANETARY VEHICLE DEFINITION

THE PLANETARY VEHICLE CONFIGURATION CHOSEN FOR THIS STUDY HAS THE MAJOR ELECTRONIC EQUIPMENT OF THE SPACECRAFT LOCATED NEAR THE CAPSULE INTERFACE SO THAT IT IS SUBJECTED TO THE HIGHEST LEVELS OF THERMAL AND NUCLEAR RADIATION, THUS PERMITTING WORST CASE ANALYSIS. SEPARATE CASES OF THE SPACECRAFT POWERED BY SOLAR OR RTG POWER ARE CONSIDERED.

Figure 3-2 shows the Planetary Vehicle configuration used in this study. The spacecraft configuration which supports the capsule is one of several described in detail in Volume II.

This particular configuration was chosen for the RTG interaction study because of the proximity of the equipment bays to the capsule RTG's and the desire to identify worst case thermal and nuclear radiation interactions. Similarly, the planet scan package is shown stowed above the solar array slant panels so that it too would be subjected to higher levels of nuclear and thermal radiation flux.

Sixteen equipment bays are used. For the purpose of estimating steady-state temperature conditions during the prelaunch phase a total heat dissipation of 330 watts from the bays is assumed.

The equipment to be studied for possible radiation effects consists of two categories: (1) the spacecraft parts and materials as defined in Volume II of this report and (2) the science payload equipment listed in Table 3-1.

The first nine instruments comprise the baseline science payload; the remaining instruments shown are considered as potential alternates or additions.

The RTG-powered spacecraft version shown on Figure 3-3 has eight RTG's circumferentially distributed and mounted on the panels normally occupied by solar cells in the solar-powered version. Except for the relative positioning of the equipment bays, this configuration is quite similar to the configuration generated in the Voyager Phase IA Task C RTG Study. Each spacecraft RTG is assumed to be rated at 1500 thermal watts. The heat rejection area (30-inch diameter) and its distance from the shroud (30 inches) conform closely with those used in the Task C study.

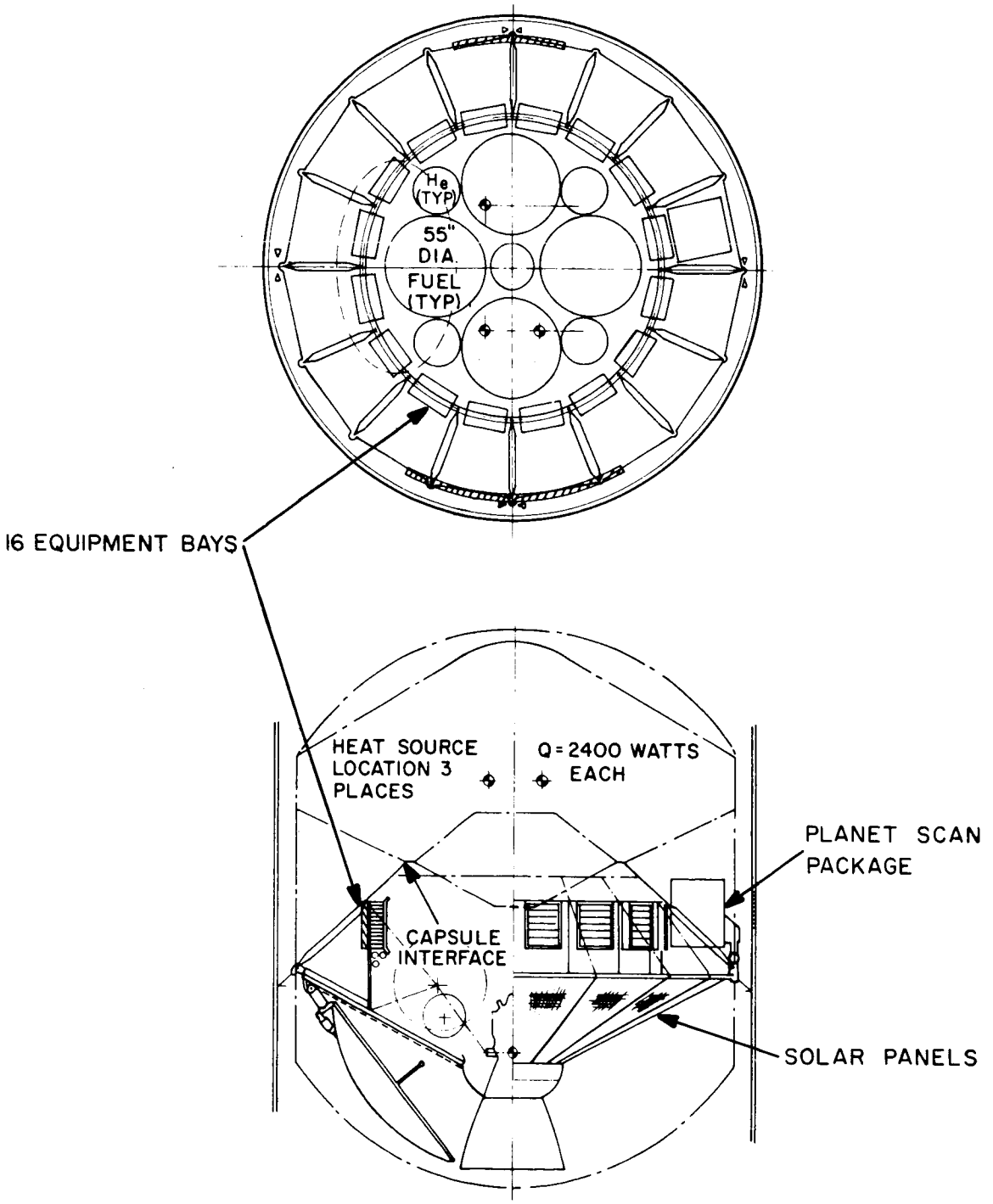

Figure 3-2. Planetary Vehicle Configuration (Solar Powered Spacecraft)

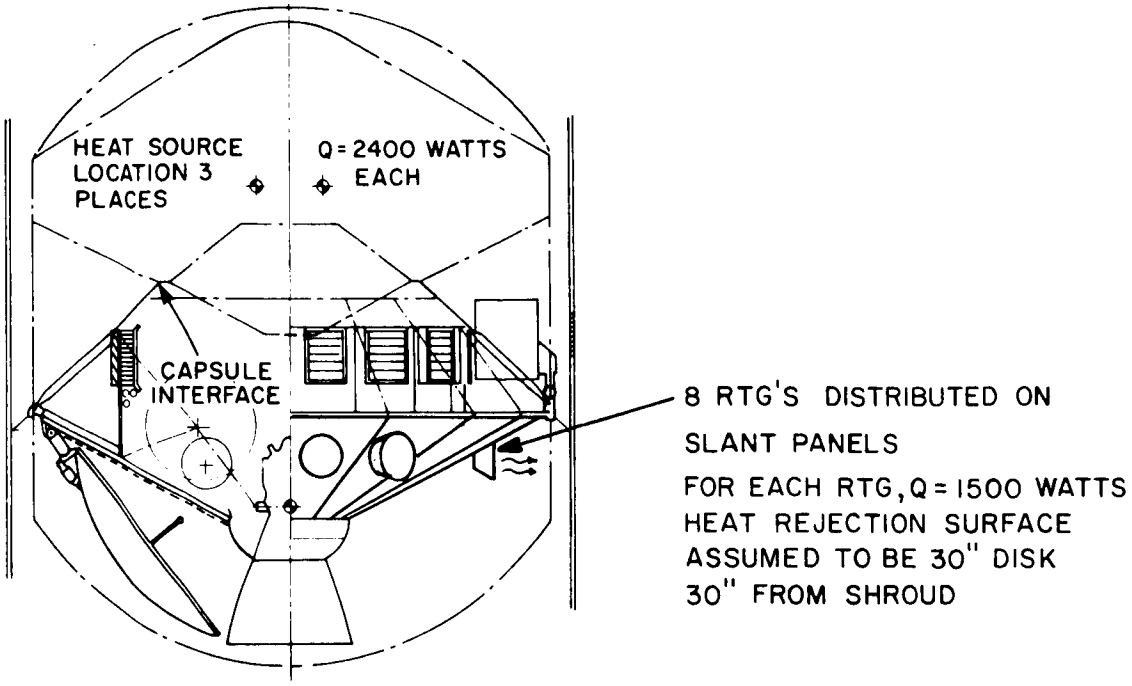

Figure 3-3. Planetary Vehicle Configuration (RTG Powered Spacecraft)

Table 3-1. Assumed Science Equipment

Baseline Science Experiments:

1. Medium Resolution TV Camera No. 1
2. Medium Resolution TV Camera No. 2
3. High Resolution TV Camera
4. High Resolution IR Spectrometer
5. Broad Band IR Spectrometer
6. IR Radiometer
7. UV Spectrometer
8. Radio Occultation
9. Celestial Mechanics

Additional or Alternate Experiments:

10. Photographic Film System
11. Gamma Ray Spectrometer
12. Cosmic Ray Telescopes (3)
13. Magnetometers (3)
14. Cosmic Dust Detector
15. Mass Spectrometer
16. Plasma Probes
17. Polarimeter
18. X-Ray Detector
19. Neutron Spectrometer
20. Bistatic Radar
21. Microwave Radiometer
22. Gradiometer

SECTION 4: THERMAL ANALYSIS

PRELAUNCH THERMAL CONDITIONS

DURING STEADY-STATE PRELAUNCH CONDITIONS, INSIDE SHROUD TEMPERATURES WILL BE 260°F IN THE REGION OF THE CAPSULE RTG RADIATORS AND 220°F IN THE REGION OF SPACECRAFT RTG'S, IF THEY ARE USED. THE AVERAGE TEMPERATURE OF THE SPACECRAFT ELECTRONIC EQUIPMENT WILL INCREASE A MAXIMUM OF 16°F FOR A FIXED VALUE OF SHROUD COOLING.

As indicated previously, the capsule RTG's reject their waste heat through radiator plates located on the circumferential periphery of the capsule. If spacecraft RTG's are used, they reject their heat directly from their cold junction fins. Several possible steady-state prelaunch conditions must be evaluated:

a. The local shroud regions receiving RTG-rejected heat will be at an elevated temperature.

b. The rejection plate temperature of the RTG's will increase because of the higher radiation heat sink temperature.

c. Spacecraft temperatures might also increase due to the increased shroud heat sink temperature.

These were the principal effects considered. The results are as follows:

a. Local Shroud Temperatures. The calculated distributions of temperature are shown on the nodal diagrams of Figures 4-1 and 4-2 for the capsule RTG's and spacecraft RTG's respectively. A maximum inner shroud wall temperature of 260°F is indicated. The calculations are based solely on radiant heat exchange without the use of circulating air cooling. Sizeable variations in the external ambient conditions would have a negligible effect on the predicted temperatures of the inner walls.

b. RTG Radiator Plate Temperatures. The effect of the increased sink (shroud) temperature on the capsule RTG radiator plate temperature is shown in Figure 4-3. Typically for plate emissivities of 0.85, the radiator temperature will rise about 70°F higher under the shroud than when radiating to free space. Similar temperature increases would apply to the spacecraft RTG's.

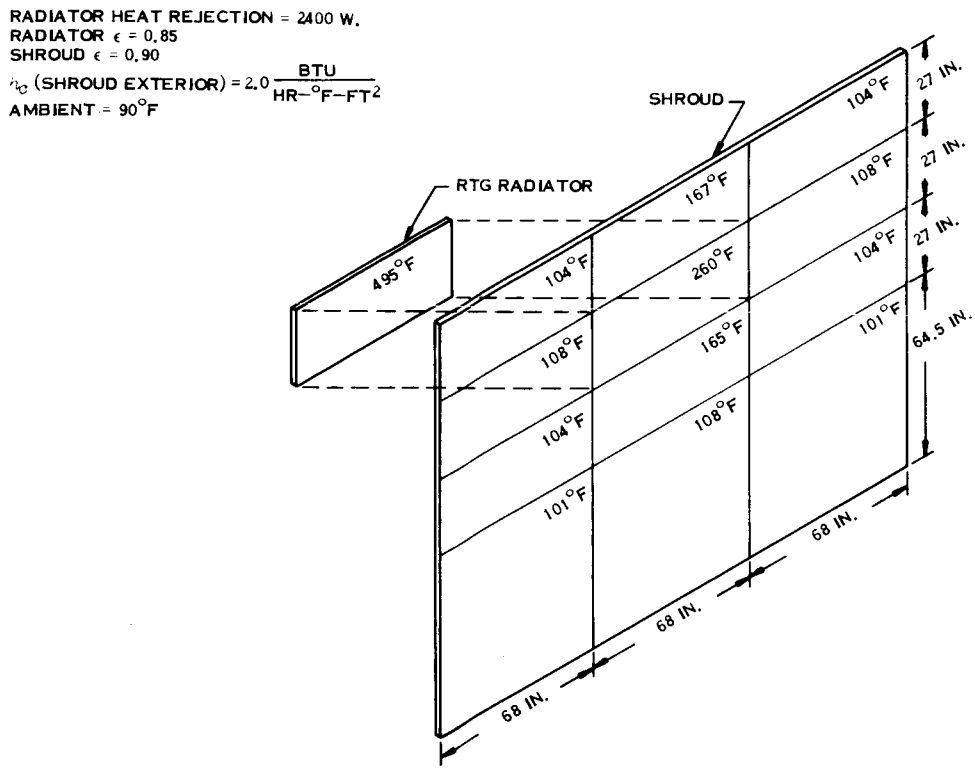

Figure 4-1. Inside Shroud Temperature Distribution Opposite Lander RTG Radiating Plate

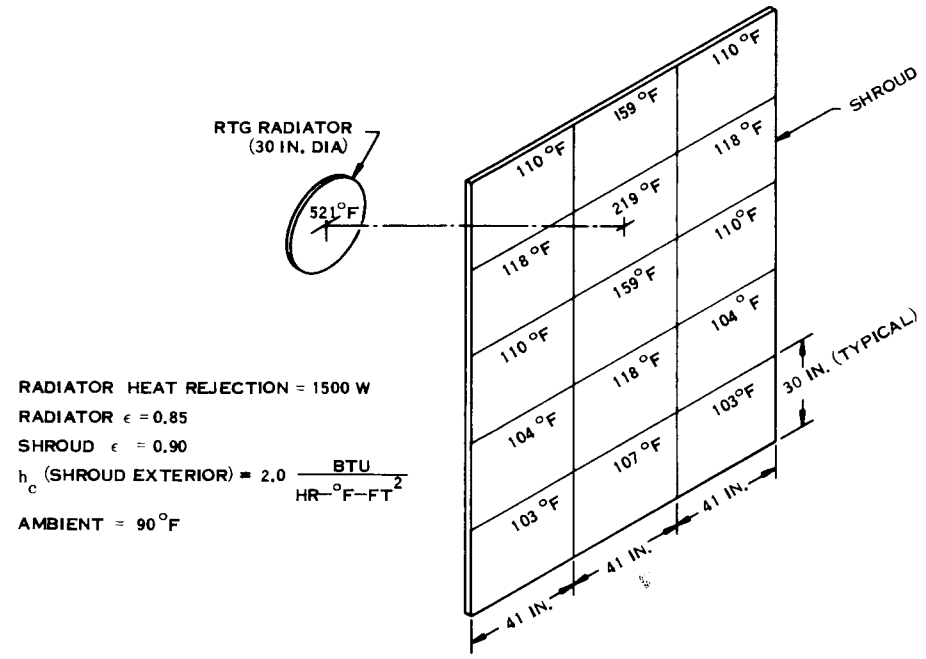

Figure 4-2. Effect of Spacecraft RTG's on Local Shroud Temperatures

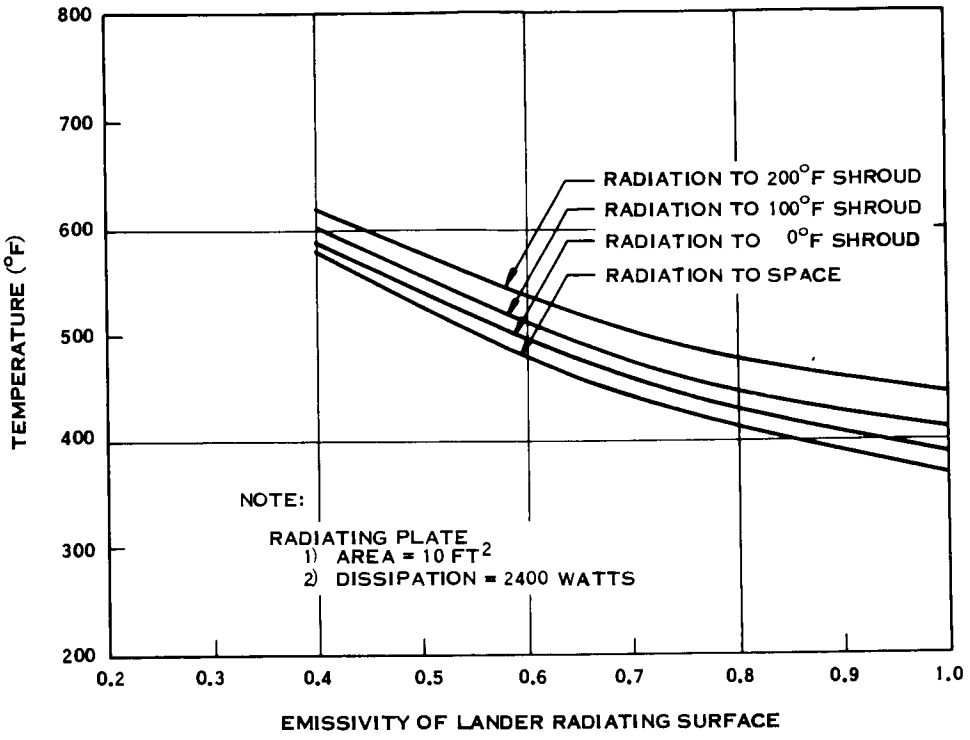

Figure 4-3. Temperature of Lander Radiating Plate Versus Radiating Plate Emissivity

c. Spacecraft Temperature. The predicted temperature of the electronic bay equipment is used as the basis for estimating the thermal effect of the capsule RTG's on the spacecraft. The particular arrangement of the capsule, spacecraft, and shroud indicates that the capsule or spacecraft RTG's may affect the bay equipment by heat conduction through the capsule-spacecraft interface or by the reradiation of the RTG rejected heat from the inner shroud wall. These effects are considered separately below:

1. Heat Through Interface. Since the internal arrangement of the capsule equipment has not been defined for this study, it is not possible to definitely predict the value of conducted heat. Nevertheless, by hypothesizing the existence of a multilayered thermal barrier located at the spacecraft/capsule interface, very small values of heat flux are predicted. Typical values for the effective emissivity of 40-layer insulation are 0.0045.* Thus for a thermal barrier of 97 square feet (corresponding to the 160-inch interface diameter),

*As established in the Planetary Vehicle Thermal Insulation Study, JPL Contract Number 951537.

an assumed average inside capsule temperature as high as 200°F, and a spacecraft temperature of 70°F, the total predicted heat flow is 24 watts. This is considered negligible in terms of effect on spacecraft temperatures.

2. Reradiated Heat. The equilibrium temperature of a particular equipment bay depends on the amount of power dissipated in that bay and the average temperature of the shroud to which the bay heat is rejected, ignoring any cooling effect which internal circulating air might provide. Figure 4-4 shows an estimate of this temperature relationship for a total electronic bay dissipation of 330 watts during prelaunch operations. The introduction of capsule or spacecraft RTG's would tend to increase the average temperature of the shroud as viewed by the bay and would increase the bay temperature accordingly. The average inner wall shroud temperature as viewed by the equipment bays is a function of the external ambient conditions, the shroud wall thermal conductivity, and the heat load through the shroud walls. Figure 4-5 summarizes this relationship in terms of required heat removal at the surface of the inner shroud wall for cases without RTG's, with RTG's in the capsule only, and with RTG's in the capsule and spacecraft. In other words, in order to achieve a desired average inner wall shroud temperature, it would be necessary to remove the indicated heat by some means of cooling. This could be accomplished by air circulation or wall cooling coils or some combination of these. It is noted that most of the heat-removal requirement results from the inflow of heat from the external ambient source rather than from the spacecraft or capsule. Thus, for the case of no RTG's in the capsule, the heat-removal requirement at a wall temperature of 100°F is zero, since this is also roughly the external shroud temperature resulting from the 90°F ambient temperature in combination with external solar heating, whereas at a wall temperature of 80°F the heat-removal requirement is 4 kilowatts and is principally associated with the inflow of ambient heat. For any given wall temperature the capsule RTG's increase the heat-removal requirement by about 1.3 kilowatts, which represents the rejected RTG heat which is not directly transferred through the shroud but rather contributes to raising the average wall temperature as viewed by the electronic bays.

For the same reasons, the spacecraft RTG's increase the heat-removal requirements by about 3 kilowatts for any given average wall temperature as viewed by the electronics. The spacecraft RTG heat directly transferred through the shroud is therefore about 9 kilowatts, based on the 12-kilowatt thermal rating of the spacecraft RTG's. The lower regions of the spacecraft will be at elevated temperatures since they will more or less achieve equilibrium with the shroud temperatures in the vicinity of the spacecraft RTG's. This is not considered serious since the affected surfaces can be appropriately insulated to prevent the flow of heat to more temperature-sensitive regions of the spacecraft.

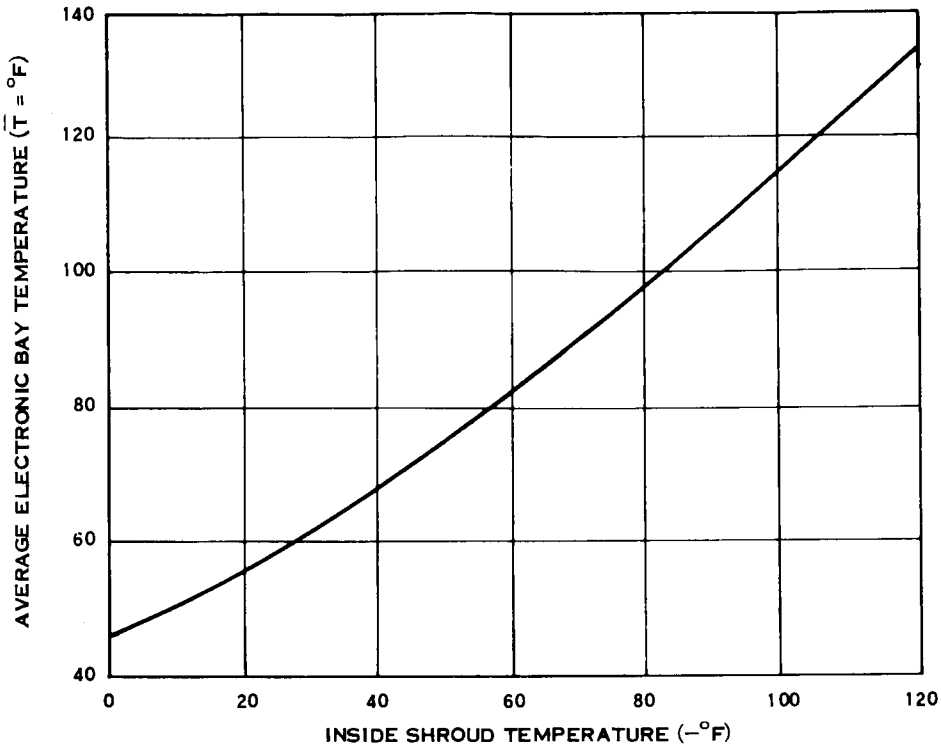

Figure 4-4. Effect of Shroud Temperature on Average Electronics Temperature

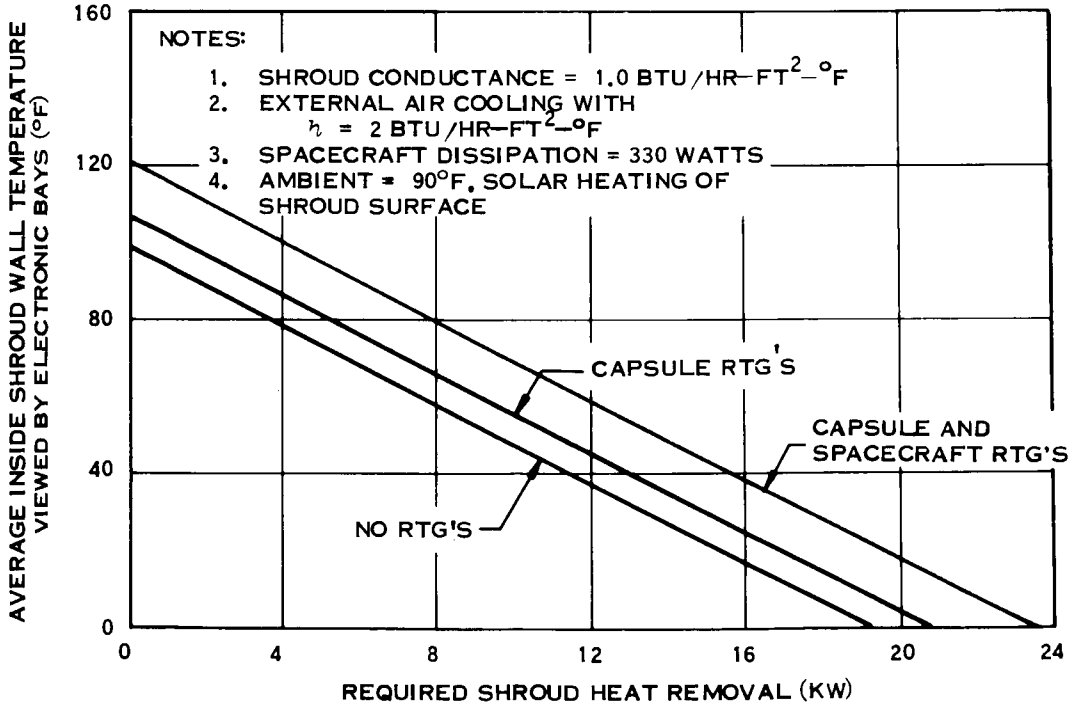

Figure 4-5. Shroud Cooling to Reduce Shroud Temperature

The data of Figures 4-4 and 4-5 are combined in Figure 4-6 to show the direct relationship of the average electronic bay temperature with the heat-removal requirement.

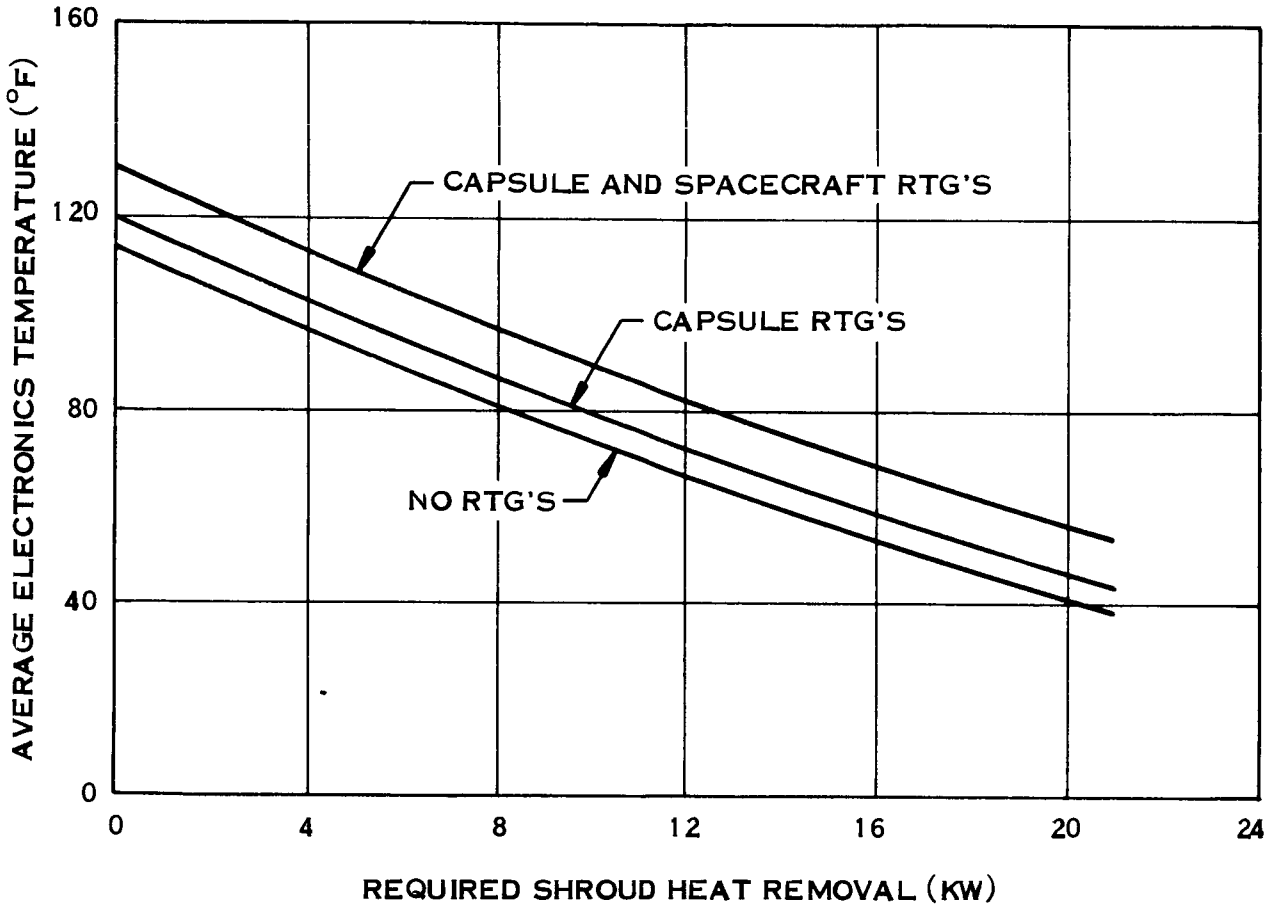

Figure 4-6. Shroud Cooling Versus Average Electronic Temperatures

SECTION 4: THERMAL ANALYSIS

ASCENT THERMAL CONDITIONS

DURING ASCENT, SHROUD TEMPERATURES IN THE REGION OF THE CAPSULE RTG RADIATOR PLATES WILL RISE TO A MAXIMUM OF 421°F, WHICH IS ABOUT 92°F HIGHER THAN IF NO RTG'S WERE USED IN THE CAPSULE. WITH SHROUD TEMPERATURE LIMITS ESTIMATED TO BE 300°F, ASCENT COOLING OF THE SHROUD WALL IS REQUIRED.

During the study, information was supplied by MSFC that shroud temperatures should not exceed around 300°F.

A thermal analysis was therefore performed to determine the temperature level of the shroud subjected to combined ascent and RTG heating. As a worst case, the shroud section opposite the capsule RTG radiating plate was selected since this section would have the highest ascent heat flux and highest initial temperature and would therefore experience the highest temperature level. As a first step, the temperature history of this shroud section was calculated with no RTG's in the capsule. The results are shown in Figure 4-7 and are quite similar to the temperature histories presented in the MSFC report entitled Voyager Shroud Thermal Analysis, dated 5 July 1967, by C. C. Wood. Inspection of this figure indicates that a peak outside shroud temperature of 329°F will be reached, starting with a launch temperature of 85°F. As a second step, the capsule RTG heat load was combined with the ascent heat flux and the resulting peak shroud temperature increased to 421°F, starting with an uncooled outside wall temperature of 230°F (inside wall at 260°F). In an attempt to reduce this peak temperature, the shroud was precooled to 80°F, and then the shroud temperature history was recalculated. The results indicated that precooling of 150°F (from 230°F to 80°F) reduces the peak shroud temperature only 7°F (from 421°F to 414°F); therefore it appears that on-the-pad precooling of the shroud does not provide much of an advantage and it is necessary to provide ascent cooling of the affected shroud section.

If some independent means were available for removing the capsule RTG heat during ascent, the temperature-time history at the shroud region in question would be no worse than that shown for the no-RTG case with a peak temperature of 329°F. Although the starting temperature would be higher, this has little influence on the peak temperature reached. It would be necessary to remove 10^6 watt-seconds (7200 thermal watts from the RTG's times 140 seconds) or 950 Btu's by the independent heat-removal means.

The heat of vaporization of 1 pound of water could accomplish this, and thus the use of some form of water boiler appears practical from a weight standpoint. Numerous other approaches could be considered for this purpose.

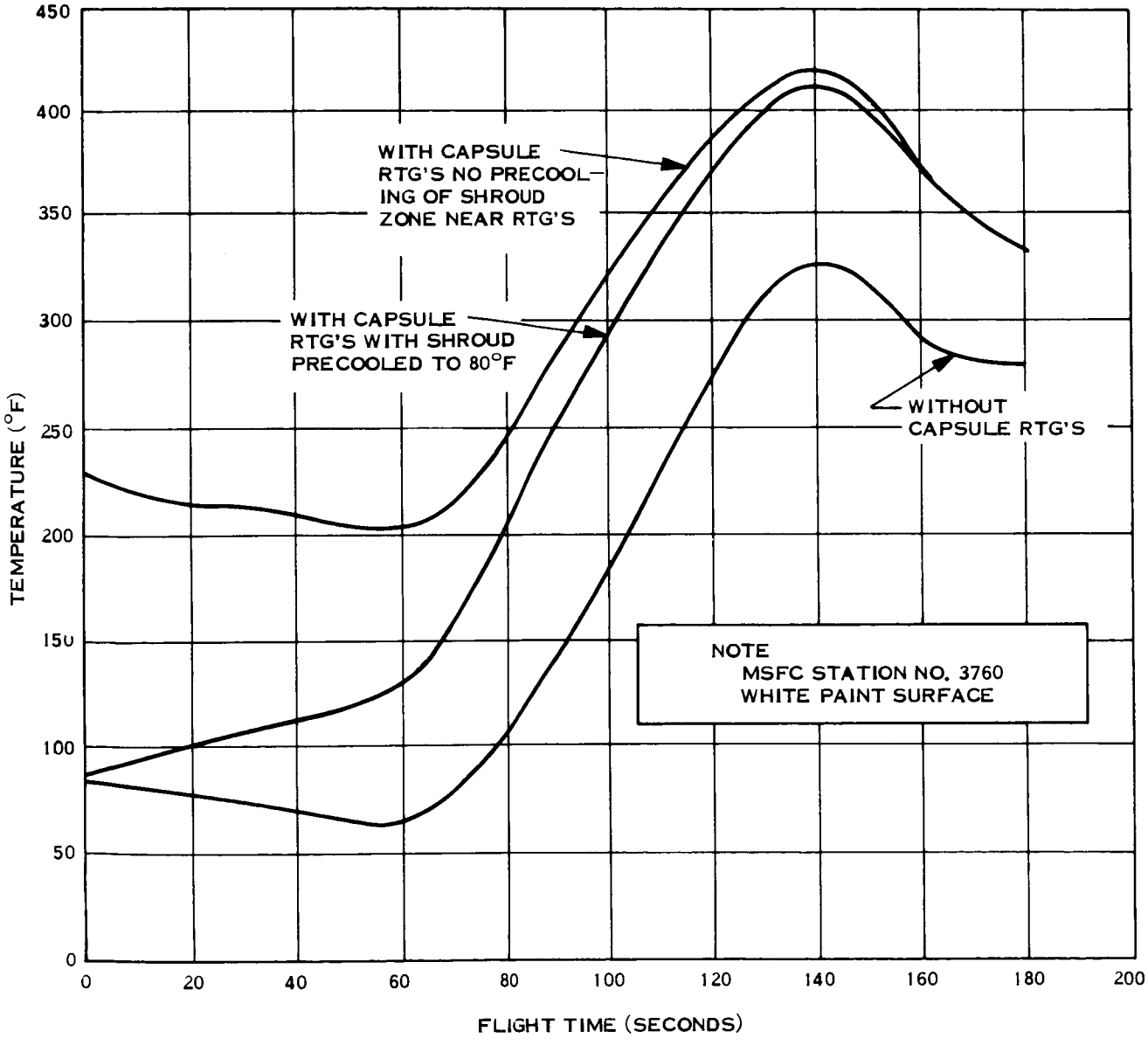

Figure 4-7. Temperature History of Outside of Shroud Opposite Capsule RTG Radiaing Plate

SECTION 5: NUCLEAR RADIATION ANALYSIS

RTG RADIATION ENVIRONMENT

AT THE TIME OF CAPSULE SEPARATION IN MARS ORBIT, THE INTEGRATED NEUTRON FLUX IN THE ELECTRONIC EQUIPMENT BAYS FROM THE CAPSULE RTG'S WILL BE ABOUT 3.2×10^{10} NEUTRONS—CM^{-2}, AND THE GAMMA RAY DOSE ABOUT 107 RADS (C). AFTER SEPARATION FOR THE CASE OF THE SPACECRAFT WITHOUT RTG'S A LOW—LEVEL RADIATION ENVIRONMENT WILL PERSIST WHICH MAY AFFECT CERTAIN SENSITIVE SCIENCE INSTRUMENTS. WITH SPACECRAFT RTG'S USED AS WELL, THE INTEGRATED NUETRON FLUX IN THE ELECTRONIC EQUPIMENT BAY AT THE END OF THE MISSION WILL BE ABOUT 5.8×10^{10} NEUTRONS—CM^{-2} AND THE GAMMA RAY DOSE ABOUT 260 RADS (C).

Alpha particle reactions with surrounding nuclei as well as spontaneous and induced fissions yield approximately 3×10^{8} neutrons-sec^{-1} from the plutonium-238 fuel in each of the capsule RTG's. The neutron emission is accompanied by gamma photon radiation associated with the fission process and with the normal decay of plutonium-238.

The neutron and gamma field intensities were calculated by means of the point isotropic-kernel, ray-tracing, shield-analysis technique described in Appendix A. The resulting flux and dose rate plots are shown in Figure 5-1. For this calculation the three non-symmetrically mounted RTG's were placed on the axis of the Planetary Vehicle; this approximation underestimates the dose to the nearest equipment bay by about a factor of 1.5; while it overestimates the average dose somewhat. The dose to the equipment bay nearest to the paired RTG's was integrated over an 8-month flight time plus a 2-month interval from assembly of the Planetary Vehicle to the beginning of the launch period. The resulting dose of 3.2×10^{10} neutrons-cm^{-2} and 107 rads (c) from gammas therefore represents an upper limit for the primary nuclear radiation to the spacecraft equipment bays from the RTG's of the mated capsule and the contribution from the second capsule during the prelaunch phase. Secondary radiation from neutron inelastic collisions, neutron absorptions, gamma scattering, etc., were not included because prior to capsule separation these secondary sources are well masked by the primary sources.

Induced radioactivity in various spacecraft materials could persist subsequent to capsule separation. Although certain instruments might not function properly in the presence of the capsule RTG's, they could be used subsequent to capsule separation with the RTG source of radiation removed. For this purpose it was decided to estimate the nature of the activation environment so that the operability of various candidate instruments could be evaluated.

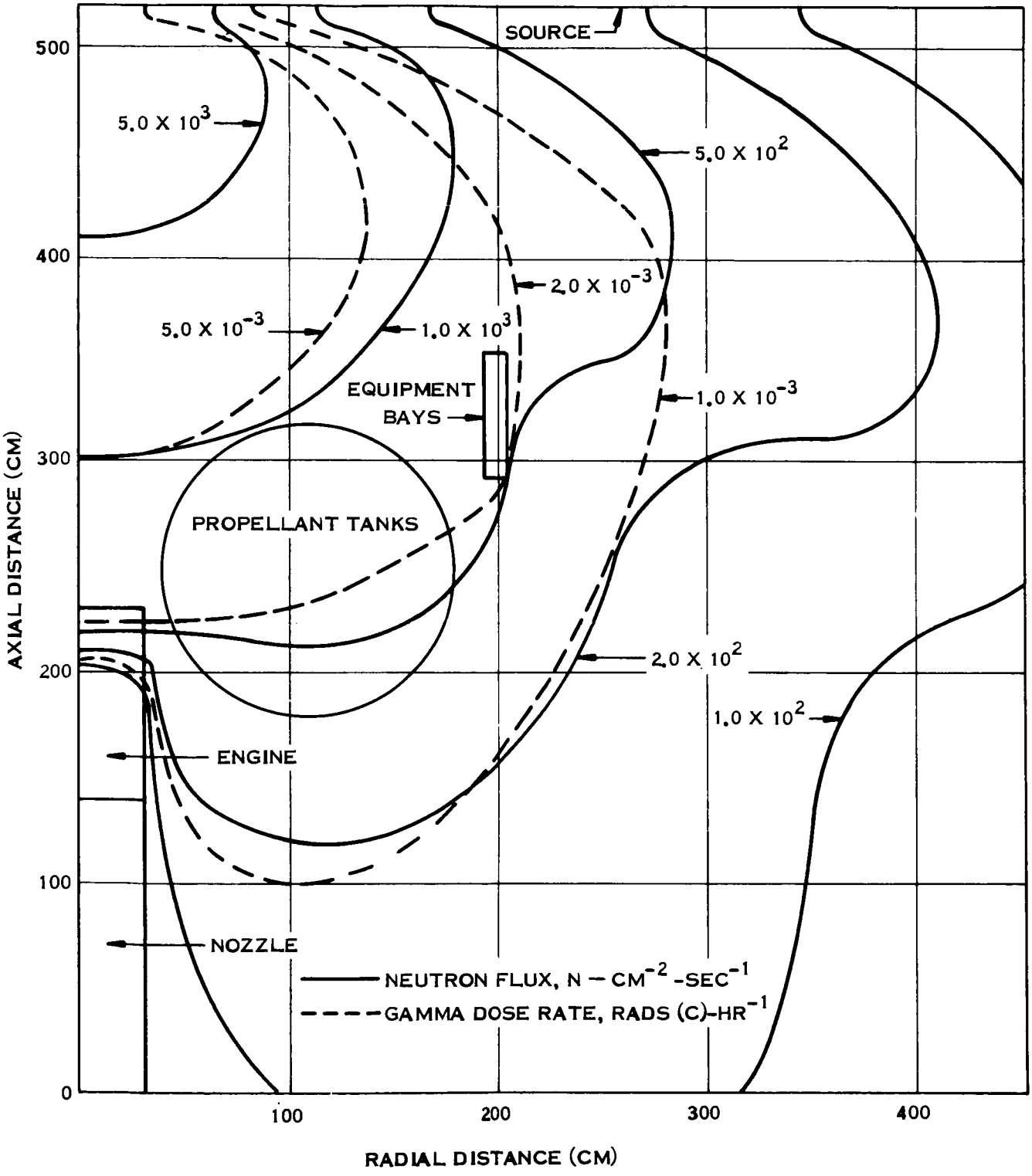

Figure 5-1. Planetary Vehicle Model With Neutron Flux and Gamma Dose Rate Isopleths

Toward this objective the effect of the relatively massive propellant fuel tanks on the neutron energy spectrum was analyzed by means of a number of neutron transport calculations, described in Appendix B. The fraction of thermal neutrons was found to be highest behind the propellant tanks: 0.563; however, just as in the analogous case of fast spectrum reactors with moderating reflectors, the thermal fraction on the tank surface facing the RTG's was nearly as much: 0.49. In the absence of pronounced thermal neutron absorbers in the spacecraft, approximately half of the neutron population outside the RTG's can be assumed to be thermal. The neutron spectra are shown in Figure 5-2 for various locations with and without Aerozene in the propellant tanks. The results of these considerations are presented in Appendix B in terms of activation dose rates for various possible spacecraft materials.

With the use of spacecraft RTG's, the integrated neutron flux and gamma ray dose are increased to take account of the spacecraft RTG's themseleves and an additional time of 6 months in Mars orbit. Using the data of Table A-3 in Appendix A, the calculated values are 5.8×10^{10} neutron-cm^{-2} and 260 rads (c).

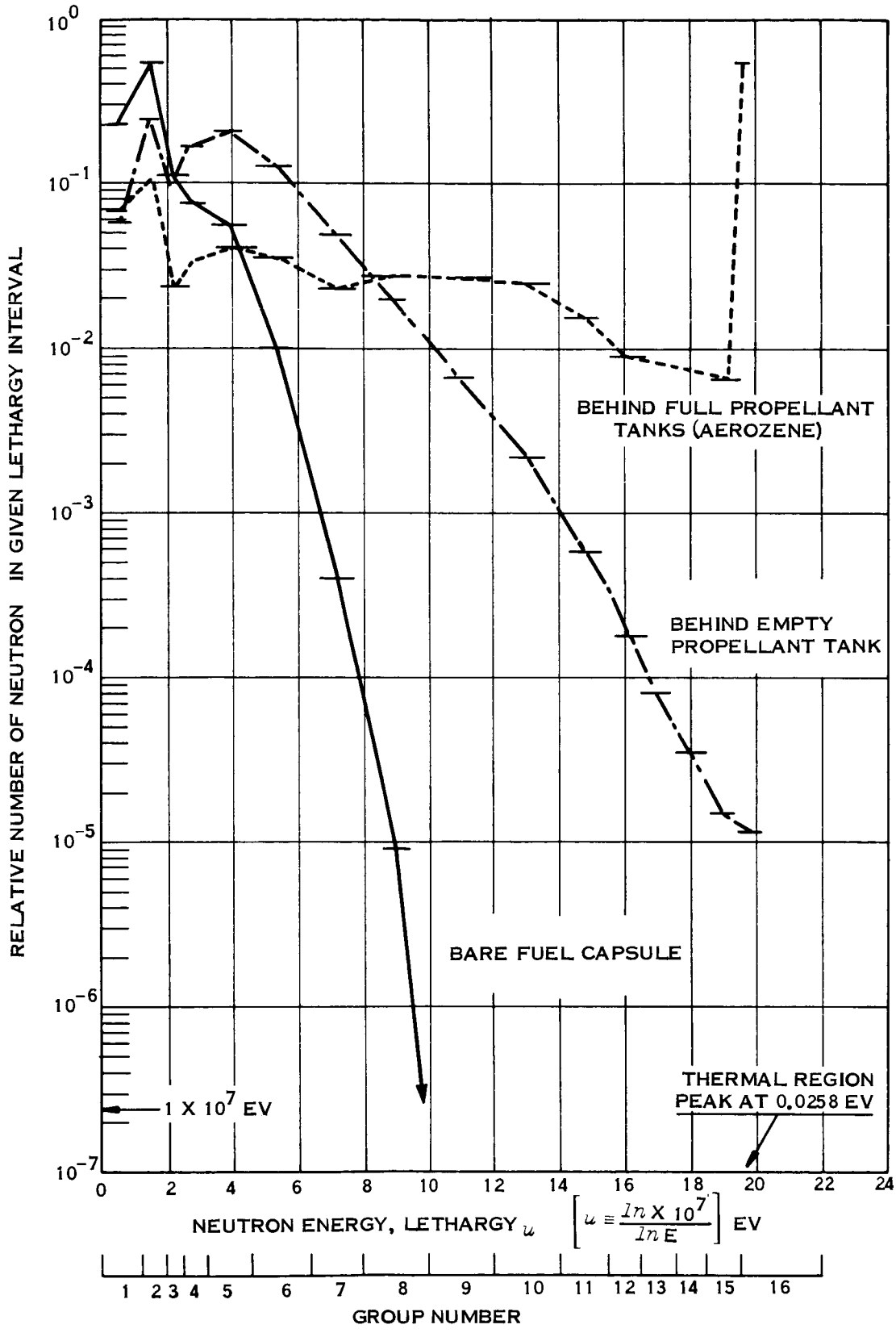

Figure 5-2. Neutron Spectra from Capsule RTG's

SECTION 5: NUCLEAR RADIATION ANALYSIS

RADIATION EFFECTS — SPACECRAFT EQUIPMENT NOT INCLUDING SCIENCE

A SURVEY AND ANALYSIS OF THE VARIOUS TYPES OF SPACECRAFT EQUIPMENT INDICATES THAT THRESHOLD RADIATION DAMAGE EFFECTS WILL RESULT AT AN INTEGRATED NEUTRON FLUX OF FROM 5×10^7 TO 5×10^{10} NEUTRONS PER SQUARE CENTIMETER AND/OR A GAMMA RAY DOSE OF FROM 10^3 TO 10^4 RADS. COMBINING THIS WITH THE RTG RADIATION ENVIRONMENT DATA REVEALS THAT NO DIFFICULTIES ARE ANTICIPATED THAT CANNOT BE HANDLED BY APPROPRIATE PIECE—PART AND CIRCUIT—DERATING TECHNIQUES.

The results of the radiation sensitivity analysis are presented, in a somewhat general form, in Figures 5-3 and 5-4. Three damage levels are shown in the figures: threshold, moderate, and severe damage. In general, a threshold level denotes that range of radiation dose where specific effects begin to occur, although for the most part, component performance is not seriously impaired. Moderate damage denotes that range of radiation dose which would degrade component performance and would require special design considerations for components to operate at this level. The severe damage levels would seriously degrade component operation, and, in many cases, cause component failure. A discussion of the derivation of these damage levels is presented in Appendix C. The most sensitive component, with respect to neutron damage, is the main regulator of the Power Subsystem. The low-frequency power transistors used in this component are the critical item. The integrated gyro package is also extremely sensitive. The critical item in this component is a low-frequency transistor in the accelerometer loop. This item is not considered limiting as it can be corrected by proper derating. Semiconductor surface effects set the gamma dose limit at 10^3 to 10^4 rads. This level should be considered as pessimistic, since surface effects are extremely variable. A piece-parts screening technique could decrease the gamma sensitivity to 10^4 to 10^5 rads.

The total radiation dose that the spacecraft equipment will receive can be determined by integrating dose rates at the equipment bays (Table A-3, Appendix A) over the total mission length. The pessimistic projection of mission lengths are 2 months prelaunch, 8 months Earth-Mars transit, and 1 month Mars orbit prior to flight capsule separation followed by an additional 5-month Mars orbit. Applying the appropriate dose rates over these time spans, the total mission doses are:

- RTG-powered capsule: $4.8 \times 10^{10} \frac{\text{EFN*}}{\text{cm}^2}$

  1.0×10^2 rads

*EFN - equivalent fission neutrons = 1.5 times neutrons emitted by RTG's. See Reports VOY-C1-TR3 and TR5 of the Voyager Task C RTG study for an explanation.

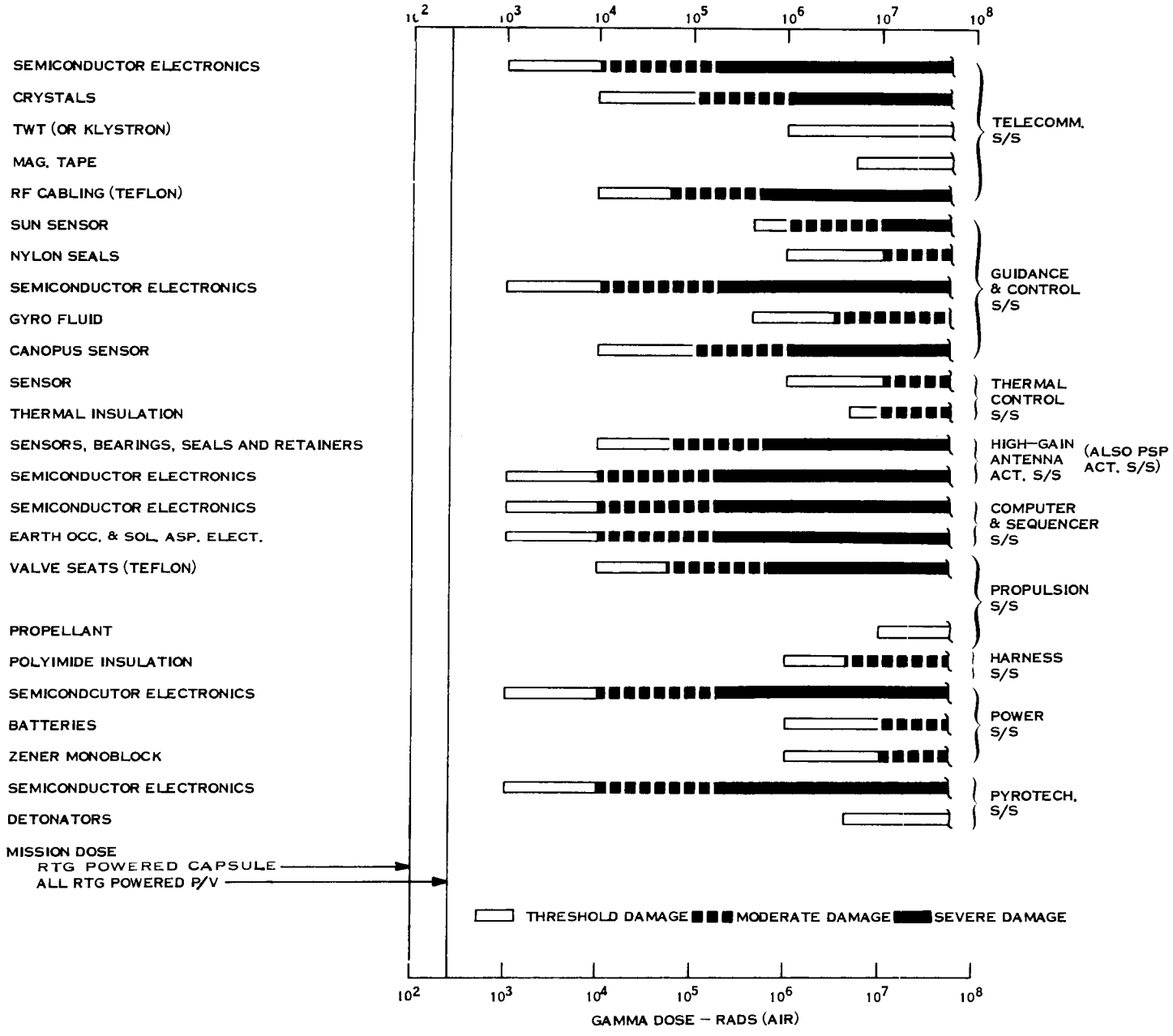

Figure 5-3. Gamma Effects Summary

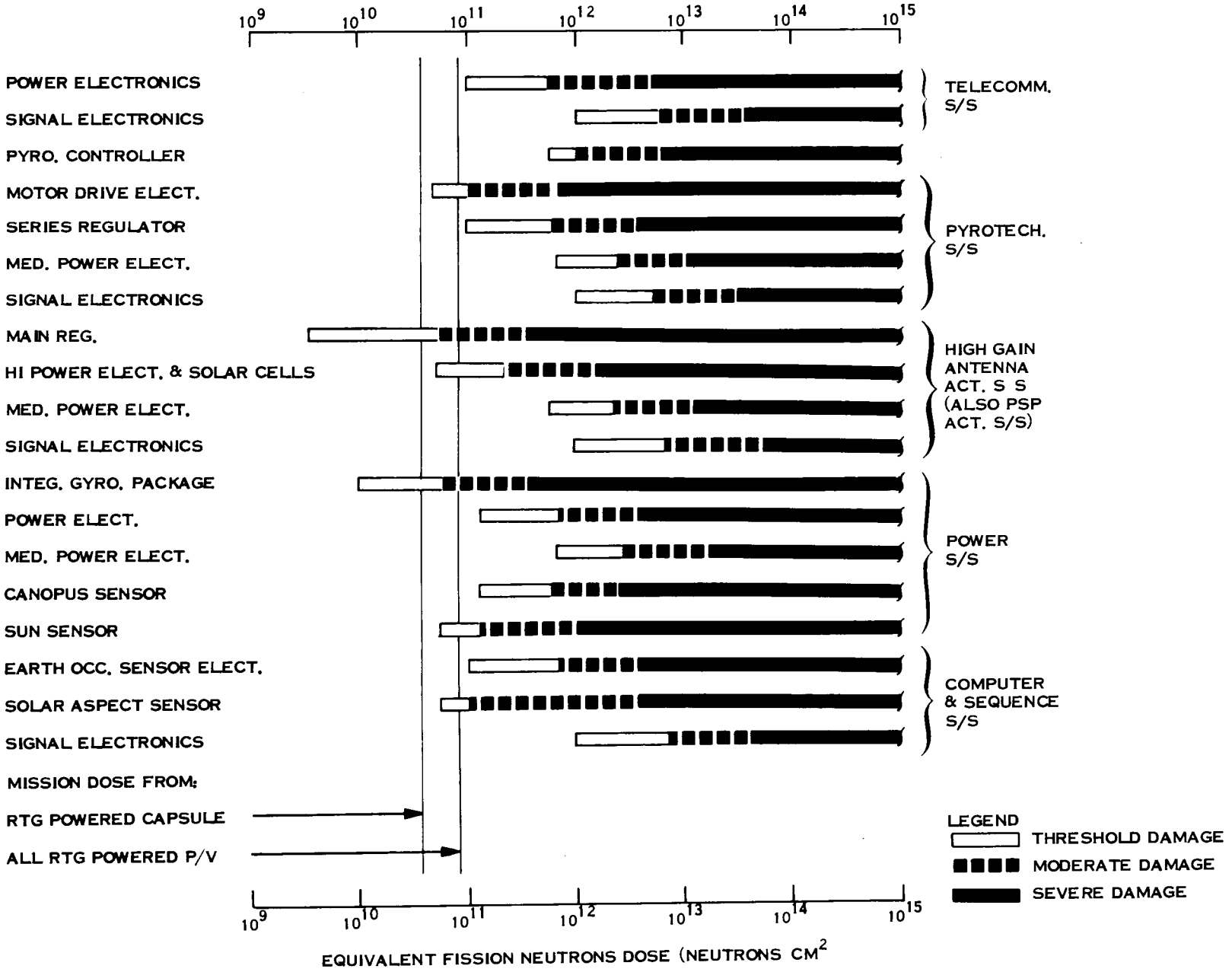

Figure 5-4. Neutrons Effects Summary

- RTG-powered lander and spacecraft: $8.7 \times 10^{10} \frac{EFN}{cm^2}$

  2.6×10^{2} rads

These doses are indicated on the equipment sensitivity bar charts (Figures 5-3 and 5-4). It is evident from the first chart that the gamma dose produces no significant effects in either the RTG-powered lander or the completely RTG-powered configuration. The neutron dose, on the other hand, indicates threshold damage for either configuration.

If RTG's are used only in the capsule, the main regulator of the Power Subsystem and the integrating gyro packages are the only affected items, while if RTG's are used in the spacecraft as well, several additional components appear to be affected.

The limiting devices in every instance are semiconductors. However, the degradations can be avoided by appropriate device and circuit-derating techniques.

RADIATION EFFECTS ON PHOTOGRAPHIC FILM

BECAUSE OF THE CAPSULE RTG'S, SHIELDING FOR PHOTOGRAPHIC FILM WILL BE REQUIRED TO LIMIT LOSS OF CONTRAST TO ACCEPTABLE LEVELS.

Radiation from RTG's or natural sources decreases the performance of photographic film as shown in Figure 5-5. The curves show the effect in terms of film granularity and signal to noise ratio as a function of absorbed radiation (rads). These curves pertain to Eastman Kodak SO-243 film which was used on the Lunar Orbiter spacecraft and is considered one of the more radiation resistant types.

With the use of film in the photoimaging system located on the Planet Scan Package, the amount of RTG radiation (rads) reaching the film is estimated below:

The neutron and gamma ray integrated fluxes over an eleven month period are 3.25×10^{10} photons/cm^2 and 2×10^{10} neutrons/cm^2. The absorbed energy equivalent to these fluxes is 82 rads (c). To reduce this level, shields consisting of lead (for gamma rays) and polyethylene (for neutrons) may be used. Figure 5-6 shows the weight of such shielding required to reduce the number of rads to other levels. These weights are based on shaping the shield to provide sufficient protection from the capsule RTG's with the Planet Scan Package in a stowed position.

By combining Figures 5-5 and 5-6, shield weight as a function of film performance is shown on Figure 5-7. It has been estimated that the loss of signal to noise ratios of 0.5 to 1.5 db could be tolerated and, therefore, a shield weight of 40 to 130 pounds would be required.

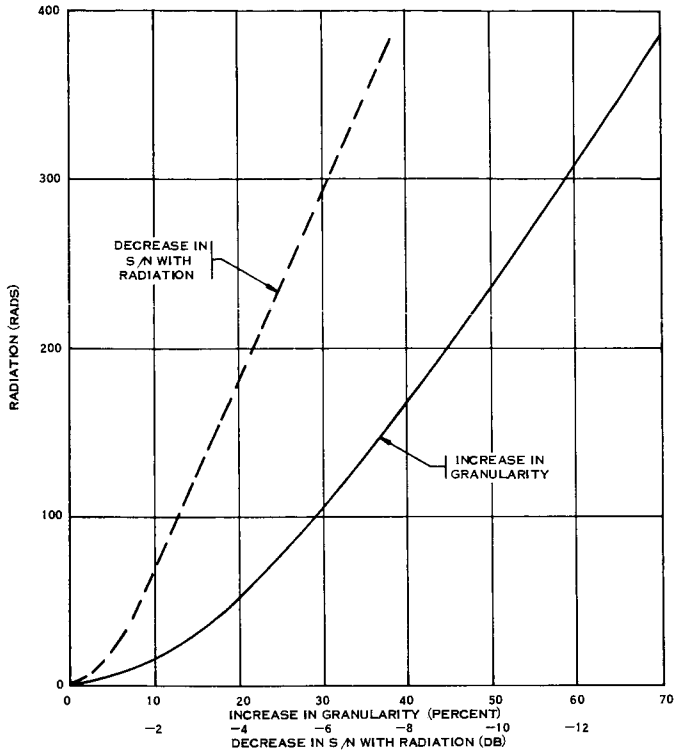

Figure 5-5. Radiation Effects on Eastman Kodak SO-243 Film

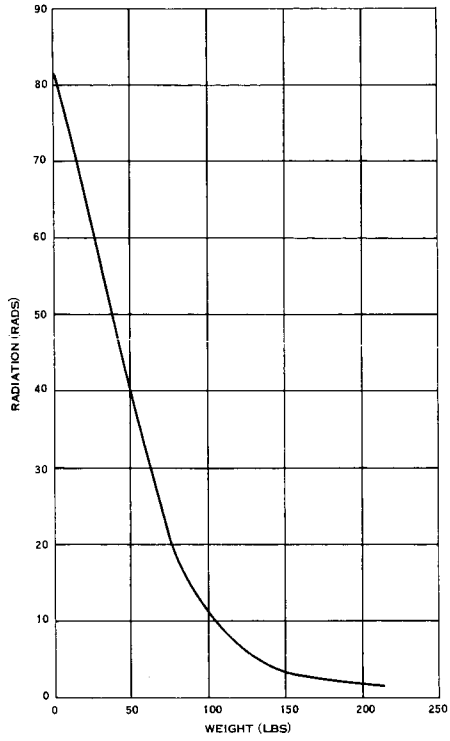

Figure 5-6. Radiation Absorption Versus Shield Weight Eastman Kodak High Definition Aerial Film SO-243

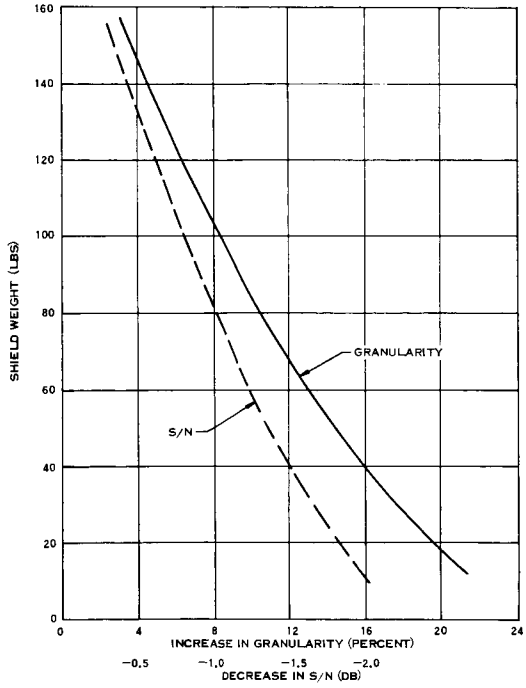

Figure 5-7. Shield Weight versus Granularity and S/N Eastman Kodak Film SO-243

RADIATION EFFECTS — SCIENCE PAYLOAD

SHIELDING MAY BE REQUIRED FOR THE ULTRAVIOLET SPECTROMETER AND TO A LESSER EXTENT FOR THE INFRARED SPECTROMETERS OF THE BASELINE SCIENCE PAYLOAD TO MINIMIZE DYNAMIC INTERFERENCE FROM THE RTG RADIATION DURING THE SEVERAL DAYS OF ORBIT OPERATION BEFORE CAPSULE SEPARATION.

The interaction of the RTG nuclear radiation with the Science payload will be in the form of dynamic interface, i.e., inability of certain instruments to distinguish between the natural radiation of interest (ultraviolet, infrared, cosmic rays, etc.) and those resulting from RTG emission. Permanent effects to the instruments will be similar to those predicted for the spacecraft equipment discussed earlier and is not considered serious.

Table 5-1 presents estimates of threshold radiation levels for the instruments defined earlier and compares these with the expected RTG radiation environment. Columns 2 and 3 show the estimated allowable flux limit that would not affect the instrument sensitivity. Since any single type of detector can be designed for sensitivity to specific flux levels, the values cited pertain to typical sensitivity ranges and should not be interpreted in any absolute sense.

Columns 4 and 5 list the flux emanating from the RTG's. These flux levels are estimated at the location of the planetary scan package without instrument sensor shielding. By comparing these levels with columns 2 and 3, it is possible to estimate the extent of dynamic interference present before capsule separation.

Column 6 provides estimates of shielding thickness for materials that would reduce the flux to acceptable levels and column 7 indicates associated shield weights. The shield weight is highly dependent on the instrument sensor size and its location relative to the RTG's. Since limited information was available with respect to these factors, the weight estimates are based on a π steradian shadow shield. The inner shield radius was taken to be 2 inches to provide volume for the detectors. Shields for the IR spectrometers and UV spectrometer of the Baseline Science consider two detectors in each instrument.

Column 8 is intended to show the influence of spacecraft material activation. The numbers indicate the elapsed time after capsule separation that the residual radiation in the spacecraft decays to the acceptable values cited in columns 2 and 3.

Table 5-2 shows estimated material weights on which the activation times are based. This information of course only applies to the use of capsule RTG's and not to spacecraft RTG's.

Table 5-1. Instrument Radiation Sensitivity

1	2	3	4	5	6	7	8
Instrument	Threshold Radiation Level		Time Integrated RTG Flux● PSP		Shield Thickness and Material	Shield Weight	Activation Decay Time
	Neutrons	Gammas					
Baseline Science Experiments (No. 1 to 9):	Integrated Flux Limit $n \cdot cm^{-2}$	Integrated Flux Limit $\gamma \cdot cm^{-2}$	Neutron	Gamma			
1. Medium Resolution TV Camera No. 1	$> 10^{12}$	$> 10^{14}$	1.23×10^{10}	1.72×10^{11}	None	0	0
2. Medium Res. TV Camera No. 2	$> 10^{12}$	$> 10^{14}$	1.23×10^{10}	1.72×10^{11}	None	0	0
3. High Resolution TV Camera	$> 10^{12}$	$> 10^{14}$	1.23×10^{10}	1.72×10^{11}	None	0	0
4. High Resolution IR Spectrometer	2.85×10^{10}	2.85×10^{10}	1.23×10^{10}	1.72×10^{11}	No neutron shielding required -- 0.43 in.-Pb	6 lb	0
5. Broad Band IR Spectrometer	2.85×10^{10}	2.85×10^{10}	1.23×10^{10}	1.72×10^{11}	No neutron shielding required -- 0.43 in. Pb	6 lb	0
6. IR Radiometer	$> 10^{12}$	$> 10^{12}$	1.23×10^{10}	1.72×10^{11}	None	0	0
7. UV Spectrometer	2.85×10^{9}	2.85×10^{8}	1.23×10^{10}	1.72×10^{11}	1.5 in. Polyethylene 1.5 in. Pb	36 lb	0
8. Radio Occultation	$> 10^{12}$	$> 10^{12}$	1.23×10^{10}	1.72×10^{11}	None	0	0
9. Celestial Mechanics	---	---	---	---	---	---	--
Additional or Alternate Experiments:							
10. Photographic Film System			-- See Separate Section --				
11. Gamma Ray Spectrometer	5.7×10^{7}	2.85×10^{6}	1.23×10^{10}	1.72×10^{11}	9.8 in. Polyethylene 2.65 in. Pb	150 lb	60 hr
12. Cosmic Ray Telescopes	2.85×10^{9}	2.85×10^{8}	1.23×10^{10}	1.72×10^{11}	1.5 in. Polyethylene 1.5 in. Pb	18 lb	0
13. Magnetometers	$> 10^{12}$	$> 10^{14}$	1.23×10^{10}	1.72×10^{11}	None	0	0
14. Cosmic Dust Detectors	$> 10^{12}$	$> 10^{14}$	1.23×10^{10}	1.72×10^{11}	None	0	0
15. Mass Spectrometer	2.85×10^{9}	2.85×10^{8}	1.23×10^{10}	1.72×10^{11}	1.5 in. Polyethylene 1.5 in. Pb	18 lb	0
16. Plasma Probes	2.85×10^{9}	2.85×10^{8}	1.23×10^{10}	1.72×10^{11}	1.5 in. Polyethylene 1.5 in. Pb	18 lb	0
17. Polarimeter	$> 10^{12}$	$> 10^{14}$	1.23×10^{10}	1.72×10^{11}	None	0	0
18. X-Ray Detector	5.7×10^{7}	2.85×10^{6}	1.23×10^{10}	1.72×10^{11}	9.8 in. Polyethylene 2.65 in. Pb	150 lb	60 hr
19. Neutron Spectrometer	2.85×10^{6}	2.85×10^{9}	1.23×10^{10}	1.72×10^{11}	18.3 in. Polyethylene 1.0 in. Pb	380 lb	0
20. Bistatic Radar	$> 10^{12}$	$> 10^{14}$	1.23×10^{10}	1.72×10^{11}	None	0	0
21. Microwave Radiometer	$> 10^{12}$	$> 10^{14}$	1.23×10^{10}	1.72×10^{11}	None	0	0
22. Gradiometer	$> 10^{12}$	$> 10^{14}$	1.23×10^{10}	1.72×10^{11}	None	0	0

Table 5-2. Assumed Constituents of Spacecraft for Activation Decay Time Estimates

Nuclide	Estimated Mass, (pounds)
Mg^{27}	300
Al^{28}	1500
Si^{31}	60
Ti^{51}	510
Fe^{59}	150
Co^{60m}, Co^{60}	16
Ni^{65}	110
Cu^{64}, Cu^{65}	300
Mo^{99}, Mo^{101}	10
Ag^{108}	5

Assumed: Point mass concentration in plane of PSP and on Z-axis.
No selfshielding or other absorptions
Weak β or gamma emitters not included
Very short half-life emitters not included

An overview of these data indicates that if UV and IR data is required during the first several days of orbit, substantial amounts of shielding may be required for the ultraviolet spectrometer and lesser amounts for the infrared spectrometers. A number of the other potential instruments will also require varying amounts of shielding. The use of active shielding techniques such as anticoincidence circuitry could significantly reduce the estimated shield weights.

SECTION 6: MISSION EFFECTS

SPACECRAFT OPERATIONAL ALTERNATIVES WITH AN RTG POWERED CAPSULE

THE CAPSULE RTG'S REMOVE THE NEED FOR THE SPACECRAFT TO SUPPLY 200 WATTS TO THE CAPSULE. HOWEVER, DUE TO SOLAR OCCULTATIONS LATE IN THE ORBITING MISSION, SOLAR ARRAY AREA CANNOT BE SIGNIFICANTLY REDUCED. EARLY IN THE MISSION ADVANTAGE CAN BE TAKEN OF THIS EXCESS POWER TO IMPROVE SPACECRAFT PERFORMANCE. THE CAPSULE RTG POWER ITSELF CAN BE USED AS A BACKUP SOURCE OF POWER DURING SPACECRAFT MANEUVERS.

The set of curves on Figure 6-1 develop solar array area requirements for each of the Voyager mission opportunities in the 1970's with and without RTG's used in the capsule. The curves of set I show predicted solar array output in watts per square foot as a function of time after encounter based on the estimated arrival times indicated. The values are based on solar array performance and predicted array temperatures from Volume II, Systems Description. Only postencounter times are shown since this is the more critical mission phase relative to solar array requirements.

Curve II shows the estimated occurrence of solar occultations which commence about 80 days after encounter depending on particular orbit characteristics. The curve shown actually envelopes the eclipse profiles corresponding to the orbits considered for the 1973 mission and is sufficient to identify the longest eclipse period of about 84 minutes. A cursory examination of the eclipse phase for the 1975, '77 and '79 missions indicates that eclipses also commence about 80 days after encounter and therefore the curve shown is considered to be appropriate for those cases as well.

Curve III shows power demand at the solar array. It is based on load estimates derived from the Spacecraft Description in Volume II and includes all power conditioning losses. Up to the time of capsule separation, the spacecraft must supply 200 watts to the capsule when no capsule RTG's are used and zero power when RTG's are used. During the solar occultation phase, the array power demand increases to provide battery charging.

Curves IV to VII show net area requirements for each of the missions and are obtained by dividing the power requirement of Curve III by the specific power shown on Curve I.

The conclusions from these curves are that the use of RTG's in the capsule have little influence on the size of the spacecraft solar array. For the 1973 and 1975 missions, the solar occultation phase establishes the array area requirements and

FOLDOUT FRAME 1

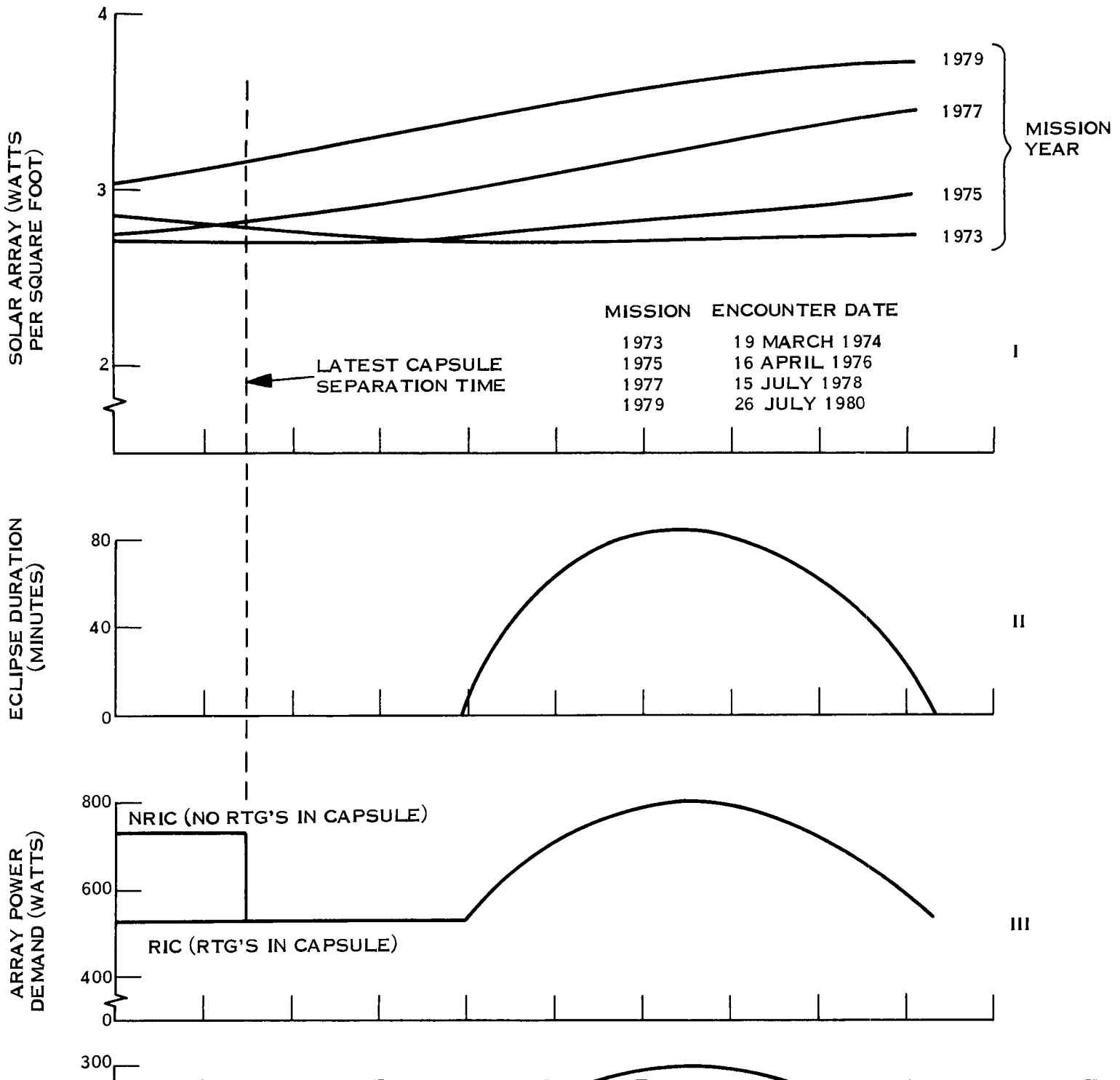

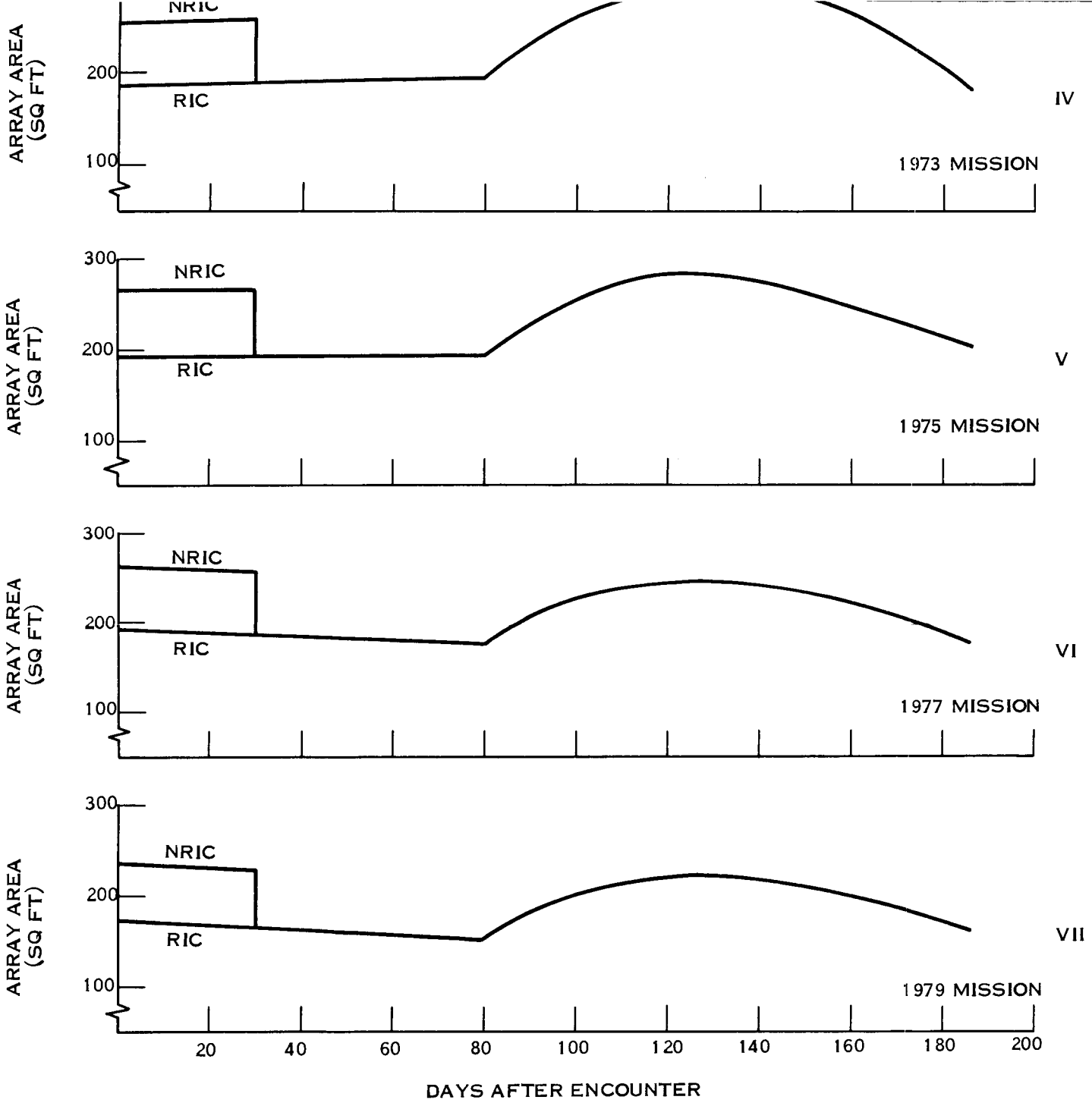

FOLDOUT FRAME 2

Figure 6-1. Array Area Requirements

the use of RTG's in the capsule do not permit any reduction of solar array area. For the 1977 and 1979 missions, the use of capsule RTG's permit a nominal area reduction of about 10 to 20 square feet. These conclusions are based on the assumption that the full spacecraft load is maintained during solar occultation periods.

About 300 square feet of solar array are required for the 1973 mission of which about 100 square feet are devoted to battery recharging during the solar occultation phase. If this area is installed for all opportunities, then the excess power capability at the time of encounter, assuming the use of an RTG powered capsule, is as follows:

Opportunity	Excess Power, watts
1973	335
1975	296
1977	305
1979	395

This excess power is available early in the orbiting phase rather than later which is favorable from the standpoint of accumulating maximum science data early in the mission.

Another way of viewing this excess power is to consider that solar occultations just subsequent to encounter can be tolerated from a power system standpoint. Just considering this from the point of view of the solar array power the percentage of allowable occultation time per orbit is estimated below:

Mission	Percent Occultation Time Per Orbit
1973	28
1975	25
1977	26
1979	31

For the nominal 1000 x 10,000 kilometer orbits these allowable percentage times are actually longer than the longest possible occultation of about 84 minutes. Thus, the excess array not only permits orbits with occultations but would also permit lower orbits with higher percentages of occultation time.

Capsule RTG's permit a reduction in battery capacity because the supply of 200 watts to the capsule during maneuver periods is unnecessary. The orbit insertion maneuver is estimated to be the longest of these with a 2-hour duration. This corresponds to a battery capacity reduction of 400 watt-hours which, at a specific energy of about

19 watt-hours per pound for silver-zinc batteries (rated at 50 percent depth of discharge), results in a saving of about 21 pounds.

The RTG power generated in the capsule could be used to advantage in the spacecraft. Although the use of this power would complicate the interface with the spacecraft, it would serve as a useful backup to the spacecraft batteries during critical maneuvers. To illustrate this possible benefit, the table below summarizes battery capacity requirements with and without RTG's in the capsule:

Battery Type	No Capsule RTG's	Capsule RTG's	Remarks
Ni-Cd	1520 w-hr	1520 w-hr	Sized by 760 w-hr solar occultation requirement late in mission; use at 50 percent depth of discharge.
Ag-Zn	1710 w-hr	910 w-hr	Sized by orbit insertion load; use at 50 percent depth of discharge.
TOTAL	3230 w-hr	2430 w-hr	

The orbit insertion maneuver requires about 1540 watt-hours of energy over a 2-hour period if no capsule RTG's are used, or about 1140 watt-hours if capsule RTG's are used (due to removal of the 200 watt capsule requirement). Thus, the installed batteries provide this at slightly less than 50 percent depth of discharge. Assuming the capsule RTG's have a 360 watt capability, they could provide 720 watt-hours of the 1140 watt-hours required. The nickel-cadmium capacity of 1520 watt-hours actually consists of two batteries rated at 760 watt-hours each. Therefore, either nickel-cadmium battery in conjunction with the capsule RTG's would suffice to supply the required energy. The silver-zinc battery could also alone provide this energy and therefore the capsule RTG's serve as a good backup in the event of failure of any two of the three spacecraft batteries.

SECTION 7: ASSEMBLY, TEST, AND PRELAUNCH EFFECTS

PERSONNEL RADIATION EXPOSURE

FROM THE TIME THE RTG POWERED CAPSULE IS MATED TO THE SPACECRAFT, RADIATION LEVELS WILL BE OF SUFFICIENT MAGNITUDE TO REQUIRE EITHER PROTECTIVE SHIELDING OR LIMITED RESIDENCE TIMES FOR WORKING PERSONNEL, OR A COMBINATION OF BOTH.

The neutron and gamma biological dose rates around the spacecraft resulting from the capsule RTG radiation are shown in Figure 7-1. The dose rates were calculated with program QAD using the Albert-Welton kernel and fast neutron removal theory for the neutron dose rates. The point isotropic gamma kernel method was used in conjunction with buildup factors to compute gamma dose rates. The spacecraft/capsule assembly was assumed to be an isolated system; there is thus no allowance for reflection from the ground or contributions from any adjacent similar system.

Assuming that the Planetary Vehicle is in a "Radiation Area," i.e. one with limited and controlled access, the permissible dose is 3 rems during any contiguous 13 week period as specified in the Code of Federal Regulations. Other typical regulations, depending on the particular facility, are that the dose shall not exceed 200 millirems per week or 60 millirems per day. According to Figure 7-1, the dose rate at the spacecraft equipment bays is 52 mrem $-hr^{-1}$ from both neutrons and gamma photons. These establish the working time limits listed below for a technician working on this equipment:

Per 13 week period:	57 hours
Per week:	3.85 hours
Per day:	1.15 hours

The permissible exposure times may be extended by use of a temporary radiation shield. A simple polyethelene slab shield with a one-tenth layer thickness* of about 6.4 inches is quite effective. The gamma contribution to the dose rate is about five percent; gamma shielding may therefore not be needed.

* Shielding thickness that attenuates radiation by a factor of ten.

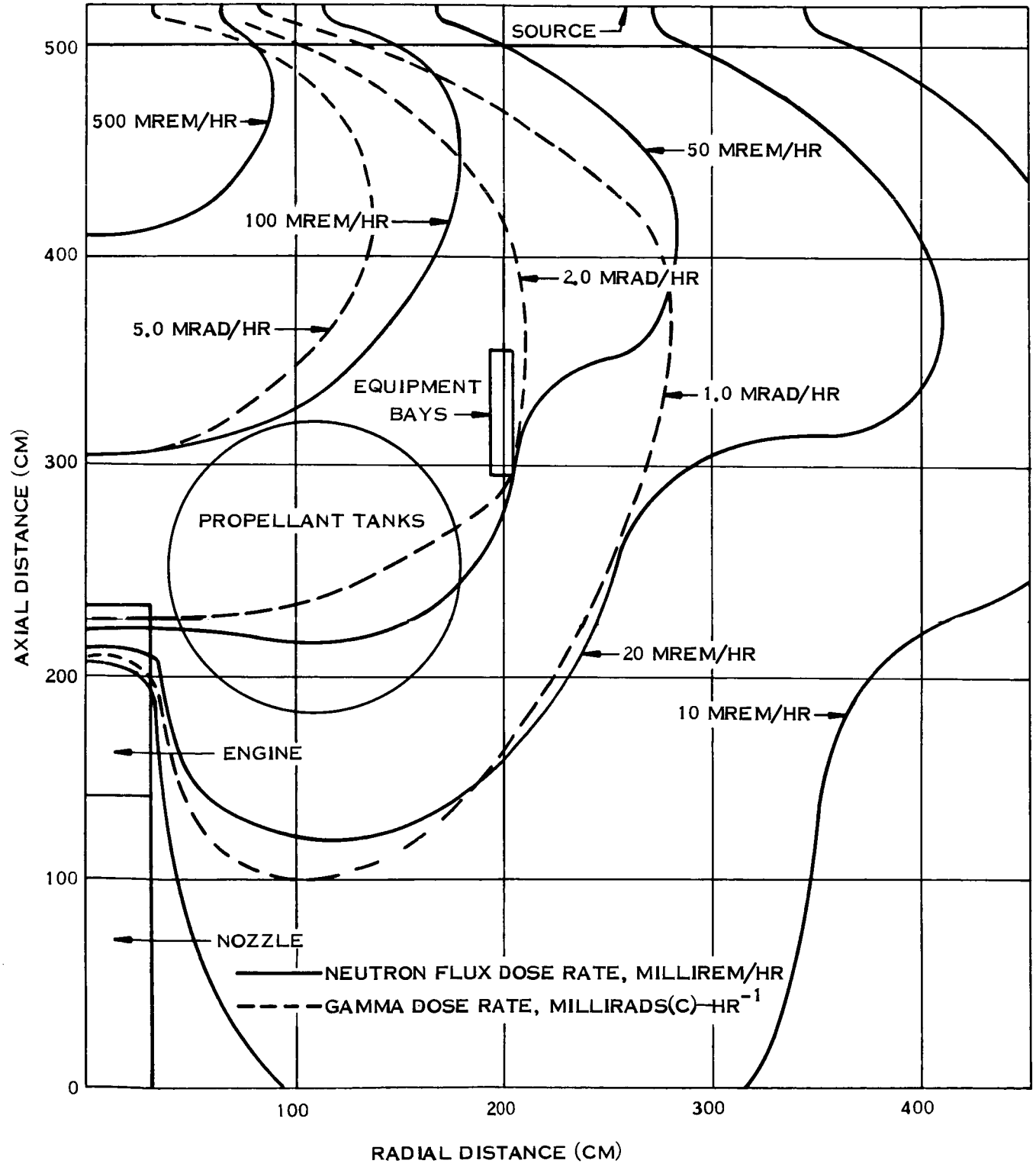

Figure 7-1. Planetary Vehicle Model with Neutron and Gamma Dose Rate Isopleths

SECTION 7: ASSEMBLY, TEST AND PRELAUNCH EFFECTS

INFLUENCE OF CAPSULE RTG'S ON SPACECRAFT TESTING

ADDITIONAL TESTING OF THE SPACECRAFT WILL BE REQUIRED PRINCIPALLY AS A RESULT OF THE CAPSULE RTG RADIATION CHARACTERISTICS.

The thermal and nuclear characteristics of the capsule RTG's will affect numerous aspects of the design, development, test and prelaunch phases of the spacecraft program.

First, early definitions of these characteristics from the capsule contractor will permit proper allowances to be taken into account in the design of the spacecraft. This will principally take the form of analytical radiation mapping studies to determine the expected environmental levels for specific items of spacecraft equipment.

The predicted radiation levels will determine the extent to which radiation resistant devices and materials will be used on various spacecraft components.

During the developmental phase, some radiation testing will be conducted on components considered to be susceptible to radiation effects including sensitive science instruments and spacecraft sensors. Certified radiation testing facilties will be required for this purpose.

At a later time in the development phase, the predicted radiation levels in the spacecraft will be verified by test. This requires a reasonable simulation of the mass distribution and materials used in the spacecraft. The materials point is emphasized since radiation interactions are highly dependent on material properties. A capsule simulator would also be required which duplicates mass distributions, materials, and RTG characteristics as defined by the capsule contractor.

Three System Test Models of the spacecraft are planned for the development phase for structural, thermal and electrical systems test. One of these, probably the Electrical System Model, could be used for the radiation test mentioned above. The question of whether a separate Radiation System Model of the spacecraft should be incorporated in test plans depends largely on whether certain spacecraft instruments predicted to be radiation sensitive will be required to function in the presence of the capsule RTG's before capsule separation. If this is so, then extensive compatability testing is likely and a separate Radiation Systems Model is desirable. In any case, such testing will require certified facilities and controlled residence times for personnel.

Proceeding to the component qualification phase, components will be tested to the measured environment with allowance made for margin. Several testing approaches might be necessary. First, regarding damage due to the integrated flux over the

mission time, accelerated test methods will be required using high radiation flux facilities. Qualification relative to dynamic interference, on the other hand, requires a close duplication of the anticipated environment and is best accomplished with the actual RTG's themselves.

Spacecraft systems qualification, as far as the radiation environment is concerned, will entail tests with the full complement of RTG fuel in a simulated flight capsule. Whether or not this should be accomplished on the Proof Test Model (PTM) spacecraft again depends on the question of sensitive instrument operations prior to capsule separation. If instrument operation is not required, the PTM would be used since the tests provide more of a compatibility check and would not entail extensive test times. If instrument operation is required, extensive test times are likely and the use of a separate System Radiation Model spacecraft would be more practical.

The thermal effect of capsule RTG's will not seriously disrupt test plans for the spacecraft and will principally involve the simulation of RTG heat in the flight capsule simulator used in spacecraft system tests. The principal effect will show up in compatibility tests with the shroud and the determination of proper cooling requirements.

The capsule RTG's will influence prelaunch sequences from the time the flight capsule is mated to the spacecraft. The principal effect thereafter will pertain to the limited residence times of personnel working near the planetary vehicle.

APPENDIX A

PLANETARY VEHICLE RADIATION MAPPING STUDY

A.1 INTRODUCTION
- A.1.1 Purpose of Study
- A.1.2 Analysis Approach
- A.1.3 Sources of Radiation

A.2 RADIATION MAPPING OF PLANETARY VEHICLE
- A.2.1 Planetary Vehicle Geometry
- A.2.2 Analytical Method
- A.2.3 Source Definition
- A.2.4 Radiation Mapping Results
- A.2.5 Dose Rates for the All-RTG Planetary Vehicle
- A.2.6 Gamma Variations with Time

A.3 ENERGY DISTRIBUTION OF NEUTRONS
- A.3.1 Calculational Model
- A.3.2 RTG Unperturbed Neutron Spectrum

A.4 DESCRIPTION OF QAD-PR COMPUTER CODE

A.5 REFERENCES

APPENDIX A

PLANETARY VEHICLE RADIATION MAPPING STUDY

A.1 INTRODUCTION

A.1.1 PURPOSE OF STUDY

This study defines the intensity and energy distribution of the neutron and gamma fields in and around the Voyager Planetary Vehicle. The radiation fields are caused by three radioisotope thermoelectric generators (RTG's) in the flight capsule. This definition of the radiation field is used to assess the effects of this radiation on the components and equipment on the spacecraft bus and associated science payload.

The mass distributions in the Planetary Vehicle are not sufficiently well defined to permit a highly sophisticated analysis at this time, nor does the present purpose of this study justify such an effort. Instead, the depth of the analysis is of the order of a "preliminary design" evaluation.

A.1.2 ANALYSIS APPROACH

The results of this study serve as radiation source definitions for:

a. Evaluation of effects of long-term exposure of the solar-powered spacecraft bus to the nuclear radiation from the RTG-powered flight capsule, and an estimate of the field intensity if both the bus and capsule were powered by RTG's.

b. Evaluation of the dynamic interference of the RTG radiation with the science payload on the bus; specifically, from secondary radiation emitted by neutron-activated bus components after separation from the flight capsule.

Generally, the long-term radiation effects are more pronounced for higher energy neutrons. The first calculation therefore contains the conservative and simplifying assumption that there is no neutron energy degradation anywhere in the Planetary Vehicle. This permits the application of the point-kernel, ray-tracing technique with a good geometry model.

Neutron activation reactions, on the other hand, have generally a higher probability at lower incident neutron energies. The maximum fraction of neutrons with low energies is found in the shadow of the spacecraft bus propellant tanks; this proportion is conservatively assumed to be representative of the neutron population throughout the Planetary Vehicle for the purpose of estimating activation rates. This assumption, in turn, permits the use of a neutron transport calculation in just one-dimensional geometry but with a fine treatment of the neutronics aspects.

A.1.3 SOURCES OF RADIATION

A.1.3.1 Primary Sources

The RTG's are fueled with a high-temperature compound form of plutonium-238; of the many such forms, $^{238}PuO_2$ is used in this study as a representative compound.

Plutonium-238 decays by two modes: by emitting an alpha particle and certain characteristic gamma photons, and by spontaneous fissioning. The alpha particles are, of course, fully contained in the fuel capsule. They may, however, interact with light element nuclei and in the process release a neutron. Because plutonium-238 is fissionable by fast (high-energy) neutrons, those neutrons released in spontaneous fissions and from alpha reactions can induce further fissions in the fuel.

The characteristic decay gammas of plutonium-238 have energies of 0.043, 0.099, 0.15, 0.716, and 0.81 Mev. There are also higher energy gamma photons, mostly from the decay of fission product nuclei and so-called "prompt" gammas emitted essentially at the time of the fission.

A.1.3.2 Secondary Sources

Secondary radiation may be generated as a result of interactions between the primary particles and spacecraft components. Most secondary neutron sources arise from radiative capture, charged particle, and neutron inelastic scatter reactions.

Secondary gamma photons are emitted in the course of the decay of neutron-activated surrounding nuclei, in Compton scattering, photoelectric reactions, pair production, and Bremsstrahlung and also in fluorescence radiation and during coherent electron scattering.

This study does not include secondary radiation because their generally low intensity is usually masked by the far-larger primary radiation fluxes. For simplicity, the cosmic and solar radiations are not included either.

A.2 RADIATION MAPPING OF PLANETARY VEHICLE

A.2.1 PLANETARY VEHICLE GEOMETRY

The geometry of the Planetary Vehicle used in this study is described earlier in this report.

A.2.2 ANALYTICAL METHOD

As indicated above in Section A.1.2, the evaluation of the effects of long-term exposure to the RTG radiation is well served with the assumption that the energy spectrum of source neutrons is not degraded outside the RTG's because it leads to conservative approximations. With this assumption it is possible to use the point-kernel, ray-tracing technique. Here the source region is subdivided into smaller volume sources which, when viewed from a given receiver point, may be treated as isotropically emitting point sources without appreciable error. (The error disappears entirely, of course, when the source volume elements approach zero in the limit: the point kernels.) A ray from the source volume element to the receiver point is traced and the exponential attenuation through the traversed materials is combined with the inverse-square reduction to yield the dose rate or particle flux at the receiver point from the source volume element. Repeated and summed over the entire source volume, this method provides a fine approximation of the total dose rate or particle flux. The scattering of gamma photons into the narrow beam is allowed for by energy-dependent buildup factors for a single representative material. For the neutron calculation, the Albert-Welton kernel is used; here a complex exponential function is used to fit measured attenuation of neutrons through slabs of the given material, which are placed in an "infinite"

water medium. The single "removal" cross section which performs the best fit is then used in analogous single energy calculations.

This study employed a version of QAD, a Los Alamos Scientific Laboratory originated shielding program which utilizes the above methods. The gamma attenuation cross sections were obtained from Reference A-1, the gamma buildup factors from Reference A-2, and the neutron removal cross sections from Reference A-3.

A.2.3 SOURCE DEFINITION

The RTG radiation sources must be described for the program in geometry, intensity, and energy spectrum.

QAD performs an essentially three-dimensional analysis in cylindrical geometry. To accommodate the code, the three RTG's were lumped together and simulated by a single cylindrical source on the z-axis and in the same plane as the three RTG's. The simulated source geometry was selected to conserve the self-absorption characteristics of the individual RTG's. To check the validity of the simulated source, a hand calculation was performed for three sensitive locations: the electronics bay nearest to the two closely spaced RTG's, the planetary scan package in the folded position, and the solar cell array at a point which has a direct view of the RTG's.

The hand calculations were performed using previously obtained results for a similar RTG and adding the contributions for the three nonsymmetric locations of the RTG's on the flight capsule. As shown in Table A-1, the results agreed quite well with the machine calculation and therefore validated the single central source assumption as well as the general computer model of the flight vehicle.

The nuclear definition of the source was based on a neutron yield of 5×10^4 neuts-sec^{-1}-g^{-1} of plutonium-238, a specific power of 0.4 watt (th) per gram plutonium-238, and on a gamma photon yield shown in Table A-2. Neutron multiplication because of induced fissions in the fuel is roughly estimated to be 1.1 to 1.3 and is not included in the results.

Table A-1. Comparison of Results

Location	Hand Calculation		QAD Calculation	
	Neutron Flux	γ Flux	Neutron Flux*	γ Flux
Planetary scan package (folded)	4.32×10^{2} $\frac{n}{cm^2 - sec}$	2.84×10^{3} $\frac{Mev}{cm^2 - sec}$	6.25×10^{2} $\frac{n}{cm^2 - sec}$	1.14×10^{3} $\frac{Mev}{cm^2 - sec}$
Electronics bay	1.04×10^{3}	7.41×10^{3}	6.91×10^{2}	1.32×10^{3}
Solar panels	3.0×10^{2}	1.93×10^{3}	2.85×10^{2}	6.89×10^{2}

*Based upon the dose calculated by QAD and an average energy of the neutron source spectrum.

Table A-2. Gamma Photon Flux for Plutonium-238 Product from a 1 kw (th) Capsule

Energy (Mev)	Source	Yield (Photons-cm^{-2}-sec^{-1}-kw^{-1})
0.1	^{238}Pu decay	0.1×10^{3}
0.15	^{238}Pu decay	3.5×10^{3}
0.776	^{238}Pu decay	2.1×10^{3}
0.81	^{238}Pu decay	1.0×10^{3}
1.0	Fission product decay and prompt fission gammas	0.11×10^{3}
1.5		0.057×10^{3}
2.3		0.031×10^{3}
3.0		0.017×10^{3}
5.0		0.008×10^{3}

A.2.4 RADIATION MAPPING RESULTS

A large number of receiver points were specified and neutron and gamma dose rates computed at those points in order to define the dose rate isopleths shown in Figure A-1. The calculations were not extended above the source plane because that area has limited significance for this study. The outline of the spacecraft bus is shown in Figure A-1 as well as those regions which are either sensitive component locations or those with appreciable radiation attenuation capability. The propellant tanks, because of their high hydrogen content, are the most significant attenuating factors on the vehicle. The propellant was assumed to be Aerozene. The vehicle structure should have little influence over the radiation field and was therefore neglected. The RTG's were assumed to be the only significant components on the flight capsule.

The biological equivalent neutron dose rate may be estimated by using an energy-integrated average conversion factor of approximately 1×10^4 $(n\text{-}cm^{-2}\text{-}sec^{-1})$ per $(rem\text{-}hr^{-1})$.

If the two Planetary Vehicles are mated for an extended period of time prior to launch, then the upper spacecraft bus may experience a considerable radiation exposure from the lower flight capsule. The minimum ground time from assembly to the beginning of the launch period is 20 days; the maximum is 40 days. As an upper limit, a ground time of 60 days was assumed.

The distance from the RTG's in the lower flight capsule to the equipment bays of the upper spacecraft bus is approximately 5 meters; from Figure A-1 the corresponding neutron flux is about 200 neutrons-cm^{-2}-sec^{-1}. The equipment bays are therefore exposed to a flux of 200 neutrons-cm^{-2}-sec^{-1} for 2 months in addition to the 8 months in-flight and 2 months ground time exposure to the flux of 690 neutrons-cm^{-2}-sec^{-1} from their own flight capsule. The integrated neutron dose is thus 2.1×10^{10} neutrons-cm^{-2}, of which the contribution from the lower vehicle is about 15 percent.

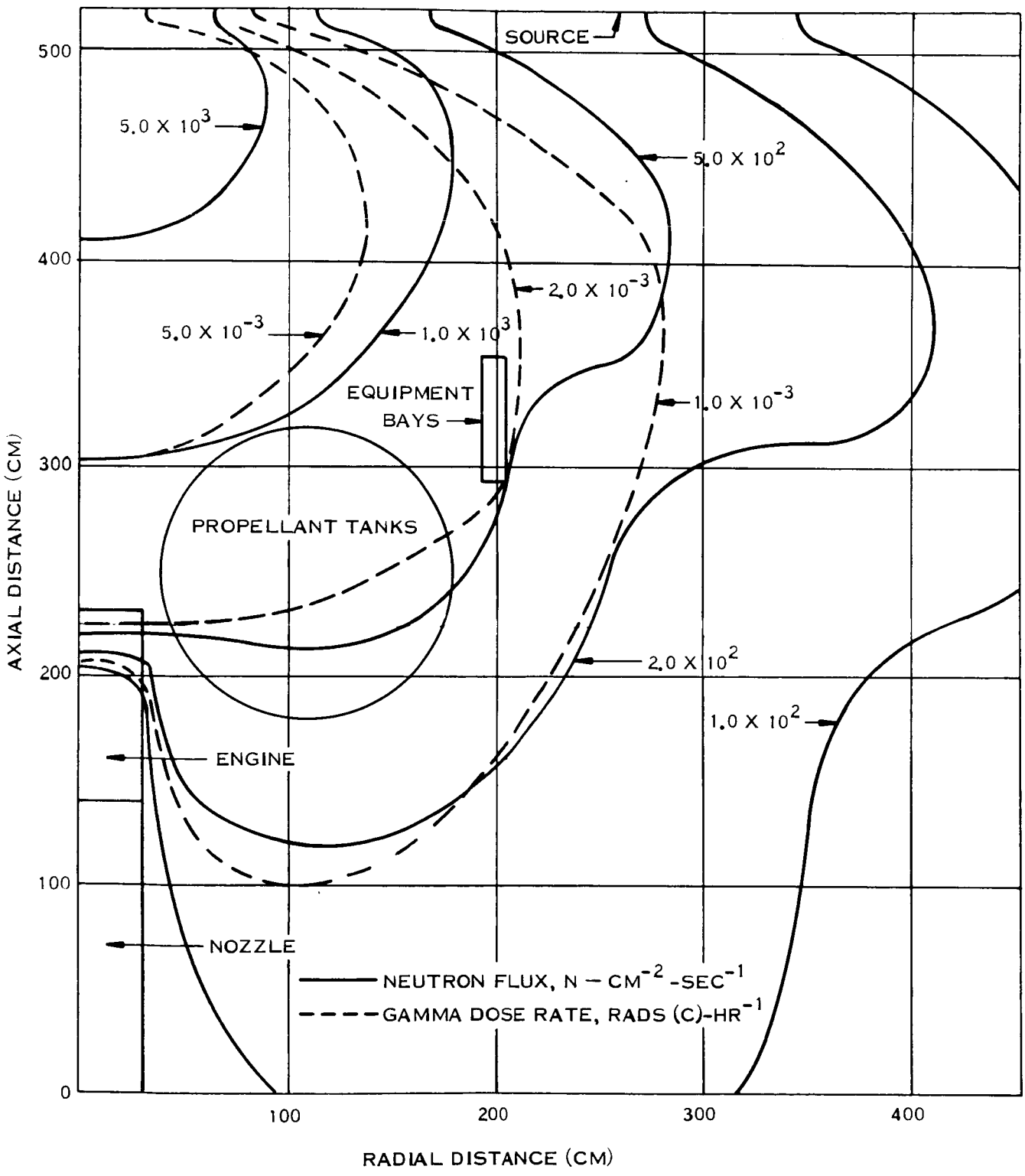

Figure A-1. Planetary Vehicle Model with Neutron Flux and Gamma Dose Rate Isopleths

A.2.5 DOSE RATES FOR THE ALL-NUCLEAR PLANETARY VEHICLE

It is interesting to combine the above dose rates at some locations on the spacecraft bus with those derived for the same locations in the Voyager Task C work for the RTG-powered spacecraft bus. Because of some changes in geometry and arrangement, the dose rates were adjusted by simple inverse-square to the Task D locations. The comparison is shown in Table A-3 for the folded planetary scan package and for the equipment bay nearest to the two closely spaced RTG's.

A.2.6 GAMMA VARIATION WITH TIME

One of the actinide impurities in plutonium-238 is the isotope plutonium-236, which is present in typical concentrations around 1.2×10^{-6} grams 236 per gram of 238 "product." The decay chain of plutonium-236 includes thallium-208, whose decay, in turn, produces a penetrating 2.614 Mev gamma photon. The half-lives of the plutonium-236 chain are so

Table A-3. Neutron Fluxes and Gamma Dose Rates from All-Nuclear Planetary Vehicle (Neutron Flux in neut-cm^{-2}-sec^{-1}; gamma dose rate in rads (c) - hr^{-1})

Region	RTG's in Flight Capsule		RTG's in Spacecraft Bus		Total RTG's	
	Neutron Flux	Gamma Dose Rate (c)	Neutron Flux	Gamma Dose Rate (c)	Neutron Flux	Gamma Dose Rate (c)
Planetary scan package, folded	4.3×10^{2}	4.8×10^{-3}	7.6×10^{2}	1.4×10^{-2}	1.2×10^{3}	1.9×10^{-2}
Equipment bay	1.0×10^{3}	1.3×10^{-2}	7.6×10^{2}	1.4×10^{-2}	1.8×10^{3}	2.6×10^{-2}

arranged that the concentration of thallium-208 builds up with time and peaks at about 17 years after fuel separation. Typical 1-meter dose rates from thallium-208 from a 1-kilowatt(th) source are listed in Table A-4 as a function of time. The gamma map in Figure A-2 assumes essentially fresh plutonium fuel.

Table A-4. Dose Rates from Thallium-208 1 Meter from a 1-kw(th) Plutonium-238 Capsule

Time (years)	Dose Rate (millirads (c)-hr^{-1})
0	0
1	0.77
2	2.6
5	9.2
10	17

A.3 ENERGY DISTRIBUTION OF NEUTRONS

In Section A.1.2 above it was shown that the neutron energy distribution has an important effect on the radiation field in the spacecraft bus after separation from the flight capsule because neutron energy degradation is associated with increased activation probabilities for many nuclides. The single most effective neutron slowing-down region in the Planetary Vehicle is unquestionably the propellant tanks using Aerozene fuel.

A.3.1 CALCULATIONAL MODEL

A one-dimensional model of the RTG and propellant was constructed in cylindrical geometry as indicated in Figure A-2. As a worst-case condition the thickness of the annular region representing Aerozene was taken as the diameter of the propellant tanks. The RTG was given in rather fine detail in order to determine the effect of the neutron moderating cold frame in the generator region. The DTF-IV computer program (Reference A-4) was used for this part of the study. DTF solves the time-independent Boltzmann equation at each space point by Carlson's Discrete Ordinate method. The calculations were carried out with a 16-group

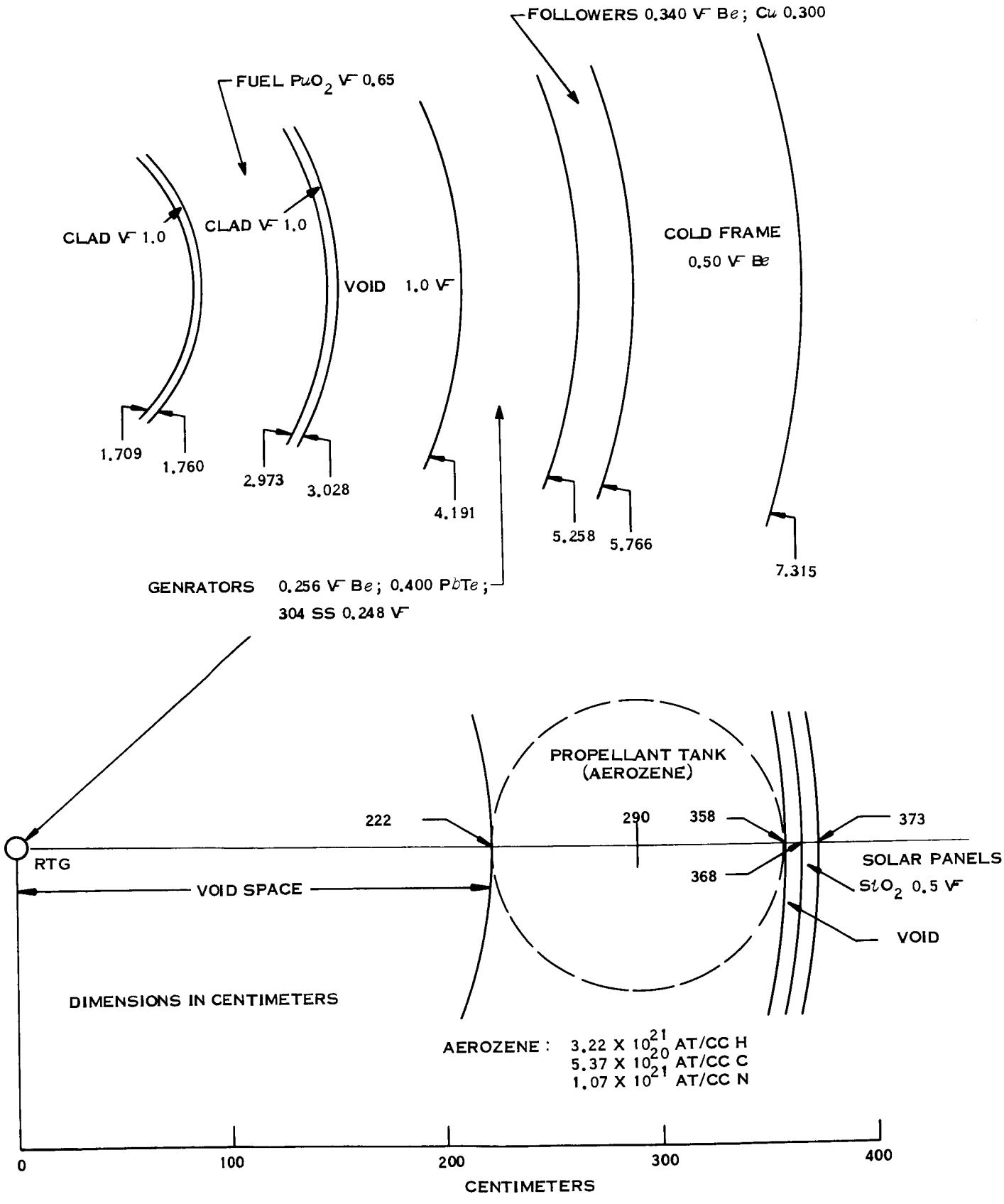

Figure A-2. Planetary Vehicle Model for One-Dimensional Neutron Transport Analysis

energy lattice and in S4 angular detail. The 84-interval spacial lattice had varying incremental widths depending on the material properties in any given interval.

The calculation was repeated for a full and for an empty propellant tank.

A. 3. 2 RTG UNPERTURBED NEUTRON SPECTRUM

The fundamental $^{238}PuO_2$ neutron spectrum will not be observed outside an RTG because of the effect of the generator components surrounding the fuel capsule. The RTG used here was modeled after an existing and well-defined design; the material selection is therefore considered appropriate. The single most important RTG component, aside from the plutonia, is the relatively thick beryllium cold frame.

The neutron spectrum used as input to describe the source is shown in Figure A-3. The total spectrum was integrated and averaged for the 16-group energy lattice. The resulting spectrum is given in Table A-5, column A. Columns B and C compare the spectra at the outer edge of the RTG with and without Aerozene in the tank, respectively. Columns D and E make the same comparison behind the propellant tank, near the center of the solar cell array.

The thermal fraction, i. e., the flux in the thermal group divided by the total flux with Aerozene present, is 2.78×10^{-10} near the center of the plutonia and 0. 0624 near the outer edge of the generator, but 0. 490 at the inner edge of the propellant and 0. 563 behind the propellant. In this energy lattice the neutron resonance region usually extends from group 13 to 10. As column D indicates, the resonance region contains about 6 percent of the total neutron population. Except for some nuclides with large resonance absorption integrals (which also produce activations of interest), the neutron activation study which will utilize the results of this report may profitably ignore the resonance region and assume a thermal fraction of 0. 56 everywhere in the spacecraft bus with corresponding thermal activation cross sections. On this basis, the total neutron flux from Section A. 2. 4 is listed in Table A-6, with the corresponding thermal component, for three selected locations.

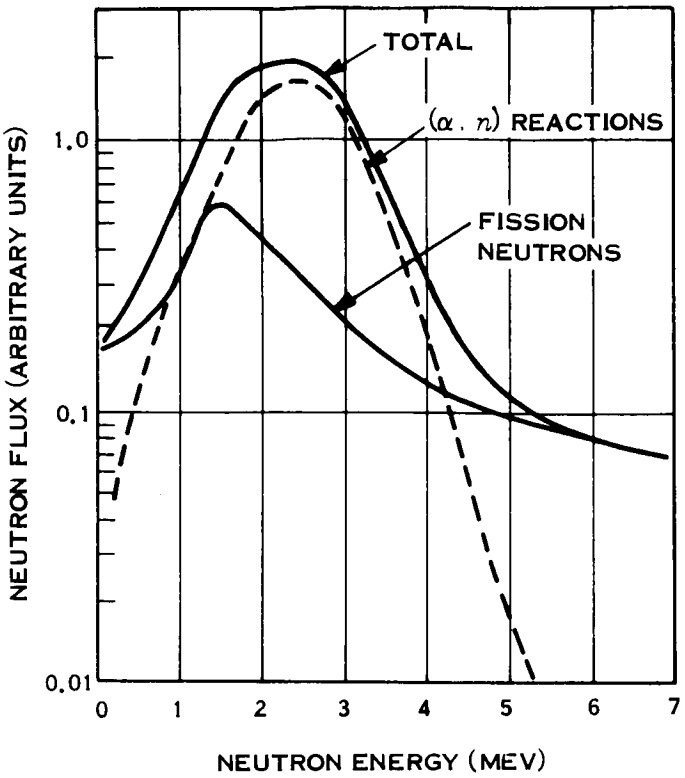

Figure A-3. Neutron Flux Energy Distribution

A.4 DESCRIPTION OF QAD-PR COMPUTER CODE

The QAD-PR code, written at the Los Alamos Scientific Laboratory, is a program used to compute fast neutron and gamma ray penetration through shielding assemblies and materials. The original version of QAD-PR, known as QAD, has since undergone revision to its present form, which is described in this appendix. The computations are based on point-kernel, ray-tracing techniques which include the use of polynominal buildup factors for gamma radiation; and for neutron penetration, removal based on NDA moments fit data and Albert-Welton kernal attenuation are used.

The code accommodates up to 20 gamma ray source group energies and 10 fast neutron energy source groups with a lower edge of 0. 33 Mev as per the moments fit data for a fission source. The source may be specified in either rectangular, cylindrical, or spherical geometry. Zones (or space regions) are formed by surface boundaries which intersect to result in the desired volume enclosures. These boundaries are, in general, curved surfaces

Table A-5. Relative Neutron Spectra

Group	Energy Range		Locations**					
	Lethargy*	Energy	A	B	C	D	E	F
1	0.0 - 1.204	10.0 - 3.0 Mev	0.279	0.0987	0.108	0.0673	0.0577	0.163
2	1.204 - 1.996	3.0 - 1.4 Mev	0.584	0.340	0.373	0.113	0.256	0.428
3	1.996 - 2.408	1.4 - 0.9 Mev	0.0852	0.125	0.138	0.0234	0.0953	0.113
4	2.408 - 3.219	0.9 - 0.4 Mev	0.0412	0.124	0.137	0.0333	0.172	0.110
5	3.219 - 4.605	0.4 - 0.1 Mev	0.0095	0.134	0.149	0.0401	0.208	0.114
6	4.605 - 6.377	100 - 17 kev	0.0012	0.0626	0.0666	0.0353	0.133	0.0489
7	6.377 - 8.0	17 - 3.354 kev	0	0.0198	0.0186	0.0229	0.0488	0.0118
8	8.0 - 10.0	3.354 - 0.454 kev	0	0.0117	6.99/-3	0.0278	0.0199	1.75/-3
9	10.0 - 12.0	454 - 61.44 ev	0	7.15/-3	1.80/-3	0.0276	6.73/-3	2.49/-4
10	12.0 - 14.0	61.44 - 8.315 ev	0	5.47/-3	4.75/-4	0.0254	2.14/-3	8.92/-5
11	14.0 - 15.5	8.315 - 1.855 ev	0	3.10/-3	1.06/-4	0.0160	5.90/-4	7.76/-5
12	15.5 - 16.5	1.855 - 0.6826 ev	0	1.67/-3	2.73/-5	0.00908	1.79/-4	2.36/-8
13	16.5 - 17.5	0.6826 - 0.2511ev	0	1.51/-3	1.08/-5	0.00819	8.04/-5	7.34/-10
14	17.5 - 18.5	0.2511 - 0.0924ev	0	1.30/-3	4.11/-6	0.00733	3.55/-5	4.15/-8
15	18.5 - 19.555	0.0924 - 0.0322ev	0	1.14/-3	1.58/-6	0.00648	1.58/-5	7.01/-11
16	19.555 - ∞	thermal	0	6.24/-2	9.98/-7	0.563	1.23/-5	2.78/-10

*Lethargy $= \frac{\ln 10^7 \text{ ev}}{\ln E}$

NOTE: $N/n = N \times 10^n$

**Locations

A: Source term; unscattered neutrons
B: Outer edge of RTG with full propellant tanks
C: Outer edge of RTG with empty propellant tanks
D: Inside solar panels with full propellant tanks
E: Inside solar panels with empty propellant tanks
F: Center of RTG fuel with full propellant tanks

Table A-6. Neutron Total and Thermal Flux Estimates at Some Locations

Region	Total Flux (neut-cm^{-2}-sec^{-1})	Thermal Flux (neut-cm^{-2}-sec^{-1})
Planetary scan package, folded	4.3×10^{2}	2.4×10^{2}
Equipment bay nearest to two RTG's	1.0×10^{3}	5.6×10^{2}
Solar panels	2.9×10^{2}	1.6×10^{2}

or planes which are described by the input information. The material composition of each zone is specified, which enables the number of mean free paths for the neutron groups to be computed from a source point to a receiver point (detector); with this, application of the material gamma attenuation, geometrical attenuation, and integration over the source volume result in computed radiation intensities at the receiver point. Any number of receiver points may be prescribed per problem.

Computed radiation intensities in the form of a variety of printout information is available from the program computations. For gamma radiation, the code prints out the direct beam energy flux and mean buildup factors for each energy group; also the dose rates and energy absorption rates for four additional materials both for direct beam penetration (without buildup) and penetration including buildup may be obtained as printout information upon supplying the appropriate conversion factors as input. The units for all the printout intensities are determined by the input. The mean buildup factors for each energy group are also listed, which are the ratios of the gamma intensity including buildup factors to the direct beam intensities.

The neutron printout information is the differential number spectrum, the number flux, and energy flux. The neutron dose rate and heating rates in four other materials may also be

obtained by supplying the appropriate input information. Provisions are also made in the program for computing an alternate neutron dose rate based on Albert-Welton and neutron removal attenuation; again, the form of the output information is determined by the input constants.

A.5 REFERENCES

A-1. Capo, M.A., Gamma Ray Absorption Coefficients for Elements and Mixtures, USAEC Report XDC 59-10-19, General Electric Co., ANP Dept., Cincinnati, Ohio, 28 September 1959.

A-2. Trubey, D.K., A Survey of Empirical Functions Used to Fit Gamma-Ray Buildup Factors, USAEC Report ORNL-RSIC-10, Oak Ridge National Lab., Oak Ridge, Tennessee, February 1966.

A-3. Edwards, W. E., et al., Gas-Cooled High-Temperature Nuclear Reactor Design Technology, 7, Shield Design, USAEC Report APEX-800 Part E, General Electric Co., NM&PO, Cincinnati, Ohio, 30 June 1962.

A-4. Lathrop, K.D., DTF-IV, A Fortran-IV Program for Solving the Multigroup Transport Equation with Anisotropic Scattering, USAEC Report LA-3373, Los Alamos Scientific Laboratory, Los Alamos, New Mexico, 15 July 1965.

APPENDIX B

RADIATION ACTIVATION STUDY

B.1 SUMMARY

B.2 INTRODUCTION

B.3 DISCUSSION
- B.3.1 Neutron Activation Calculation
- B.3.2 Environment
- B.3.3 Creation of Radioisotopes
- B.3.4 Activation-Produced Dose Rates

B.4 REFERENCES

APPENDIX B

RADIATION ACTIVATION STUDY

B.1 SUMMARY

The material activation resulting from neutrons produced by the lander RTG's is examined in this appendix. It was determined that for a nominal Voyager (as described in Task D) mission, the activation produced radiation is insignificant compared to the primary RTG radiation as long as the lander and spacecraft are mated. Activation will not produce radiation levels sufficient to cause dynamic interference in spacecraft equipment with the exception of some of the scientific instruments. The activation per gram of each element from Z = 1 to Z = 82 was determined and is described in Section B-3. Table B-1 presents the results of these calculations.

B.2 INTRODUCTION

The Voyager Planetary Vehicle as defined for the Task D RTG Study consists of the spacecraft bus and a lander capsule which separates from the bus sometime after Mars orbit has been achieved. The electrical power for the bus is supplied by a solar cell array, while that of the capsule is supplied by Radioisotope Thermoelectric Generators (RTG's). These RTG's emit photons and neutrons which are damaging to the spacecraft equipment. In addition, the neutrons activate materials in the spacecraft bus, and this activity persists after the capsule separates from the bus. The effects of the primary RTG radiations are discussed in Appendix C while this appendix is limited to the activation problem.

In order that the radiation resulting from neutron activation be of the same order of magnitude as the primary radiation, each RTG neutron must interact with the spacecraft materials and thus produce a radioactive nucleus which decays in such a fashion that at least one photon is emitted. Comparing the number of activated nuclei to the number of parent nuclei present, on a per gram basis, there are at least nine orders of magnitude fewer radioactive nuclei for the neutron flux level and time interval of the Voyager mission. Therefore, as long as the lander is present, the magnitude of radiation resulting from activation will be insignificant compared to the primary RTG radiation.

B. 3 DISCUSSION

To determine the magnitude of material activation in the Voyager spacecraft resulting from neutrons emitted by the RTG's used to provide electrical power for the planetary vehicle, the residual activity per gram of each element was calculated.

B. 3. 1 NEUTRON ACTIVATION CALCULATION

When a beam of neutrons impinges upon a slab of material the activation reaction can be written:

$$ {}_{z}X^{a} + {}_{o}n^{1} \rightarrow {}_{z}X^{a+1} \qquad \text{(B-1)} $$

where

z = atomic number

X = isotope

a = atomic weight

${}_{o}n^{1}$ = neutron (z = o a = 1)

If the neutron flux is constant throughout the sample, the production rate of the new isotope $({}_{z}X^{a+1})$ is:

$$ \frac{dN^*}{dt} = \phi(E)\,\sigma(E)\,(N-N^*) \qquad \text{(B-2)} $$

where

N* = number of new isotope nuclei

t = time

$\phi(E)$ = neutron flux (neutrons - cm^{-2}-sec^{-1})

E = neutron (n) energy

σ = microscopic cross-section (cm^2)

N = number of parent nuclei

The newly created isotope which may be unstable decays with a characteristic time constant (λ). The decay rate can be expressed as:

$$\frac{dN^*}{dt} = -\lambda N^* \tag{B-3}$$

The number of activated nuclei present at any time (T) can be determined by combining the production and decay rate:

$$\frac{dN^*}{dt} = \phi(E)\,\sigma(E)\,\{N - N^*\} - \lambda N^* \tag{B-4}$$

Rearranging and integrating this equation becomes:

$$\int_0^{N^*} dN^*/\{\phi(E)\,\sigma(E)\,N - [\phi(E)\,\sigma(E) + \lambda]\,N^*\} = \int^T dt \tag{B-5}$$

Integrating over the indicated limits:

$$\frac{\ln\{\phi(E)\,\sigma(E)\,N - [\phi(E)\,\sigma(E) + \lambda]\,N^*\} - \ln\{\phi(E)\,\sigma(E)\,N\}}{-\{\phi(E)\,\sigma(E) + \lambda\}} = T \tag{B-6}$$

Solving equation (B-6) for N* and assuming monoenergetic neutrons, equation (B-7) is obtained.

$$N^* = \frac{\phi\sigma N}{\phi\sigma + \lambda}\left\{1 - e^{-(\phi\sigma + \lambda)\,T}\right\} \tag{B-7}$$

Equation B-7) is an expression for the number of new isotope nuclei (N*) after a time (T) during which the sample has been exposed to a neutron flux (ϕ).

B.3.2 ENVIRONMENT

The number and energy spectrum of the neutron environment in the Voyager spacecraft, due to 7200 watts (thermal) produced by RTG's located in the capsule, has been estimated in Appendix A. The neutron flux in the equipment bays is estimated to be 1.0×10^{3} n-cm^{-2}-sec^{-1}. Using the simplifying assumptions that the major portion of the activation is caused by thermal neutrons, and a thermal fraction of 0.56 exists everywhere in the spacecraft, for purposes of activation analysis the neutron flux is taken as 5.6×10^{2} n-cm^{-2}-sec^{-1}.

B.3.3 CREATION OF RADIO-ISOTOPES

The radio activity created by a neutron flux of 5.6×10^{2} n-cm^{-2}-sec^{-1} was examined by determining the number of radioactive nuclei of each isomer created per gram of each element from z = 1 through z = 82, and the resulting radio activity from each isomer created. The isomeric activity was determined by:

$$A = N^{*}\lambda \qquad \text{(B-8)}$$

where

A = activity in disintegrations per second per gram of parent element dps/g

N* = number of isomer nuclei from (3-7)

λ = characteristic isomer time constant = $0.693/T_{1/2}$(half-life)

The results of this calculation appear in Table B-1. The microscopic cross-section values used for the calculation were taken from Reference B-1. Only single activation was considered.

B.3.4 ACTIVATION PRODUCED DOSE RATES

Since each radioactive isotope has its own peculiar decay scheme, and since the resultant dose rate is a function of the number of emissions per disintegration and the energy of each emission, the activities calculated previously were not converted to dose rates. If it is assumed that: all emissions other than photons are absorbed in the materials in which they are created, one photon is emitted per disintegration, and the material is a point source, the dose rate per disintegration per second one meter from the source can be determined as a function of energy. This relationship is displayed in Figure B-1. Comparing this figure with Table B-1, it is observed that large amounts of material are required to produce dose rates on the order of 10 percent of the RTG dose rate.

B.4 REFERENCES

B-1 Hughes, D. J. and Schwartz, R.B., Neutron Cross Sections Brookhaven National Laboratory, Upton, New York, Report No. BNL-325, 1 July 1958.

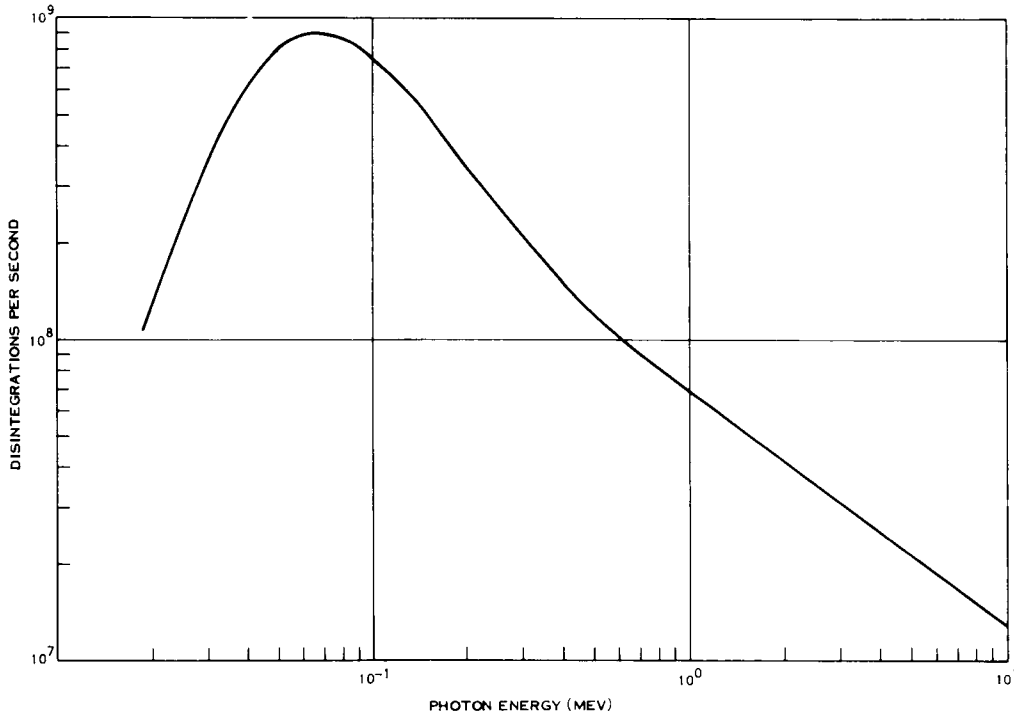

Figure B-1. Activity Required to Produce a Dose Rate of 1.0×10^{-3} r/hr at 1 Meter from a Point Source

Table B-1. Summary of RTG Produced Activity

Element	Radioactive Isotope(s)	Half-life (sec)	11 Month Activity dps/grams(N)	Disintegration Scheme
Hydrogen	H^3	3.87E+08*	1.44E-06	β^-
Helium	H^3	3.86E+08	2.09E-02	β^-
Lithium	Li^3	8.60E+01	1.48E+00	$\beta^- \rightarrow Be^8$ 2α
Beryllium	Be^{10}	7.87E+13	9.56E-08	β^-
Boron	B^{12}	2.20E-02	1.27E+00	β^-, γ
Carbon	C^{14}	1.76E+11	2.48E-08	β^-
Nitrogen	N^{16}	7.36E+00	2.11E-06	β^-, γ
Oxygen	O^{19}	2.94E+01	9.02E-06	β^-, γ
Fluorine	F^{20}	1.12E+01	1.60E-01	β^-, γ
Neon	Ne^{23}	3.76E+01	5.30E-02	β^-, γ
Sodium	Na^{24}	5.40E+04	7.70E+00	β^-, γ
Magnesium	Mg^{27}	5.67E+02	4.24E-02	β^-, γ
Aluminum	Al^{28}	1.38E+02	2.87E+00	β^-, γ
Silicon	Si^{31}	9.54E+04	4.11E-02	β^-, γ
Phosphorus	P^{32}	1.23E+06	2.28E+00	β^-
Sulphur	S^{35}	7.51E+06	1.07E-01	β^-
	S^{37}	3.02E+02	2.51E-04	β^-, γ
Chlorine	Cl^{36}	1.02E+13	5.91E-04	β^-, E.C.
	Cl^{38m}	1.00E+00	1.17E-02	IT $\rightarrow$ Cl^{38}
	Cl^{38}	2.25E+03	1.31E+00	β^-, γ
Argon	A^{37}	2.94E+06	1.72E-01	E.C.
	A^{39}	8.19E+09	7.54E-06	β^-
	A^{41}	6.59E+03	4.46E+00	β^-, γ
Potassium	K^{40}	4.00E+16	3.13E-08	β^-, γ, E.C.
	K^{42}	4.99E+04	6.97E-01	β^-, γ
Calcium	Ca^{41}	6.30E+12	5.70E-06	E.C.
	Ca^{45}	1.41E+07	9.08E-02	β^-
	Ca^{47}	4.23E+06	6.93E-05	β^-, $\gamma \rightarrow Sc^{47}$ β^-, γ
Scandium	Sc^{46m}	1.95E+01	7.50E+01	IT $\rightarrow$ Sc^{46}
	Sc^{46}	7.33E+06	8.42E+01	β^-
Titanium	Ti^{51}	3.47E+02	5.19E-02	β^-, γ

*Read as $3.87 \times 10^{+8}$

Table B-1. Summary of RTG Produced Activity (Cont)

Element	Radioactive Isotope(s)	Half-life (sec)	11 Month Activity dps/grams(N)	Disintegration Scheme
Vanadium	V^{52}	2.26E+02	3.36E+01	β^-, γ
Chromium	Cr^{51}	2.40E+06	4.20E+00	E.C.
	Cr^{55}	2.11E+03	5.72E-02	β^-
Manganese	Mn^{56}	9.29E+03	8.19E+01	β^-, γ
Iron	Fe^{55}	9.26E+07	1.58E-01	E.C.
	Fe^{59}	1.66E+08	1.83E-01	β^-, γ
Cobalt	Co^{60m}	6.30E+02	9.14E+01	IT $\rightarrow$ Co^{60}
	Co^{60}	1.66E+08	1.30E+01	β^-, γ
Nickel	Ni^{59}	2.52E+12	1.30E-04	E.C.
	Ni^{63}	2.52E+09	2.50E-02	β^-
	Ni^{65}	3.09E+02	3.28E+00	β^-, γ
Copper	Cu^{64}	4.62E+04	1.50E+01	β^-, β^+, E.C., and γ
	Cu^{66}	3.09E+02	3.28E+00	β^-, γ
Zinc	Zn^{65}	2.11E+07	6.18E-01	β^+, E.C., and γ
	Zn^{67m}	8.80E-06	2.87E-05	IT
	Zn^{69m}	4.97E+04	9.31E-02	IT $\rightarrow$ Zn^{69}
	Zn^{69}	3.12E+03	9.59E-01	β^-
	Zn^{71}	1.32E+02	2.88E-03	β^-
Gallium	Ga^{70m}	1.90E-02	4.95E+00	IT $\rightarrow$ Ga^{70} β^-, γ
	Ga^{72}	5.11E+04	9.44E+00	β^-, γ
Germanium	Ge^{71m}	2.00E-02	3.16E+00	IT $\rightarrow$ Ge^{71} E.C.
	Ge^{73m}	5.30E-01	1.25E+00	IT
	Ge^{75m}	4.80E+01	9.38E-01	IT $\rightarrow$ Ge^{75} β^-, γ
	Ge^{77m}	5.20E+01	2.85E-02	β^-, $\gamma \rightarrow As^{77}$ β^-, γ or IT Ge^{77}
	Ge^{77}	4.32E+04	4.11E-02	β^-, $\gamma \rightarrow As^{77}$ β^-, γ
Arsenic	As^{76}	9.58E+04	1.89E+01	β^-, γ
Selenium	Se^{75}	1.10E+07	8.11E-01	E.C.
	Se^{77m}	1.75E+01	2.70E+00	IT
	Se^{79m}	2.34E+02	4.02E-01	IT $\rightarrow$ Se^{79} β^-
	Se^{81m}	3.41E+03	6.38E-02	IT $\rightarrow$ Se^{81}

Table B-1. Summary of RTG Produced Activity (Cont)

Element	Radioactive Isotope(s)	Half-life (sec)	11 Month Activity dps/grams(N)	Disintegration Scheme
Selenium (Cont)	Se^{81}	1.09E+03	1.06E+00	β^-
	Se^{83m}	6.70E+01	1.96E-02	$\beta^-, \gamma \rightarrow Br^{83}$ β^-, γ
	Se^{83}	1.50E+03	1.57E-03	$\beta^-, \gamma \rightarrow Br^{83}$ β^-, γ
Bromine	Br^{79m}	1.62E+04	6.18E+00	IT $\rightarrow Br^{79}$
	Br^{79}	1.11E+03	1.81E+01	β^-, γ and E.C.
	Br^{82}	1.29E+05	6.48E+00	β^-, γ
Krypton	Kr^{79}	1.24E+05	2.85E-02	E.C. and B^+, γ
	Kr^{81m}	1.30E+01	8.68E+00	IT $\rightarrow Kr^{81}$ E.C.
	Kr^{83m}	6.77E+03	2.10E+01	IT
	Kr^{85m}	1.58E+03	2.29E-01	β^-, γ and IT $\rightarrow Kr^{85}$
	Kr^{85}	3.34E+08	8.00E-03	β^-, γ
	Kr^{87}	4.68E+03	4.20E-02	β^-, γ
Rubidium	Rb^{86}	1.60E+06	2.28E+00	β^-, γ
	Rb^{88}	1.07E+03	1.32E-01	β^-
Strontium	Sr^{85}	5.61E+06	2.06E-02	E.C. $\rightarrow Rb^{85m}$ IT
	Sr^{87m}	9.08E+03	4.94E-01	IT
	Sr^{89}	4.35E+06	1.58E-02	β^-
Yttrium	Y^{90}	2.31E+05	4.82E+00	β^-
Zirconium	Zr^{93}	3.46E+13	9.15E-08	β^-
	Zr^{95}	5.46E+06	5.01E-02	$\beta^-, \gamma \rightarrow Nb^{95}$ β^-, γ
Niobium	Nb^{94m}	3.96E+02	3.63E+00	IT $\rightarrow Nb^{94}$ β^-, γ
Molybdenum	Mo^{93m}	2.50E+04	3.36E-03	IT $\rightarrow Mo^{93}$ E.C.
	Mo^{99}	2.41E+05	3.77E-01	$\beta^-, \gamma \rightarrow Tc^{99m}$ IT $\rightarrow Tc^{99}$ β^-
	Mo^{101}	8.76E+02	6.77E-02	$\beta^-, \gamma \rightarrow Tc^{101}$ β^-, γ
Ruthenium	Ru^{97}	2.50E+05	3.85E-02	E.C. $\rightarrow Tc^{97}$ E.C.
	Ru^{103}	3.54E+06	1.26E+00	$\beta^-, \gamma \rightarrow Rh^{103m}$ IT
	Ru^{105}	1.62E+04	4.52E-01	$\beta^-, \gamma \rightarrow Rh^{105m}$ IT Rh^{105} $\beta^- \gamma$

Table B-1. Summary of RTG Produced Activity (Cont)

Element	Radioactive Isotope(s)	Half-life (sec)	11 Month Activity dps/grams(N)	Disintegration Scheme
Rhodium	Rh^{104m}	2.64E+02	3.93E+01	IT - Rh^{104}
	Rh^{104}	4.20E+01	4.59E+02	$\beta^-,\gamma \rightarrow Pd^{104m}$ IT
Palladium	Pd^{103}	1.47E+06	1.46E-01	E.C $\rightarrow Rh^{103m}$ IT
	Pd^{109m}	2.88E+02	5.91E-02	IT $\rightarrow Pd^{109}$
	Pd^{109}	4.90E+04	9.29E+00	$\beta^-, \rightarrow Ag^{109m}$ IT
	Pd^{111}	1.32E+03	1.12E-01	$\beta^-,\gamma \rightarrow Ag^{111}$ β^-,γ
Silver	Ag^{108}	1.38E+02	7.32E+01	β^-, γ
	Ag^{110m}	2.33E+07	2.45E+00	β^-, γ and IT $\rightarrow Ag^{110}$
	Ag^{110}	2.42E+01	1.72E+02	β^-, γ
Cadmium	Cd^{107}	2.41E+04	3.63E-02	E.C. $\rightarrow Ag^{102m}$ IT
	Cd^{109}	4.09E+07	1.02E-02	E.C. $\rightarrow Ag^{109m}$ IT
	Cd^{111m}	2.92E+03	7.44E-02	IT
	Cd^{113m}	4.41E+08	9.63E-04	$\beta^- \rightarrow In^{113m}$ IT
	Cd^{115m}	3.71E+06	1.20E-01	$\beta^-,\gamma \rightarrow In^{115}$ β^-,γ
	Cd^{115}	1.91E+05	9.54E-01	$\beta^-,\gamma \rightarrow In^{115}$ IT $\rightarrow In^{115}$ β^-,γ
	Cd^{117m}	9.44E+03	3.41E-01	IT $\rightarrow Cd^{117}$ $\beta^-,\gamma \rightarrow In^{117m}$ β^-,γ
Indium	In^{114m}	4.23E+06	6.90E+00	IT $\rightarrow In^{114}$ β^-, γ
	In^{114}	7.20E+01	2.49E+00	β,γ
	In^{116m}	3.25E+03	4.08E+02	β^-, γ
	In^{116}	1.30E+01	1.46E+02	β^-
Tin	Sn^{113}	9.92E+06	3.05E-02	E.C. $\rightarrow In^{113m}$ IT
	Sn^{117m}	1.21E+06	2.42E-03	IT
	Sn^{119m}	2.37E+07	3.89E-03	IT
	Sn^{120}	1.10E-05	6.83E-04	IT
	Sn^{121m}	1.58E+08	1.11E-04	β^-
	Sn^{121}	9.90E+04	1.31E-01	β^-
	Sn^{123m}	1.13E+07	1.11E-04	β^-
	Sn^{123}	2.40E+03	2.15E-01	β^-, γ
	Sn^{125m}	5.70E+02	3.40E-02	$\beta^-,\gamma \rightarrow Sb^{125}$ $\beta^-,\gamma \rightarrow Te^{125m}$ IT
	Sn^{125}	8.19E+05	6.80E-04	$\beta^-,\gamma \rightarrow Sb^{125}$ $\beta^-,\gamma \rightarrow Te^{125m}$ IT

Table B-1. Summary of RTG Produced Activity (Cont)

Element	Radioactive Isotope(s)	Half-life (sec)	11 Month Activity dps/grams(N)	Disintegration Scheme
Antimony	Sb^{122}	2.41E+05	9.51E+00	$\beta^-,\gamma \rightarrow Te^{122m}$ IT
	Sb^{124m_2}	1.26E+03	3.56E-02	IT $\rightarrow Sb^{124m_1}$
	Sb^{124m_1}	7.80E+01	3.56E-02	IT $\rightarrow Sb^{124}$
	Sb^{124}	5.17E+06	2.90E+00	β^-,γ
Tellurium	Te^{121m}	1.33E+07	1.28E-01	IT $\rightarrow Te^{121}$ E.C.
	Te^{123m}	8.97E+06	6.38E-02	IT $\rightarrow Te^{123}$
	Te^{123}	3.15E+21	3.19E-11	E.C.
	Te^{125m}	5.00E+06	7.18E-01	IT
	Te^{127m}	9.06E+06	3.96E-02	IT $\rightarrow Te^{127}$
	Te^{127}	5.61E+02	3.95E-01	β^-,γ
	Te^{129m}	2.85E+06	1.26E-02	IT $\rightarrow Te^{129}$
	Te^{129}	4.44E+03	1.09E-01	$\beta^-,\gamma \rightarrow I^{129}$ β^-,γ
Iodine	I^{128}	9.36E+03	5.35E-02	β^-,γ
Xenon	Xe^{129m}	6.90E+05	2.47E-01	IT
	Xe^{131m2}	1.03E+06	5.24E-01	IT $\rightarrow Xe^{131m_1}$ IT
	Xe^{133m}	1.98E+05	1.38E-01	IT Xe^{133} β^-,γ
	Xe^{135m}	9.36E+02	5.35E-02	IT $\rightarrow Xe^{135}$ $\beta^-,\gamma \rightarrow C,^{135m}$ IT $\rightarrow Cs^{135}$ β^-
	Xe^{137}	2.28E+02	3.42E-02	$\beta^- \rightarrow Cs^{137}$ $\beta^- \rightarrow Be^{137m}$ IT
Cesium	Cs^{134m}	1.15E+04	4.31E-02	IT $\rightarrow Cs^{134}$
	Cs^{134}	7.25E+07	1.59E+01	β^-,γ
Barium	Ba^{131}	1.00E+06	2.51E-02	E.C. $\rightarrow Cs^{31}$ E.C.
	Ba^{133}	2.27E+08	1.41E-03	E.C.
	Ba^{135m}	1.03E+05	1.19E-01	IT
	Ba^{137m}	1.56E+02	7.68E-02	IT
	Ba^{139}	5.10E+03	1.14E+00	$\beta^-,\gamma \rightarrow La^{139m}$ IT
Lanthanum	La^{140}	1.45E+05	1.99E+01	β^-,γ

Table B-1. Summary of RTG Produced Activity (Cont)

Element	Radioactive Isotope(s)	Half-life (sec)	11 Month Activity dps/grams(N)	Disintegration Scheme
Cerium	Ce^{137m}	3.17E+04	3.79E-02	IT → Ce^{137}
	Ce^{137}	1.24E+04	2.79E-03	E.C. → La^{137} E.C.
	Ce^{139m}	5.50E+01	4.21E-05	IT → Ce^{139}
	Ce^{139}	1.21E+07	4.78E-03	E.C.
	Ce^{141}	2.80E+06	6.60E-01	β^- → Pr^{141} IT
	Ce^{143}	1.19E+05	2.67E-01	β^-,γ → Pr^{143} β^-
Praseodymium	Pr^{142}	6.95E+04	2.78E+01	β^-,γ
Neodynium	Nd^{144}	6.30E+22	8.68E-12	α → Ce^{141} β^- → Pr^{141m} IT
	Nd^{147}	9.75E+05	7.29E-01	β^-,γ → Pm^{147} α → Nd^{144}
	Nd^{149}	7.20E+03	4.30E-01	β^-,γ → Pm^{149} β^-,γ
Samarium	Sm^{145}	3.10E+07	6.74E-02	E.C. → Pm^{145} E.C.
	Sm^{153}	1.69E+05	8.36E+01	β^-,γ → Eu^{153m} IT
	Sm^{155}	1.44E+03	2.78E+00	β^-,γ → Eu^{155} β^-,γ
Europium	Eu^{152m}	3.31E+04	1.84E+03	β^-,γ → Gd^{152} α
	Eu^{152}	4.10E+08	7.05E+01	E.C. → Sm^{152m} IT
	Eu^{154}	5.04E+08	1.89E+01	β^-,γ
Gadolinium	Gd^{153}	2.04E+07	3.36E+01	E.C. → Eu^{153m} IT and E.C.
	Gd^{159}	6.48E+04	2.14E-00	β^-,γ
	Gd^{161}	2.18E+02	3.76E-01	β^-,γ → Tb^{161} β^-,γ
Terbium	Tb^{160}	6.30E+06	8.95E+01	β^-,γ → Dy^{160m} IT
Dysprosium	Dy^{165m}	7.50E+01	2.99E+02	IT → Dy^{165} $\beta^-\gamma$
	Dy^{168}	8.35E+03	1.23E+03	β^-,γ
Holmium	Ho^{166m}	9.45E+08	2.74E+00	β^-,γ
Erbium	Er^{169}	8.11E+05	1.09E+00	β^- → Tm^{169m} IT
	Er^{171}	2.70E+04	2.70E+00	β^-,γ → Tm^{171m} IT → TM^{171} β^-
Thulium	Tm^{170}	1.10E+07	1.98E+02	β^-

Table B-1. Summary of RTG Produced Activity (Cont)

Element	Radioactive Isotope(s)	Half-life (sec)	11 Month Activity dps/grams(N)	Disintegration Scheme
Ytterbium	Yb^{169}	2.76E+06	3.00E+01	E.C $\rightarrow Tm^{169m}$ IT
	Yb^{175m}	6.70E-02	3.72E+01	IT $\rightarrow Yb^{175}$ β^-,γ
	Yb^{177m}	6.50E+00	1.36E+00	IT $\rightarrow Yb^{177}$ β^-,γ Lu^{177} β^-,γ
Lutetium	Lu^{176m}	1.34E+04	6.57E+01	$\beta^- \rightarrow Hf^{176m}$ IT
	Lu^{177}	5.78E+05	2.00E+02	β^-,γ
Hafnium	Hf^{175}	6.05E+06	4.92E+00	E.C.
	Hf^{178m}	4.80E+00	1.33E+02	IT
	Hf^{179m}	1.90E+01	3.85E+01	IT
	Hf^{180m2}	1.95E+04	1.70E+01	IT $\rightarrow Hf^{180m1}$ IT
	Hf^{181}	3.97E+06	7.87E+00	$\beta^- \rightarrow Ta^{181m}$ IT
Tantalum	Ta^{182m}	9.90E+02	5.59E-03	IT
	Ta^{182}	9.66E+06	3.10E+01	β^-,γ
Tungsten	W^{181}	1.21E+07	6.02E-02	E.C.
	W^{183m}	5.50E+00	9.70E+00	IT
	W^{185}	6.38E+06	1.08E+00	β^-,γ
	W^{187}	8.64E+04	1.77E+01	$\beta^-,\gamma \rightarrow Re^{187m}$ IT $\rightarrow Re^{187}$ β^-
Rhenium	Rh^{186}	3.28E+05	6.73E+01	$\beta^-\gamma \rightarrow Os^{186m}$ IT
	Rh^{188}	6.12E+04	7.87E+01	$\beta^-\gamma \rightarrow Os^{188m}$ IT
Osmium	Os^{185}	8.19E+06	5.84E+02	E.C.
	Os^{191}	1.38E+06	3.75E+00	$\beta^- \rightarrow Ir^{191m}$ IT
	Os^{193}	1.03E+05	1.16E+00	β^-, γ
Iridium	Ir^{192m}	8.70E+01	1.76E+02	IT $\rightarrow Ir^{192}$
	Ir^{192}	6.43E+06	4.53E+02	β^-, γ
	IR^{194m}	4.70E+01	1.43E+02	IT $\rightarrow Ir^{194}$ β^-, γ
Platinum	Pt^{191}	2.59E+05	1.58E-04	E.C.
	Pt^{193m}	3.02E+05	1.21E+00	IT $\rightarrow Pt^{193}$ E.C.
	Pt^{195m}	5.17E+05	6.81E-01	IT
	Pt^{197}	6.48E+04	3.52E-01	β^-, γ
	Pt^{199m}	1.40E+01	4.98E-01	IT $\rightarrow Pt^{139}$ $\beta^-,\gamma \rightarrow Au^{199}$ $\beta^-,\gamma \rightarrow Hg^{199m1}$ IT

Table B-1. Summary of RTG Produced Activity (Cont)

Element	Radioactive Isotope(s)	Half-life (sec)	11 Month Activity dps/grams(N)	Disintegration Scheme
Gold	Au^{198}	2.33E+05	1.68E+02	β^-, γ
Mercury	Hg^{197m}	8.64E+04	7.36E+00	IT $\rightarrow$ Hg^{197} E.C.
	Hg^{203}	3.95E+06	1.98E+00	β^-, γ
	Hg^{205}	3.30E+02	4.95E-02	β^-, γ
Thallium	Tl^{204}	1.29E+08	7.69E-01	β^-, γ
	Tl^{206}	2.52E+02	1.16E-01	β^-
Lead	Pb^{205m}	4.80E-03	1.35E-04	IT $\rightarrow$ Pb^{205} E.C.
	Pb^{207m}	8.40E-01	9.61E-03	IT
	Pb^{209}	1.20E+04	5.11E-04	β^-

APPENDIX C

RADIATION SENSITIVITY STUDY - SPACECRAFT EQUIPMENT NOT INCLUDING SCIENCE

C.1 INTRODUCTION

C.2 SUMMARY

C.3 SUBSYSTEM RADIATION SENSITIVITY ANALYSIS
- C.3.1 Telecommunications Subsystem
- C.3.2 Guidance and Control Subsystem
- C.3.3 Temperature Control Subsystem
- C.3.4 Structure Subsystem
- C.3.5 Pyrotechnic Subsystem
- C.3.6 High-Gain Antenna Actuation Subsystem
- C.3.7 Power Subsystem
- C.3.8 Computer and Sequencer Subsystem
- C.3.9 Propulsion Subsystem
- C.3.10 Planetary Scan Platform Actuation Subsystem
- C.3.11 Harness Subsystem

C.4 REFERENCES

APPENDIX C

RADIATION SENSITIVITY STUDY - SPACECRAFT EQUIPMENT NOT INCLUDING SCIENCE

C.1 INTRODUCTION

This appendix describes the radiation sensitivity of the Voyager spacecraft exclusive of the lander and scientific payload. The sensitivity analysis considers the interaction of photons and neutrons from the plutonium-fueled radioisotope thermoelectric generators (RTG's) with the spacecraft. The functional description of the spacecraft used to perform the radiation sensitivity analysis is that given in the General Electric Company's Voyager Spacecraft System - Phase 1A Task B Preliminary Design - Spacecraft Functional Description, (Reference C-1) with appropriate modifications delineating the Task D systems update effort. These changes to the functional description have been provided by the cognizant subsystem and component engineers.

Since much of the system remains unchanged or simply reconfigured, the radiation sensitivities are those reported in the previous study (Reference C-2). The sensitivity analysis of such subsystems and components is presented in Reference C-3, and will not be repeated in this document. New radiation sensitivity data has been incorporated into this report for components for which it was available. The analysis of radiation sensitivity of components not previously evaluated has been performed in a manner similar to that described in Reference C-2.

The results of the radiation sensitivity analysis are summarized in Section C.2. Section C.3 describes the changes to the Voyager spacecraft in terms of the impact upon radiation sensitivity.

C.2 SUMMARY

The radiation effects upon the Voyager spacecraft from RTG-produced radiations are summarized in Figures C-1 and C-2. Figure C-1 is a summary of the principal neutron effects, and Figure C-2 is a summary of the principal gamma effects in the system. The major changes to the previous study are the addition of the solar panels and the associated circuitry, the substitution of a single Propulsion Subsystem for the Retropropulsion and Midcourse Orbit Adjust Subsystems, and the consideration of a Harness Subsystem. In general, the radiation sensitivity of the Voyager spacecraft remains unchanged from that previously given in Reference C-2.

C.3 SUBSYSTEM RADIATION SENSITIVITY ANALYSIS

The subsystem radiation sensitivities have been determined by analyzing the piece parts and materials comprising the subsystem. The piece-part and material sensitivities have been utilized to determine damage thresholds for the appropriate components. Three damage levels have been determined: threshold, moderate, and severe. The threshold damage range indicates those radiation doses at which device degradation has begun but at which the component is still operable within design tolerances. Moderate damage generally denotes that range of radiation doses at which device degradation is appreciable but at which component operation would have been within design tolerances if the device parameters had been derated initially. Severe damage represents those radiation doses at which the devices have failed and/or those doses at which special design techniques and component selection must be utilized to obtain an operating component.

Many of the components of the present Voyager spacecraft system are unchanged from that which was examined in the prior radiation sensitivity analysis. These components were not reexamined during this study. A listing of the major components of the Voyager spacecraft exclusive of scientific instruments appears in Tables C-1 through C-11. The radiation sensitivities of these components are summarized in Figures C-1 and C-2. The ensuing discussion is limited to those new components which have been identified during

this study. In some cases, better definition of components was available and is noted in Tables C-1 through C-11. However, since the radiation sensitivity was unchanged, the analysis does not appear in this report. Analyses of components not appearing in this report can be found in Reference C-2 or Reference C-3.

C.3.1 TELECOMMUNICATIONS SUBSYSTEM

The Telecommunications Subsystem is essentially unchanged, with the exception of the optical end-of-tape sensor in the magnetic tape recorders. This sensor has been replaced by a nonoptical device (undefined at this time) which will perform this function. The sensitivity of this device is assumed to be similar to that of the signal electronics.

C.3.2 GUIDANCE AND CONTROL SUBSYSTEM

Two changes in the Guidance and Control Subsystem are under consideration. A study of the Canopus sensor has been concluded with the recommendation for use of an improved sensor utilizing an in-flight calibration source and slightly different logic (Reference C-5). Also, a tradeoff study of the integrating gyro package is being conducted.

C.3.2.1 Canopus Sensor

The electronic and optical components of the Canopus sensor have radiation sensititivies similar to the sensor analyzed in Reference C-3, and the image disector tube is identical. The calibration source, however, has been changed. The present calibration source is a Cherenkov light source. A typical Cherenkov light source consists of a radioisotope which emits charged particles and a quartz disc within which the particles lose energy. A fraction of this energy is then re-emitted in the form of visible light. Cherenkov radiation occurs only if the particle velocity is greater than the phase velocity of light in the medium. The phase velocity is equal to "c/n", where "c" is the velocity of light in vacuum and "in" is the index of refraction of the medium. The particle velocity is equal to βc, where β is the particle velocity expressed as a fraction of the velocity of light. In order that Cherenkov radiation occur:

$$\beta n > 1$$

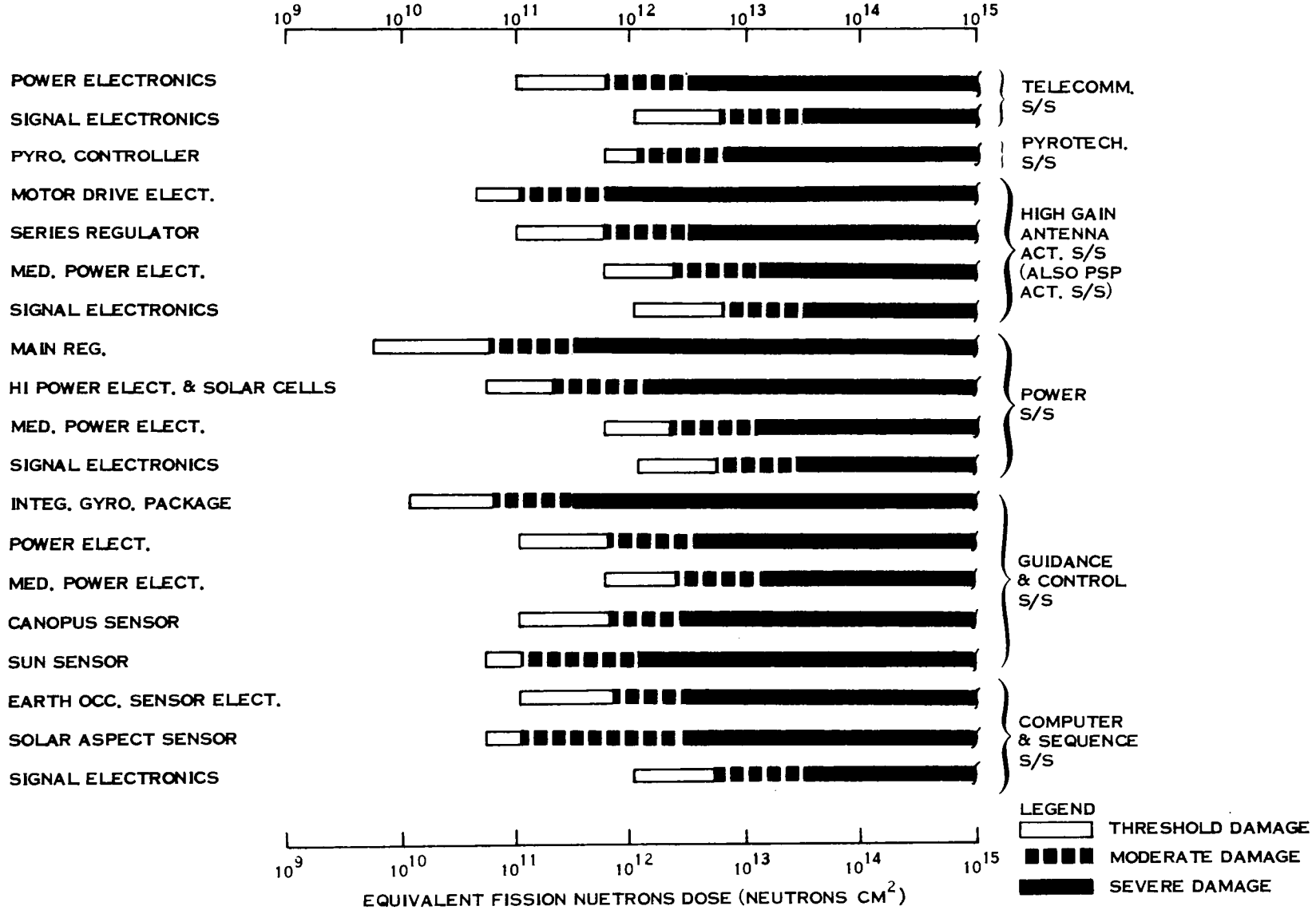

Figure C-1. Neutron Sensitivity Summary

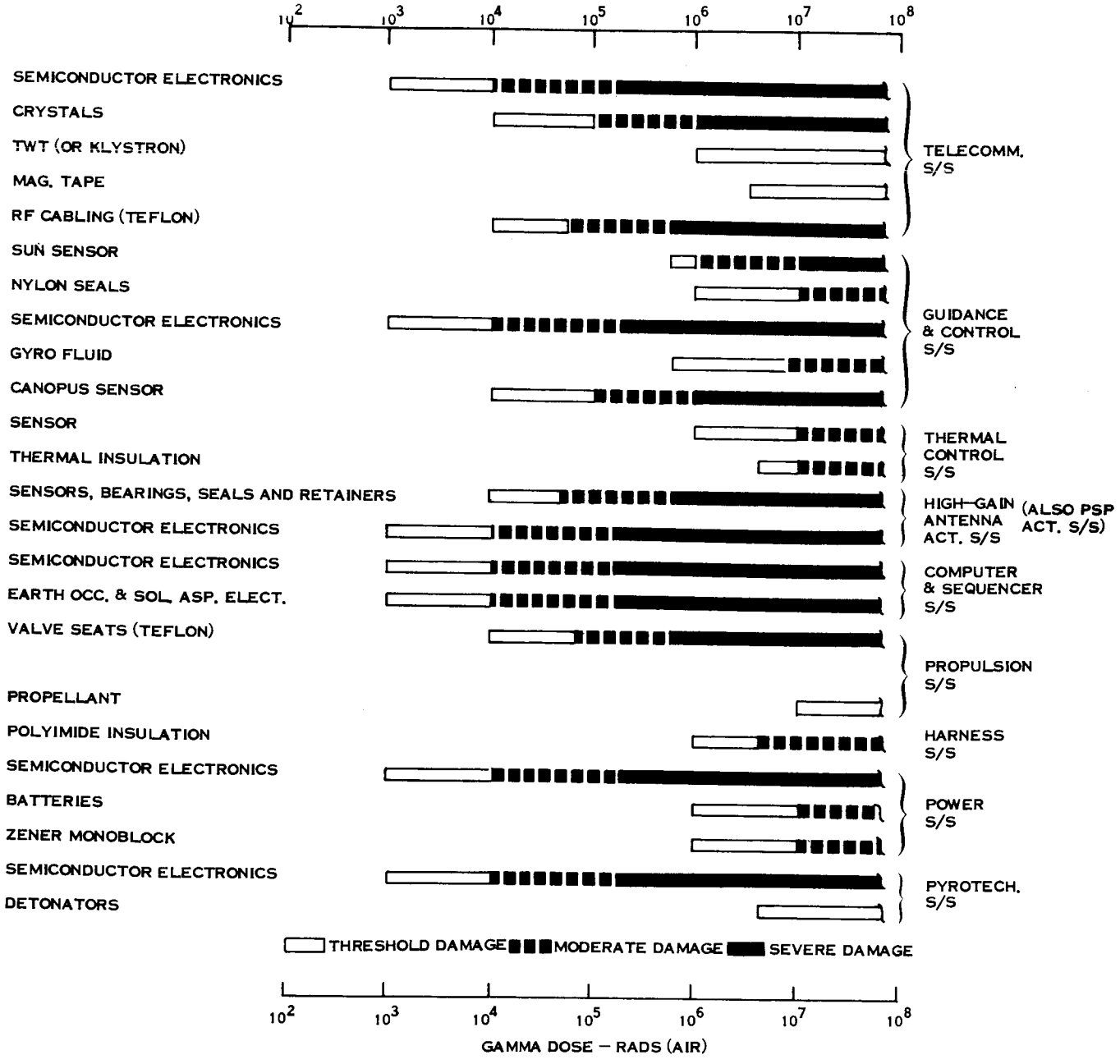

Figure C-2. Gamma Effects Summary

A typical Cherenkov source is comprised of a quartz plate (Corning #7940) and several millicuries of strontium 90. The index of refraction of quartz is approximately 1.5, so the energy of the electrons emitted by strontium 90 (Sr-90) must have velocities in excess of 0.667 c or energies in excess of 0.2 Mev. Sr-90 decays to yttrium 90 (Y-90) by emission of a 0.6-Mev electron. This decay has a characteristic half-life of 28 years. Y-90 subsequently decays to zirconium 90 (Zr-90) by emitting a 2.25-Mev electron. The decay to Zr-90, which is stable, has a characteristic half-life of approximately 62 hours. Both electrons have sufficient energy to produce Cherenkov radiation. Photons and neutrons from the RTG's which interact with the quartz plate do not cause Cherenkov radiation directly as they are uncharged. However, secondary interactions within the quartz plate or nearby material can produce secondary electrons which will undergo Cherenkov interactions if they have sufficient energy. In order to cause an appreciable interference signal in the light source, RTG photons would have to create a secondary electron flux of the same order of magnitude as that resulting from the radioistope used in the source. The Sr-90 source strength used in typical Cherenkov light sources is 2 millicuries. A millicurie is equal to 3.7×10^{7} disintegrations per second (dps). Since two electrons are emitted per disintegration and since the source strength is approximately 2 millicuries, the Sr-90 source produces approximately 1.5×10^{8} electrons/second. If we assume that the quartz plate is 1 centimeter (cm) away from the source and consider the source to be a point, the electron flux in the quartz is approximately 10^{7} electrons-cm^{-2}-sec^{-1}. The energy averaged cross section for electron production in quartz by the RTG photons is approximately 6×10^{-4} cm^{-1}. If the quartz is 1 cm thick, approximately 10^{8} photons-cm^{-2}-sec^{-1} are required to cause a 1 percent increase in light output. Hence, the dynamic interference level is approximately 2.3×10^{4} rads (air)/hour. The other deleterious effect is darkening of the quartz plate. This effect is discussed in detail in Reference C-3. The threshold damage levels determined (Reference C-3) are 10^{8} rads and 10^{12} EFN/cm^{2}.

C.3.2.2 Integrating Gyro Package

Selection of an integrating gyro package is presently under study. The gyros under consideration are one- and two-axis ball and gas bearing types. In general, the radiation damage levels of all gyros under consideration are similar. Hence the damage levels determined for the Kearfott Alpha Ball Bearing Gyro are expected to hold true for any candidate gyro.

C.3.2.3 Cold Gas Jet Subsystem

A recent report (Reference C-6) indicated that the threshold damage levels of the temperature and pressure sensors are 5×10^4 rads, 10^{14} EFN/cm^2 and 10^7 rads, 10^6 EFN/cm^2 respectively. The ionization dose of 5×10^4 rads is the threshold damage dose for positive coefficient thermistor temperature transducer. If this type of transducer is not used, the threshold damage dose is 2×10^6 rads.

C.3.3 TEMPERATURE CONTROL SUBSYSTEM

Bimetallic actuators have replaced the fluid-filled bellows as the thermal control louver actuating mechanisms. The outer surface of the louvers will be highly polished aluminum rather than being aluminum oxide coated. Both these modifications result in components which are less sensitive to radiation. In order to affect the operation of the actuators or change the heat transfer characteristics of the louvers, the structural properties of the materials must be changed. The threshold damage levels at which such changes begin are in excess of 10^{17} EFN/cm^2 and 10^9 rads.

Thermal control coatings Z-93 (zinc oxide pigment in a potassium silicate binder) and PV-100 (titanium oxide pigmented silicone alkyd) are being considered. These coatings were analyzed previously and have damage thresholds of 6×10^7 and 2×10^8 rads respectively (Reference C-3).

The superinsulation blankets may be modified by the addition of a thin outer layer of Kapton and the substitution of gold deposition instead of aluminum. The addition of a Kapton layer and the substitution of gold for aluminum are not expected to change the radiation damage levels of the superinsulation blankets.

The temperature sensors and louver position indicators are presently being reviewed. The temperature sensor identified in the Task B design (Reference C-1) is a platinum wire resistance type having a damage threshold of 10^6 rads and 10^{15} EFN/cm^2. The louver position indicator defined in Reference C-1 is a differential transformer type exhibiting a threshold damage level of 10^6 rads and 10^{15} EFN/cm^2. Since information on possible substitutions is unavailable, these damage levels are used.

C.3.4 STRUCTURE SUBSYSTEM

The materials utilized in the Structure Subsystem remain unchanged from those reported in Reference C-1, and the damage levels are the same as noted in References C-2 and C-3.

C.3.5 PYROTECHNIC SUBSYSTEM

The safe-arm and igniter components have been deleted (Reference C-4).

C.3.6 HIGH GAIN ANTENNA ACTUATION SUBSYSTEM

This subsystem remains unchanged with two exceptions. All lubricants noted under the lubrication heading in Reference C-3 have been replaced by molybdenum disulfide (MoS_2) dry films. The lubricity of MoS_2 is unaffected by radiation (Reference C-7). The control and sensory harness is to be fabricated from polyimide-insulated wire rather than Teflon-insulated wire. The threshold damage level of polyimide insulation is greater than 10^8 rads (References C-8 and C-9). Reference C-10 indicates essentially no change in tensile strength or elongation at a dose of 10^{15} EFN/cm^2. However, the same reference indicates that cobalt-60 gamma ray exposures of approximately 10^6 rads produce the following changes in 0.001-inch-thick polyimide film: volume resistivity

+37 percent, dielectric constant +2.9 percent, dissipation factor +15 percent, and dielectric strength -13 percent. Since only the dielectric strength and dissipation factors are degraded while the other parameters are improved, 10^6 rads will be used as the threshold damage level.

C.3.7 POWER SUBSYSTEM

The Power Subsystem considered in the previous radiation sensitivity analysis utilized a RTG power source. The Task D design utilizes a solar array as the prime power source. This results in several changes to the Power Subsystem, which are discussed in Sections C.3.7.1 through C.3.7.5.

C.3.7.1 Solar Cell Array

The solar array is comprised of series and parallel combinations of N on P silicon solar cells. The effects of proton and electron bombardment upon silicon solar cells have been studied extensively (for example, Reference C-11). However, very little data is available describing the effects of neutron and gamma radiation upon solar cells. A recent experiment (Reference C-4) performed by the General Electric Company subjected N/P silicon solar cells to neutron bombardment. A summary of the tests results appears in Figure C-3. The threshold damage level from Figure C-3 is 10^{10} to 1.4×10^{11} EFN-cm^{-2}. The ionization threshold damage dose can be determined from electron damage data utilizing the damage correlation reported in Reference C-11. The ionization threshold damage dose from Reference C-12 ranges from 3×10^{12} to 3×10^{13}, 1. Mev electrons/cm^2, or 9.5×10^5 to 9.3×10^6 rads. Reference C-11 notes that Co-60 gamma rays are less damaging by a factor of 100. Hence, the threshold damage range is approximately 9×10^7 to 9×10^8 rads (air).

C.3.7.2 Zener Monoblock

The Zener monoblocks consist of 16 Zener diodes and two isolation diodes. The Zener diodes are connected in two parallel strings of eight series-connected diodes. Each diode is rated at 7 volts and 3 watts. Extensive reactor tests (Reference C-13) indicate

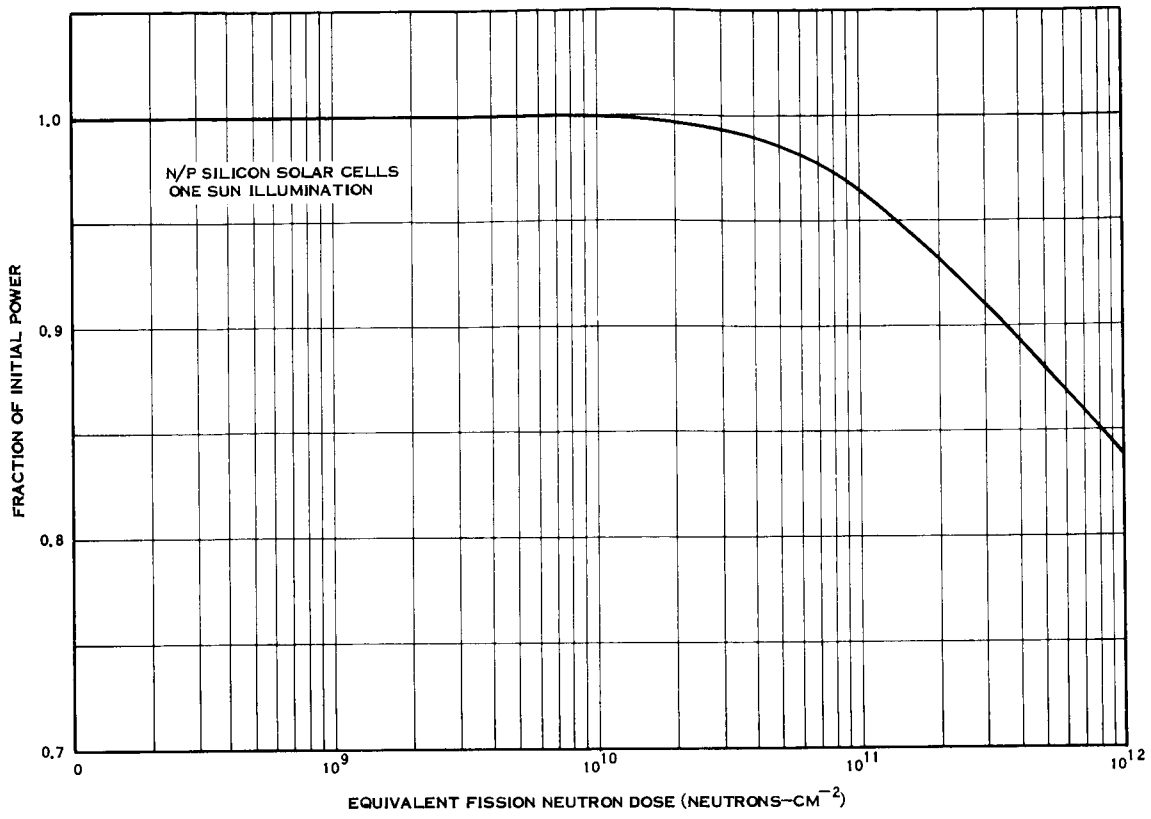

Figure C-3. Solar Cell Power Degradation

that the damage threshold is approximately 10^{14} EFN/cm^2. Radiation tests performed to determine the ionizing radiation sensitivity of Zener diodes denote no change in Zener voltage at a dose of approximately 10^7 rads (air). (See Reference C-14.) However, the devices tested had a lower power rating and hence a smaller junction area. Therefore, the threshold damage level of the Zener monoblock is taken as 10^6 rads.

C.3.7.3 Batteries

The silver-cadmium batteries noted in Reference C-3 are to be replaced with nickel-cadmium (Ni-Cd) cells. Reference C-15 indicates that the radiation sensitivity of this type of cell is similar to the silver-cadmium type it replaced.

C.3.7.4 Load-Sharing Circuitry

The most sensitive portions of this component are the integrated circuits. The damage levels are those noted for the signal electronics in Reference C-2. The threshold level is 10^{12} EFN/cm^2 and 10^3 to 10^4 rads.

C.3.7.5 Ampere-Hour Meter

The medium-frequency transistors and signal diodes used in this component require that the threshold damage level be that noted for the load-sharing circuitry.

C.3.8 COMPUTER AND SEQUENCER SUBSYSTEM

This subsystem remains unchanged with respect to its radiation damage threshold.

C.3.9 PROPULSION SUBSYSTEM

The Propulsion Subsystem replaces the Midcourse Adjust and Retropulsion Subsystems. In general, this subsystem is made up of combinations of components of the two subsystems it replaced. The fuel and pressurant tanks are similar to those of the Midcourse Adjust Subsystem except they are bladderless. The threshold damage levels are in excess of 10^{15} EFN/cm^2 and 10^8 rads. The major change in this subsystem is the propellant. A bipropellant system using Monomethyl Hydrazine (MMH) or Aerozine (A-50) with N_2O_4 oxidizer has replaced the monopropellant midcourse adjust component and the solid-fueled retropulsion unit. Both MMH and A-50 have threshold damage levels of 10^{15} EFN/cm^2 and 10^7 rads, while the N_2O_4 thresholds are in excess of these levels (Reference C-7). The thrust chamber will either be all ablative or ablative chamber and insulated skirt. Although not of identical construction to the nozzle described in Reference C-3, similar materials will be utilized, and the damage thresholds are expected to be the same. The rest of the components are identical (in terms of radiation sensitivities) to their corresponding component in the Midcourse Orbit Adjust Subsystem as noted in References C-2 and C-3.

C.3.10 PLANETARY SCAN PLATFORM ACTUATION SUBSYSTEM

This subsystem remains unchanged with respect to radiation sensitivity.

C.3.11 HARNESS SUBSYSTEM

It is anticipated that the polyolefin-insulated cables will be replaced by flat polyimide cables. The radiation sensitivity of polyimides was discussed in Section C.3.6, and the threshold damage level is 10^{15} EFN/cm^2 and 10^6 rads.

C.4 REFERENCES

C-1 Voyager Spacecraft System - Phase 1A Task B Preliminary Design - Spacecraft Functional Description, Volume A, Books 1 and 2, General Electric Company, Valley Forge, Pennsylvania, 31 January 1966.

C-2 J.C. Peden, et. al., Spacecraft Electronics and Materials Radiation Sensitivity Study Report for the RTG Study - Voyager Task C, General Electric Company, Valley Forge, Pa., 15 October 1966, Document No. VOY-C1-TR3.

C-3 J.C. Peden, et. al., Spacecraft Electronics and Materials Radiation Sensitivity Study Report for the RTG Study - Voyager Task C Appendices, General Electric Company, Valley Forge, Pa., 15 November 1966, Document No. VOY-C1-TR15.

C-4 General Electric Company, Voyager Subsystem and Component Engineers, private communications, July 1967 to October 1967.

C-5 Daly, G.B.,"Interim Final Report and Technical Paper on D.A. #L05-32, Automatic Canopus Identification," General Electric Company, Valley Forge, Pa., PIR Number U-41M8-125, 11 August 1967.

C-6 Chaplin, W.E., et. al., The Effect of Nuclear Radiation on Transducers, Battelle Memorial Institute, Columbus, Ohio, Report Number REIC-43, 31 October 1966.

C-7 Space Materials Handbook, 2nd edition, Air Force Materials Laboratory, RTD-AFSC, Wright-Patterson Air Force Base, Ohio, Report No. ML-TDR-64-40, January 1965.

C-8 Radiation Effects State of the Art 1964-1965, Battelle Memorial Institute, Columbus, Ohio, Report Number REIC-38, 30 June 1965.

C-9 Radiation Effects State of the Art 1965-1966, Battelle Memorial Institute, Columbus, Ohio, Report Number REIC-42, 30 June 1966.

C-10 Milek, J.T., Polyimide Plastics: A State of the Art Report, Hughes Aircraft Company, Culver City, California, Report No. S-8, 1 October 1965.

C-11 Aukerman, L.W., Proton and Electron Damage to Solar Cells, Battelle Memorial Institute, Columbus, Ohio, Report Number REIC-23, 1 April 1962.

C-12 Rasmussen, R., "Calculation of 1 Mev Electron Flux and Irradiation Degradation of Solar Cell I-V Curves by Computer," presented at the Sixth Photovoltaics Specialists Conference, Cocoa Beach, Florida, 28, 29, 30 March 1967.

C-13 Hendershott, D., Nuclear Radiation Test Results On Electronic Parts, Report 3, General Electric Company, Valley Forge, Pa., Report Number TIS-66SD277, June 1966.

C-14 Cocoa, U. and Keopp-Baker, N., Radiation Induced Surface Effects on Selected Semiconductor Devices, General Electric Company, Oklahoma City, Oklahoma, Report Number R64MCD502, 1 May 1964.

C-15 Argue, G.R., et. al., The Effects of Radiation on Nickel-Cadmium Battery Electrodes 1, Atomics International, Canoga Park, California, Report Number A1-64-11, 6 February 1964.

Table C-1. Telecommunications Subsystem

Subsystem	Components	Remarks	References
S-Band Subsystem	High-gain antenna	Possible use of Teflon	C-3, C-4
	Primary low-gain antenna	Possible use of Teflon	C-3, C-4
	Secondary low-gain antenna	Possible use of Teflon	C-3, C-4
	Medium-gain antenna	Possible use of Teflon	C-3, C-4
	Antenna RF transmission lines	Spiraline coaxial cable Aluminum jacket and Teflon dielectric	C-3, C-4
	RF test probes	Teflon connectors (probably)	C-3, C-4
	Phase lock receiver	a. Crystal filter b. Crystal VCO c. High-frequency transistors d. Operational amplifier* e. Tantalum film capacitors*	C-3, C-4 C-4 C-4
	Exciter	a. Auxiliary crystal oscillator b. High-frequency transistors	C-3, C-4
	Receiver power supply	a. Series regulators @ 2.2 and 5.5 watts input b. Transformer-rectifier*	C-3, C-4 C-4
	Exciter power supply	a. Series regulators @ 1.2 and 7.5 watts b. Transformer-rectifier supply*	C-3, C-4 C-4

* Better component definition, not a new device

Table C-1. Telecommunications Subsystem (Cont'd)

Subsystem	Components	Remarks	References
S-Band Subsystem (continued)	50-watt power amplifier	a. RF amplifier 1. Traveling wave tube or klystron 2. High-frequency transistors	C-3, C-4
		b. Power supply (dc-dc converter) 1. Low frequency power transistors 2. 143 watts input power	C-3, C-4
	3-watt solid state amplifier	12-watt power transistors @ 400 MHz*	C-3, C-4
	Diplexer	a. Mechanical components b. Possible use of Teflon	C-3, C-4
	Transfer switch	Possible use of Teflon	C-3, C-4
	Coaxial switch	Possible use of Teflon	C-3, C-4
	Hybrid coupler	a. Possible use of Teflon b. Stripline construction*	C-4
Telemetry Subsystem	Commutator	a. Integrated circuits b. High-frequency transistors	C-3, C-4 C-3, C-4
	Signal conditioners	High-frequency transistors	C-3, C-4
	Address decoding matrix	High-frequency transistors	C-3, C-4
	Subcommutator Drive	High-frequency transistors	C-3, C-4

* Better component definition, not a new device

Table C-1. Telecommunications Subsystem (Cont'd)

Subsystem	Components	Remarks	References
Telemetry Subsystem (continued)	Phaser	High-frequency transistors	C-3, C-4
	Psuedo noise generator	High-frequency transistors	C-3, C-4
	Format programmer	High-frequency transistors	C-3, C-4
	Analog-to-digital converter	a. High-frequency transistors b. Field effect transistors*	C-3, C-4
	Data transfer register	High-frequency transistors	C-3, C-4
	Digital data accumulator	a. Integrated circuits b. High-frequency transistors	C-3, C-4 C-3, C-4
	Data selector	High-frequency transistors	C-3, C-4
	Frequency divider	High-frequency transistors	C-3, C-4
	Rate control	High-frequency transistors	C-3, C-4
	Real-time data modulator	High-frequency transistors	C-3, C-4
	Stored data sub-carrier modulator	High-frequency transistors	C-3, C-4
	Subcarrier combiner and selector	High-frequency transistors	C-3, C-4
	Power supply	a. Zener diodes b. Operational amplifiers 1. Integrated circuits 2. High-frequency transistors	C-3, C-4

* Better component definition, not a new device

Table C-1. Telecommunications Subsystem (Cont'd)

Subsystem	Components	Remarks	References
Data Storage Subsystem	Magnetic tape recorder	a. Integrated circuits	C-3, C-4
		b. Internal power supply	
		1. Transformer	
		2. Rectifiers	
		3. Filters	
		c. End-of-tape sensor*	C-4
	Playback sequence control	Integrated circuits	C-3, C-4
	Power supply	a. Transformer	C-3, C-4
		b. Diodes	C-3, C-4
		c. Resistors and capacitors	C-3, C-4
		d. Relay	C-3, C-4
Command Subsystem	Command detector	a. Integrated circuits	C-3, C-4
		b. High-frequency transistors	C-3, C-4
	Command decoder	a. Integrated circuits	C-3, C-4
		b. High-frequency transistors	C-3, C-4
	Command access switch	a. Integrated circuits	C-3, C-4
		b. High-frequency transistors	C-3, C-4
	Power supply	Transformer-rectifier	C-3, C-4
Relay Radio Subsystem (GFE)	Relay antenna	Possible use of Teflon in connectors	C-3, C-4
	Antenna cable	Teflon dielectric	C-3, C-4
	RF test probe	Possible use of Teflon in connectors	C-3, C-4

* New device or component

Table C-1. Telecommunications Subsystem (Cont'd)

Subsystem	Components	Remarks	References
Relay Radio Subsystem (GFE) (continued)	Receiver	a. High-frequency transistor	C-3, C-4
		b. Crystal local oscillator	C-3, C-4
		c. Crystal filter	C-3, C-4
	Preselector and preamplifier	High-frequency transistors	C-3, C-4
	Data detector	High-frequency transistors	C-3, C-4
	Output selector	High-frequency transistors	C-3, C-4
	Power supply	Internal regulator at 15 watts	C-3, C-4

Table C-2. Guidance and Control Subsystem

Subsystem	Component	Remarks	References
Attitude Control	Acquisition sun sensor	a. 10 Ω-cm N/P silicon solar cell	C-3, C-4
		b. Corning 2600 filter	C-3, C-4
	Cruise sun sensor	a. 10 Ω-cm N/P silicon solar cell	C-3, C-4
		b. Corning 2600 filter	C-3, C-4
		c. Cerium borosilicate lens	C-3, C-4
	Coarse sun gate	Cerium borosilicate lens	C-3, C-4
	Fine sun gate	Cerium borosilicate lens	C-3, C-4
	Canopus sensor	a. Image disector tube (similar to CBS Lab type CL 1147)	C-3, C-4, C-5
		1. Corning 7052 envelope	
		2. Corning 0122 saphire face plate	
		3. K, Na, and Sb photocathode	
		4. Ag, Mg dynodes	
		b. Optics	C-3, C-4, C-5
		c. Electronics	C-3, C-4, C-5
		1. Medium-frequency transistors	
		2. Silicon-controlled rectifier	
		3. Integrated circuits	
		4. Cd S photoresistive device	
		d. In-flight calibration*	C-4, C-5
		1. Cherenkov light source	
	Integrating gyro package	See text	C-4
	Output Amplifier**	Medium- and high-frequency transistors	C-1, C-4
	Buffer Amplifier**	Medium- and high-frequency transistors	C-1, C-4

* New device or component

** Better component definition, not a new device

Table C-2. Guidance and Control Subsystem (Cont'd)

Subsystem	Component	Remarks	References
Attitude Control (continued)	Summing Amplifier*	Integrated circuits	C-1, C-4
	Rate-limiting coupler*	a. Resistors	C-1, C-4
		b. Diodes	C-1, C-4
	Rate-limiting lead network*	Medium- and High-frequency transistors	C-1, C-4
	Derived rate network*	a. Resistors	C-1, C-4
		b. Capacitors	C-1, C-4
	Threshold detector*	Integrated circuits	C-1, C-4
	Pneumatics driver*	Low-frequency power transistors	C-1, C-3, C-4
	Roll bias generator*	Integrated circuits	C-1, C-4
	Null detector*	Integrated circuits	C-1, C-4
	Logic control unit*	Integrated circuits	C-1, C-4
	Power supply*	a. Transformer	C-1, C-4
		b. Rectifier	
Cold Gas Jet Subsystem	Gas storage reservoir	a. 6 Al-4V titanium	C-3, C-4
		b. Gaseous nitrogen	C-3, C-4
	Check valve	Buna-N "0" ring	C-3, C-4
	Relief valve	a. Stainless steel	C-3, C-4
		b. Titanium	C-3, C-4

* Better component definition, not a new device

Table C-2. Guidance and Control Subsystem (Cont'd)

Subsystem	Component	Remarks	References
Cold Gas Jet Subsystem (continued)	Sensors	1. Temperature (platinum wire or thermistor resistance element)*	C-1, C-3, C-4
		2. Pressure (potentiometer type)*	C-1, C-3, C-4
	Heaters	Strip heaters	C-3, C-4
	Nozzles	Titanium	C-3, C-4
	Filters	Stainless steel screens	C-3, C-4
	Pressure regulators	Redundant nylon seats	C-3, C-4
	Solenoid valves	Metal, plastic, or elastomer seats	C-3, C-4
Autopilot Subsystem	Power amplifier	Medium-frequency transistors	C-3, C-4
	Lead-lag networks	Medium-frequency transistors	C-3, C-4
	Inverter	Medium-frequency transistors	C-3, C-4
	Servo gain amplifier	Medium-frequency transistors	C-3, C-4
	Buffer amplifiers	Medium-frequency transistors	C-3, C-4
	Power supply	Transformer rectifier	C-4
		Medium-frequency transistor	C-3, C-4

* Better component definition, not a new device

Table C-3. Temperature Control Subsystem

Component	Remarks	References
Active thermal control louvers	a. Bimetallic actuators*	C-4
	b. Highly polished aluminum*	C-4
Heaters	a. Strip heaters	C-3, C-4
	b. Bimetallic thermoswitches	C-3, C-4
	c. Resistor-diode-capacitor EMI modules	C-3, C-4
Thermal control coatings	a. Alzac (chemically brightened aluminum)	C-3, C-4
	b. White paint (zinc oxide and Potassium silicate)* Z-93 or PV 100 (titanium oxide and silicone alkyd)	C-4
	c. Black paint on interior surfaces (parsons or** catalac)	C-4
Super insulation blankets	a. Stainless steel and aluminized or gold plated* mylar with Kapton outer layer	C-4
	b. Aluminized mylar	C-3, C-4
	c. Stainless steel, Johns Manville microquarts fiber and aluminized mylar	C-3, C-4
Telemetry temperature sensor	Platinum wire	C-3, C-4
Louver position indicator	Differential transformer	C-3, C-4

* New device or component

** Better component definition, not a new device

Table C-4. Structure Subsystem

Component	Remarks	References
Structures	Mostly aluminum and some magnesium	C-3, C-4

Table C-5. Pyrotechnic Subsystem

Component	Remarks	References
Cold gas thruster	a. Materials similar to Cold Gas Jet Subsystem b. High pressure nitrogen	C-3, C-4 C-3, C-4
Pyrotechnic controller	a. SCR's b. Capacitors	C-3, C-4 C-3, C-4
Pin pullers	Pyrotechnic devices	C-3, C-4
Valves	Pyrotechnic devices	C-3, C-4

Table C-6. High-Gain Antenna Activation Subsystem

Component	Remarks	References
Series regulator	Medium frequence power transistors	C-3, C-4
Regulated dc power supply	Medium frequency power transistors	C-3, C-4
Signal conditioning Electronics	Medium frequency power transistors	C-3, C-4
Control logic	a. Latching relays	C-3, C-4
	b. Integrated circuits	C-3, C-4
Motor driver	a. High frequency transistors	C-3, C-4
	b. Silicon controlled switches	C-3, C-4
Deployment mechanism	a. Stored energy spring device	C-3, C-4
	b. Silicone oil damper	C-3, C-4
A-axis actuator	a. Step motor	C-3, C-4
	b. Viton A garter seal	C-3, C-4
	c. MoS_2 dry film coating	C-3, C-4
	d. Versilube G-300 coating	C-3, C-4
B-axis actuator	a. Step motor	C-3, C-4
	b. Welded or hydraulically formed bellows	C-3, C-4
	c. Bendix "free flex" pivots	C-3, C-4
	d. Rublon-C bushings	C-3, C-4
	e. Viton garter seal	C-3, C-4
Bearings and pivots	a. Ball bearings 1. 440 C CRES 2. LLB phenolic or Rublon-C retainer 3. Glass-reinforced Teflon or Viton-A seals	C-3, C-4

Table C-6. High-Gain Antenna Activation Subsystem (Cont'd)

Component	Remarks	References
Bearings and pivots (continued)	b. Sleeve bearings 1. Teflon 2. Glass or asbestos filter	C-3, C-4
	c. Pivots 1. Bendix "free flex"	C-3, C-4
Lubrication	MoS_2 dry film	C-4
Seals and bellows	a. Diaphragm 1. 18-8 CRES or Molybdenum	C-3, C-4
	b. Housings 1. Vitron quad rings and silicone grease	C-3, C-4
	c. Bellows 1. Beryllium Copper	C-3, C-4
	d. B-Axis actuator deployment shaft 1. Inert gas sealed by frangible seals and Viton quad rings	C-3, C-4
Stowed and deployed latch position sensor	Microswitch 1 HM 1 switches - Teflon insulation	C-3, C-4
A & B axis limit sensing switches	Same as above	C-3, C-4
Deployment axis rotation sensor	Potentiometer	C-3, C-4
Step sensor	Magnetically actuated read switch	C-3, C-4
A & B axis motor temperature sensor	Thermal resistor	C-3, C-4
Motor pressure sensor	Silicon strain gage	C-3, C-4
Control and sensory harness	Polyimide insulated wire*	C-4

* New device or component

Table C-7. Power Subsystem

Component	Remarks	References
Solar cell array*	a. Silicon solar cells, N/P	C-1, C-4
	b. Cover glass - Corning #7940, 10 mils thick	C-1, C-4
	c. Adhesives - RTV-602, RTV-560	C-1, C-4
Zener monoblock*	a. 7-volt, 3-watt zener diodes	C-1, C-4
	b. Isolation diodes	C-1, C-4
Batteries	Silver-zinc and nickel-cadmium*	C-4
Battery charge regulators	Low frequency power transistors	C-3, C-4
Load sharing circuitry*	a. Integrated circuits	C-1, C-4
	b. Resistor-capacitor	C-1, C-4
	c. Relay	C-1, C-4
Main regulator	Very low frequency power transistors	C-3, C-4
2.4 kHz inverter	Very low frequency power transistors	C-3, C-4
1-phase 400 Hz inverter	Low frequency power transistors	C-3, C-4
3-phase 400 Hz inverter	Low frequency power transistors	C-3, C-4
Power and switching logic	Medium frequency transistors	C-3, C-4
Clock and synchronizer	a. Medium frequency transistors	C-3, C-4
	b. Crystal oscillator	C-3, C-4
Failure detectors**	a. Operational amplifier	C-3, C-4
	b. Medium frequency transistors	C-3, C-4

* New device or component

** Better component definition, not a new device

Table C-7. Power Subsystem (Cont'd)

Component	Remarks	References
Telemetry electronics	Medium frequency transistors	C-3, C-4
Amp-hour meter*	a. Relay b. Passive components c. Medium frequency transistors d. Diodes	C-1, C-4

* New device or component

Table C-8. Computer and Sequencer Subsystem

Component	Remarks	References
Master sequencer	a. Magnetic core logic b. Integrated circuits	C-3, C-4 C-3, C-4
TTG registers	Integrated circuits	C-3, C-4
ΔV register	Integrated circuits	C-3, C-4
Gimbal sequencer	Integrated circuits	C-3, C-4
PSP turn ON/OFF	Integrated circuits	C-3, C-4
Telemetry registers	Integrated circuits	C-3, C-4
Power supply	a. Transformer b. Rectifier	C-3, C-4 C-3, C-4
Solar aspect sensor	a. Fused quartz reticule b. 10-ohm-centimeter N/P silicon solar cells c. Low and medium frequency transistors	C-3, C-4 C-3, C-4 C-3, C-4
Earth occultation sensor	Similar to GE SAM unit a. Silver & antimony doped tellurium IR detector b. Silicon or germainium filter c. H-film substrate d. Mylar tape e. One low frequency transistor f. FET's & high frequency transistors	C-3, C-4

Table C-9. Propulsion Subsystem*

Component	Remarks	References
Pressurization tank	a. Titanium 6AL-4V	C-1, C-4
	b. He	C-1, C-4
Propellant tank	a. Titanium 6A1-4V	C-1, C-4
	b. Monomethyl Hydrazine fuel of H-50	C-1, C-4
	c. N_2O_4 oxidizer	C-1, C-4
Thrust chamber	All ablative (silica phenolic) or ablative plus insulated skirt	C-4
Fill and vent valves	Teflon seals	C-1, C-4
Test ports	Teflon seals	C-1, C-4
Regulator	Metallic hard seats	C-1, C-4
Solenoid valves	Teflon seals	C-1, C-4
Tubes and fittings	Brazed construction	C-1, C-4
Valves	Squibb actuated	C-1, C-4
Relief valves		C-4
Sensors	a. Temperature	C-1, C-4
	b. Pressure	C-1, C-4

* New Subsystem

Table C-10. Planetary Scan Platform Actuation Subsystem

Component	Remarks	References
Entire Subsystem	Assumed similar to high-gain antenna actuation subsystem	C-3, C-4

Table C-11. Harness Subsystem

Component	Remarks	References
Harness	Polyamide (flat cables)	C-4

* New device or component